GLACIER CHANGES ACROSS NORTHERN ELLESMERE ISLAND

ADRIENNE C. WHITE

Thesis submitted to the University of Ottawa
in partial fulfillment of the requirements for the
Doctorate of Philosophy in Geography

Department of Geography, Environment and Geomatics
Faculty of Arts
University of Ottawa

ABSTRACT

This thesis investigates the causes and patterns of glacier and ice shelf changes across Northern Ellesmere Island, including rapid recent changes to marine-terminating glaciers and the mass balance of the Milne Ice Shelf along Ellesmere Island's northern coastline.

The first part describes the change in the areal extent of 1773 glacier basins across northern Ellesmere Island between ~1999 and ~2015 that were measured from optical satellite imagery. The results show that the regional ice coverage decreased by 1705.3 km^2 over the ~16-year period, a loss of ~5.9%. This indicates a marked acceleration compared to the 3.4% loss recorded by Sharp et al. (2014) between ~1960 and ~2000. Ice shelves had the greatest losses relative to their size, of ~42.4%. Glaciers feeding into ice shelves reduced in area by 4.7%, while tidewater glaciers reduced in area by 3.3%. Marine-terminating glaciers with floating ice tongues reduced in area by 4.9% and 19 of 27 ice tongues disintegrated, causing these glaciers to retreat to their grounding lines. Land-terminating glaciers lost 4.9% of their 1999 area, including the complete loss of three small ice caps (<1.5 km^2). These changes indicate the high sensitivity of the ice cover of northern Ellesmere Island to recent climate warming, and that continued losses are likely to occur in the future. In particular, the ice masses most susceptible to further losses are marine-terminating glaciers with floating termini and small land-terminating ice caps at low elevations.

To further investigate the forcings leading to the recent losses of floating ice tongues, the second part focuses on marine-terminating glacier changes in the Yelverton Bay region of northern Ellesmere Island since 1959. From 1959-2017, the total ice tongue area decreased by 49.07 km^2, with the majority of this loss occurring from 2005-2009 (34.68 km^2). The loss of ice tongues since 2005 occurred when open water replaced multi-year landfast sea ice and first-year sea ice in the regions adjacent to the ice tongues. These changes were accompanied by an increase in mean annual mid-depth (i.e., 100 and 200 m) ocean temperatures from -0.29°C from 1999-2005 to 0.67°C from 2006-2012. Despite the recent return of ocean temperatures to below pre-2006 levels, atmospheric summer temperatures have continued to rise (+0.15°C $decade^{-1}$ between 1948 and 2016), with open water continuing to occur. This suggests that loss of buttressing from sea ice appears to be the primary control on ice tongue losses, with air and ocean warming

important in weakening the sea ice and ice tongues, together with offshore wind events in some years. Based on current climate it is unlikely that ice tongues will reform in the future.

To examine the stability of the remaining ice shelves, the Milne Ice Shelf was selected as a case study to analyse the processes and patterns of surface mass balance. In 2008 a mass balance network of eight stakes was established across the Milne Ice Shelf and over the past 10 years has revealed a mean annual surface mass balance of -0.33 ±0.04 m water equivalent yr^{-1}. Comparison of this surface mass balance rate with past ice thickness change measurements made by Mortimer et al. (2012) indicate that recent thinning may be limited to the surface, and accelerating over time. Individual stake and snow measurements reveal a surface mass balance gradient, whereby ablation decreases with proximity to the seaward edge of the ice shelf. The ablation gradient is driven by the microclimatology recorded at three automatic weather stations installed along the ice shelf, which show that air temperature and solar radiation decreases towards the coastline, while snow accumulation increases. Climate analysis suggests that the entire Milne Ice Shelf is in a state of negative mass balance in years with >200 melting degree days (MDD), while the one net positive balance year (in 2013) occurred when MDD totals were 105 yr^{-1}. Although the Milne Ice Shelf is the most stable remaining ice shelf along the northern coast of Ellesmere Island, the relationship between climate and mass balance, along with a recent increase in calving along its landward margins, indicate that it is out of equilibrium with current climate.

Overall, the ice coverage across northern Ellesmere Island is shrinking. The land-terminating ice that formed under cooler climatic conditions of the past, particularly low-lying small ice caps, are out of equilibrium with current climatological conditions. In addition, recent changes in the ice tongues and ice shelves demonstrate that the northern coastline of Ellesmere Island is approaching a future where the permanent floating ice cover can no longer be sustained.

PREFACE

This thesis presents the original research of the author, conducted under the supervision of Luke Copland. The thesis is presented as three manuscripts (Chapters 2, 3 and 4) of which I am the primary author. I am responsible for the research methodology, satellite data processing and analysis and manuscript writing with guidance and suggestions provided by my supervisor and any co-authors. Derek Mueller (Carleton University) is a co-author on Chapter 4 for providing field data and satellite data. Sergey Samsonov (Natural Resources Canada) is also a co-author on Chapter 4 for providing satellite data.

Chapter 2, which is published, and Chapter 3 which is in press, incorporate suggestions from editors and anonymous reviewers from the Journal of Glaciology. Chapters 2, 3 and 4 are already published or in preparation to be published as:

White A and Copland L (2018) Area changes of glaciers across Northern Ellesmere Island, Nunavut, between ~1999 and ~2015. *Journal of Glaciology*, **64**(246), 609-623, doi: 10.1017/jog.2018.49

White A and Copland L (In press) Loss of floating glacier tongues from the Yelverton Bay region, Ellesmere Island, Canada. *Journal of Glaciology*.

White A, Copland L, Mueller D and Samsonov S (In preparation) Connections between climate, mass balance and stability of the Milne Ice Shelf, Northern Ellesmere Island.

Difficulties are just things to overcome, after all

- Sir Ernest Shackleton (1874-1922)

TABLE OF CONTENTS

LIST OF TABLES

LIST OF FIGURES

LIST OF ACRONYMS

AAR	Accumulation area ratio
ASTER	Advanced Spaceborne Thermal Emission and Reflection Radiometer
AWS	Automatic weather station
CAA	Canadian Arctic Archipelago
CMEMS	Copernicus Marine Environment Monitoring Service
EL	Equilibrium line
ELA	Equilibrium line altitude
ERS-1	European Remote-Sensing Satellite-1
ETM+	Enhanced Thematic Mapper Plus
FYI	First-year ice
GCP	Ground control point
GLIMS	Global Land Ice Measurements from Space
GPR	Ground-penetrating radar
MDD	Melting degree day
MLSI	Multi-year landfast sea ice
MODIS	Moderate Resolution Imaging Spectroradiometer
NCAR	National Center for Atmospheric Research
NCEP	National Center for Environmental Prediction
OLI	Operational Land Imager
PCA	Principal component analysis
PDD	Positive degree day
PV-AWS	Purple Valley-automatic weather station
QEI	Queen Elizabeth Islands
RGB	Red, green and blue
RMSE	Root mean square error
RWV	Radio-wave velocity
SAR	Synthetic aperture radar
SPOT	Satellite Pour l'Observation de la Terre
TIRS	Thermal Infrared Sensor
w. eq.	Water equivalent

ACKNOWLEDGEMENTS

I would like to thank the various organizations that funded this research through grants and scholarships. Support for this project was provided by ArcticNet, the Association of Canadian Universities for Northern Studies, Canada Foundation for Innovation, Ontario Research Fund, the Garfield Weston Foundation, the National Sciences and Engineering Research Council (NSERC) of Canada, the Northern Scientific Training Program, Ontario Graduate Scholarship, Polar Continental Shelf Program, the Royal Canadian Geographic Society, the Society of Naval Architects and Marine Engineers, the Norwegian Centre for International Cooperation in Education (SIU), and the University of Ottawa. I would also like to acknowledge the Polar Geospatial Center (University of Minnesota) for providing early access to the ArcticDEM.

I would like to express my deepest thanks to my supervisor, Dr. Luke Copland of the Laboratory for Cryospheric Research for his guidance and tremendous support throughout my graduate career. I sincerely appreciate all the time and patience he has given me, and for providing me with countless opportunities to grow my passion for the Polar Regions. I would like to extend my appreciation to Dr. Denis Lacelle (University of Ottawa), Dr. Michael Sawada (University of Ottawa), Dr. Brian Moorman (University of Calgary), and Dr. Derek Mueller (Carleton University) for serving as my committee members on this thesis. I would also like to acknowledge Dr. Derek Mueller for sharing mass balance and remote sensing data, and for his support and cooperation during field work on Ellesmere Island.

I would also like to thank members of the LCR (past and present) for their support and friendship. In particular I would like to acknowledge Abigail Dalton and Dorota Medrzycka for assistance with field data collection. I would also like to thank members of the Water and Ice Research Laboratory (Carleton University) for field assistance and data sharing.

This work would not have been possible without the support of my friends and family. To my mother, Elisabeth Churcher and my step-father, Timothy Denton, I am so grateful for all your love and support throughout this research. To the Tyler family, your kindness and words of encouragement have meant so much to me. To Christopher Tyler, thank you for joining me on this journey, I could not have done this without you. Last but not least, thank you to my side-kick, Eska, you've earned this PhD with me.

This thesis is dedicated to my late father, Richard Thomas White

CHAPTER 1: INTRODUCTION

1.1 GLACIER CHANGE IN THE QUEEN ELIZABETH ISLANDS

The glaciers and ice caps in Canada's Queen Elizabeth Islands (QEI) hold the largest area of ice (~104,000 km^2 in 2000) outside of Greenland and Antarctica, comprising ~14% of Earth's total ice-covered area outside of the ice sheets (Sharp et al., 2011). As a result of warming air temperatures, glaciers in the QEI have experienced a recent acceleration in their mass losses. Since the 1960s, surface mass balance monitoring has been undertaken on several ice masses in the QEI, including Devon Ice Cap, Meighen Ice Cap, Melville South Ice Cap, Agassiz Ice Cap and White Glacier (Figure 1.1a). With the exception of Meighen Ice Cap, results from 1960 to 2003 reveal a negative mass balance with a weak but significant trend to increasingly negative balances, particularly since the late 1990s (Koerner, 2005). Koerner (2005) linked the negative mass balance trends to a <1°C summer warming observed over the period 1950-1998 in the eastern Arctic (Zhang et al., 2000). The Meighen Ice Cap, on the north-west edge of the QEI, showed little trend in mass balance which, along with its prevalence at low-altitude, was linked to melt-suppressing fog from the nearby Arctic Ocean (Alt, 1979). More recently, downscaled estimates from the regional climate model RACMO2.3 extend surface mass balance estimates to a 58-year period (1958-2015; Noël et al., 2017). Accompanied by a +1.1°C increase in near-surface warming, glaciers and ice caps in the QEI have recently doubled (28.2 ±11.5 Gt yr^{-1}) in their rate of surface mass loss compared to their pre-1996 average (11.9 Gt yr^{-1}; Noël et al., 2017). Combined with ice discharge, total ice loss has accelerated at a rate of 1.0 ±0.1 Gt yr^{-2} (1991-2014), making the QEI one of the largest contributors to sea level rise outside of Greenland and Antarctica since 2005 (Millan et al., 2017). Recent estimates from Arctic Canada indicate a 3.21 ±0.72 mm contribution to sea level rise from 1971-2017, a contribution that represents ~14% of pan-Arctic land ice contributions (Box et al., 2018).

1.2 GLACIERS ON ELLESMERE ISLAND

The largest single icefield in the QEI is situated on Northern Ellesmere Island, with a total ice-covered area of 26,629 km^2 in 2000 (Sharp et al., 2014). Ellesmere Island comprises the largest island (196,236 km^2) in the northern Canadian Arctic Archipelago, with Northern Ellesmere Island separated from its southern counterpart by Greely Fiord and the Hazen Plateau (Figure

1.1). This region is characterized by a mountainous terrain with a maximum elevation of 2616 m at Barbeau Peak (Figure 1.1b). Land-terminating glaciers comprise 60% of the Northern Ellesmere Icefield and are located along the southern and eastern extent of the icefield (Millan et al., 2017). The remaining glaciers are marine-terminating and are located along the northern and western coastlines of the icefield (Millan et al., 2017). The northern coastline has several ice shelves and ice shelf remnants with a total area of 535 km^2 in 2015 (Mueller et al., 2017a). Long-term glaciological studies specific to Northern Ellesmere Island have been focused on regional elevation and velocity changes (including surging glaciers), small ice caps on the Hazen Plateau, and the floating ice shelves and ice tongues along the northern coastline. The following sections (1.2.1 to 1.2.3) provide a brief synthesis of these glaciological findings so far.

1.2.1 Glacier surface elevation changes across Northern Ellesmere Island

Repeat-track laser altimetry measurements have been collected across Northern Ellesmere Island over several years between 1995 and 2015 with NASA's Airborne Topographic Mapper conical laser scanning system. Measurements collected in 1995 and 2000 showed thinning in western areas (along Otto Glacier), transitioning into thickening towards the east, including areas of low elevation (<~750 m above sea level) thickening (>+0.5 m yr^{-1}) on Grant Ice Cap (Abdalati et al., 2004; Mortimer et al., 2018). Based on the elevation changes between 1995 and 2000, Abdalati et al. (2004) estimated a volumetric change of -3.59 km^3 yr^{-1} for the entire ice-covered region of northern Ellesmere Island, the highest rate calculated for the QEI. More recently, elevation changes between 2000 and 2005/06 showed thinning in areas that had previously shown thickening along the southwest, between Otto Glacier and Yelverton Glacier (Mortimer et al., 2018). Elevation measurements collected in 2005/06 to 2012/14 showed thinning nearly everywhere on Northern Ellesmere Island (Mortimer et al., 2018). This increased thinning has been attributed to changes in summer melt across the QEI, driven by increasing mean summer near surface (2 m) and upper-air (700 hPa) temperatures (1.0-1.2°C higher between 2005 and 2012 compared to the 1948-2015 mean), amplified by decreasing mean summer glacier surface albedo (0.029 ±0.025 $decade^{-1}$ from 2001-2016; Mortimer et al., 2016; Mortimer and Sharp, 2018; Mortimer et al., 2018).

1.2.2 Glacier velocities across Northern Ellesmere Island

Velocities across the interior of the Northern Ellesmere Icefield are typically low (<20 m yr^{-1}) but tend to increase along glacier trunks, which may indicate a transition from cold to warm basal conditions as glaciers become channelized into deep and narrow troughs or travel over changing bed conditions (e.g., bedrock type, presence or absence of subglacial sediments, or change in sediment types) in the ablation zone (Van Wychen et al., 2016). From 1991 to 2015, the main tidewater glaciers flowing from the Northern Ellesmere Icefield (i.e., Disraeli, Milne, DeVries, M'Clintock, Otto, Marine, Marine North, and Yelverton; Figure 1.1b) had a total average dynamic discharge rate of 0.48 ±0.08 Gt yr^{-1} (Millan et al., 2017). The average dynamic discharge rate for these glaciers has shown considerable interannual variability, with an increase in discharge after 2001, peaking in 2006 (0.53 ±0.12 Gt yr^{-1}), followed by a slowdown in 2015 (0.31 ±0.1 Gt yr^{-1}) due to a decrease in the velocity of most glaciers (Millan et al., 2017). The main driver of the peak discharge in 2006 was the active surge phase of Otto Glacier, which was reported to be stagnant by 2015 (Van Wychen et al., 2016; Millan et al., 2017). Otto Glacier is one of 13 glaciers showing evidence of surge characteristics (e.g., looped and folded surface moraines, and heavy crevassing) on Northern Ellesmere Island, although only Otto and Chapman glaciers have been observed during their active surge phases (Figure 1.1b; Hattersley-Smith, 1969; Copland et al., 2003; Van Wychen et al., 2016). Since 2010 the majority (>50%) of dynamic ice discharge has been driven by the Yelverton and Milne glaciers (Figure 1.1b), with an average total discharge rate of 0.15 ±0.06 Gt yr^{-1} (Millan et al., 2017).

1.2.3 The Hazen Plateau ice caps, Northern Ellesmere Island

Glaciers and ice caps <10 km^2 in size make up 90% of the ice masses across Northern Ellesmere Island and underwent the greatest relative area changes (>22% mean loss) between 1959/1960 and 1999/2000 (Sharp et al., 2014). Two pairs of small (<7.5 km^2 in 1959) ice caps along the Hazen Plateau (~300 m to >1000 m above sea level) have been the subject of intermittent mass balance studies since the 1970s, and provide the only long-term record of glacier mass balance on Northern Ellesmere Island (Hattersley-Smith and Serson, 1973; Bradley and Serreze, 1987; Braun et al., 2004; Serreze et al., 2017). These ice caps include the St. Patrick Bay Ice Caps (unofficially named; 7.48 km^2 and 2.94 km^2 in 1959) on eastern Northern Ellesmere Island, and Simmons and Murray Ice Caps (7.45 km^2 and 4.37 km^2, respectively, in 1959) located 110 km southwest of the St. Patrick Bay Ice Caps (Figure 1.1b; Serreze et al., 2017). The first

observations of the St. Patrick Bay Ice Caps were made from aerial photography collected in July 1947 and August 1959 (Hattersley-Smith and Serson, 1973; Bradley and Serreze, 1987). Mass balance stakes were installed and surveyed occasionally in the 1970s and 1980s, and annually from 1999 to 2002 (Hattersley-Smith and Serson, 1973; Bradley and Serreze, 1987; Serreze et al., 2017). The St. Patrick Bay Ice Caps were resurveyed in 1999 and 2000, a network of 11 accumulation stakes were established in 1999 and resurveyed in 2000, 2001 and 2002 on the Murray Ice Cap, and a new network of 15 stakes was established in 2000 and resurveyed in 2001 on the Simmons Ice Cap.

Based on results of both aerial and satellite imagery, and the mass balance measurements (1971/1972 and 1982/1983), the ice caps on the Hazen Plateau experienced a period of reduced loss or occasional growth from the 1960s through part of the 1970s, and in some years such as 1982/1983, in response to cool atmospheric temperatures. Since then, the annual mass balance for all four ice caps has been negative (Braun et al., 2004). All the ice caps reduced in area between 1959 and 2016; the St. Patrick Bay Ice Caps reduced to 5% of their original area, while the Murray and Simmons ice caps reduced to 39% and 25% of their original areas, respectively (Serreze et al., 2017). The accelerated loss of the St. Patrick Bay Ice Caps has been linked to increasing air temperatures since the start of the 21st century, and to the reduction in the frequency of summer snowfall combined with the reduction in summer albedo as dirt layers become exposed. Compared to the St. Patrick Bay Ice Caps, the less pronounced loss from the Simmons and Murray ice caps has been linked to their higher elevations and cooler summer temperatures and perhaps due to greater overall thickness and regional differences in temperature lapse rate (Serreze et al., 2017).

1.2.4 Ice shelves and floating ice tongues on the northern coast of Ellesmere Island

Arctic Ice Shelves are thick (≥20 m) masses of floating ice that are attached to the coast and typically have an undulating surface made up of troughs and ridges (Dowdeswell and Jeffries, 2017). There are three types of ice shelves that are distinguished by the source (i.e., meteoric or marine) of their formation and growth. Classical ice shelves form from one or many floating ice tongues that spread and coalesce to occupy an embayment or fiord, while sea-ice ice shelves form initially from multi-year landfast sea ice that acts as a basement from which surface and basal thickening occurs (Dowdeswell and Jeffries, 2017). Composite ice shelves are composed of

both glaciers ice and sea ice (Lemmen et al., 1988). The ice shelves that fringe the Antarctic coastline extend hundreds of kilometers from the grounding zone and are classified as the classical type. In the Canadian Arctic, ice shelves are limited to the northern coast of Ellesmere Island, where the lowest glaciation levels and equilibrium line altitudes are found (Miller et al., 1975). The ice shelves of Northern Ellesmere Island have a combined area of 535.2 km^2 (as of 2015; Mueller et al., 2017a), and include sea-ice ice shelves and composite ice shelves. Unlike ice shelves, ice tongues (also referred to as glacier tongues) are the floating extensions of a single valley glacier (Mueller et al., 2017a). Once established, an ice shelf gains mass through snowfall and basal accretion, and losses mass through surface and basal melting. The margins of an ice shelf can lose mass through calving, but in some instances can be replaced by multi-year landfast sea ice that freezes to the margin of the ice shelf and thickens through time (e.g., the Milne Re-entrant; Jeffries, 1986).

The first observations of the northern coast of Ellesmere Island were made by explorers during the British Arctic Expedition of 1875-76 (Parliamentary Paper v LVI, 1877) and the Peary Arctic Expedition of 1905-06 (Peary, 1907), that described the undulating surface topography as they travelled along the coastline. Based on these observations, the northern coastline was likely fringed by one continuous ice shelf, unofficially known as the Ellesmere Ice Shelf, that extended along the entire coastline and had an estimated area of 8597 km^2 in 1906 (Vincent et al., 2001; Mueller et al., 2017a). Scientific expeditions to the region began in the 1950s and have continued intermittently to present day, to study the ice shelves and the ice islands (i.e., tabular icebergs) that calve from them (Jeffries, 2017).

The Ellesmere Island ice shelves formed ~4000 years ago and remained stable until 1400 years ago when fracturing occurred, then later reformed 800 years ago (Antoniades et al., 2011). The Ellesmere Ice Shelf that fringed the coastline at the turn of the 20^{th} century underwent rapid reduction in the 1930s and 1940s, during regional warming, producing large ice islands (up to 1030 km^2 in area) observed by American military and Soviet scientists in the Arctic Ocean during the 1930s and 1940s (Koenig et al., 1952; Belkin and Kessel, 2017).

Using a combination of aerial photographs and satellite imagery, Mueller et al. (2017a) quantified the change in ice shelf and ice tongue area for 12 individual years between 1959 and 2015, which provides the most comprehensive analysis to date of change in the floating ice cover

of northern Ellesmere Island. These results show that by 1959 the Ellesmere Ice Shelf had broken up into 15 individual ice shelves with a total area of 2168 km^2, and eight ice tongues with a total area of 94 km^2 (Mueller et al., 2017a). By 2015 the total ice shelf extent reduced to 535 km^2, including the complete loss of 11 ice shelves during the 1990s and two ice shelves (Ayles and Markham) during the 2000s (Mueller et al., 2017a). The loss of several ice shelves left behind ice tongues (e.g., Serson Ice Shelf; Figure 1.1b), with nine ice tongues remaining in 2015 with a total area of 23 km^2 (Mueller et al., 2017a). The long-term causes of ice shelf thinning and weakening have been linked to warming air and ocean temperatures, and negative mass balance, including a reduction in glacier inputs (Mortimer et al., 2012; White et al., 2015). The calving events themselves are typically initiated by open water conditions caused by the loss or reduction of multiyear landfast sea ice, epishelf lake or fiord ice cover (Copland et al., 2017).

In addition to changes in area extent due to calving or disintegration, overall thinning was detected across the Milne Ice Shelf (Figure 1.1b) by Mortimer et al. (2012). Based on a comparison of radio-echo sounding data from 1981 with ground-penetrating radar (GPR) surveys completed in 2008 and 2009, an average total thinning of 8.1 ±2.8 m was measured. However, the total overall thinning was not uniformly distributed across the ice shelf; the southern half (known as the central unit) showed a higher rate of thinning, compared to the northernmost half where thickness change was positive (7.5 to 15 m) in some areas. While these measurements provide an overall estimate of ice thickness change and mass balance, they do not indicate whether the thinning occurred from the base or surface of the ice shelf.

The only comprehensive surface mass balance data previously collected over an Ellesmere ice shelf was conducted across the Ward Hunt Ice Shelf, intermittently between 1959 and 2008 (Braun, 2017; Figure 1.1b). In spring 1959, 114 ablation stakes were installed in a grid-like pattern covering an area of 1.91 km^2 across the northern margin of the Ward Hunt Ice Rise and extending onto the Ward Hunt Ice Shelf (Walker and Mattox, 1961). The stakes installed on the ice shelf were lost after a calving event in 1961/62 (Hattersley-Smith, 1963), but were established, following this event, in a grid covering an area of 0.9 km^2 to the east of Ward Hunt Island (Braun 2017). In 2002 a north-south transect was installed on the Ward Hunt Ice Rise and in 2006 five clusters with six stakes (50-100 m apart) were installed east, west and south of Ward Hunt Island to examine spatial variability in ablation (Mueller and Vincent, 2006). Although the

distribution, number of stakes, and site visits has varied over time, Braun (2017) summarized the 1959-2004 surface mass balance measurements to reveal a total average 1.68 m water equivalent (w.eq.) loss on the ice rise, compared to a 3.1 m w.eq. loss for the ice shelf. The most negative year over this time period was in 2002/2003, when the ice rise lost 0.33 m w.eq. and the ice shelf lost 0.54 m w.eq. According to the spatial distribution of surface mass balance conducted by Mueller and Vincent (2006), ablation stakes installed in marine ice sites that surround Ward Hunt Island had a significantly higher ablation (mean: -0.75 ±0.17 m w. eq.) compared to the stake clusters installed on meteoric ice sites (-0.29 ±0.05 m w. eq.). Mueller and Vincent (2006) suggested that the spatial variability in ablation could be linked to the distribution of fog. Walker Hill (450 m above sea level) on Ward Hunt Island acts as a topographic barrier that prevents fog from reaching the leeside of the island, which allows increased solar radiation to reach the ice surface and increase ablation (Mueller and Vincent, 2006).

1.3 FOCUS AND OBJECTIVES

While Northern Ellesmere Island has a rich history of exploration and scientific research dating back to the turn of the 20th century, this region's logistical challenges have left many observational gaps. Although satellite imagery has advanced glaciological research, up until recently the high northerly position of Northern Ellesmere Island was beyond the reach of Landsat imagery, which prevented complete coverage of its ice masses (Jeffries et al., 1992). This has added difficulty in monitoring and quantifying Northern Ellesmere's changing ice-covered area, which is important for assessing glacier change and placing these into a global context (Raup et al., 2007). Although a comprehensive database of glacier area for Northern Ellesmere Island has been developed, it is restricted to 1959 and 2000, and does not capture recent changes or provide in-depth analysis (Sharp et al., 2011). Mueller et al. (2017a) has generated an impressive database of ice shelf and ice tongue changes for the northern coast of Ellesmere Island that captures the scale of losses from floating ice masses, but to date the factors causing these reductions have focused on the ice shelves, and the causes and implications for ice tongue loss in this region remain largely unknown. Recent studies on the ice shelves have highlighted the external factors leading to their area changes (i.e., Ayles and Petersen ice shelves; Copland et al., 2007; White et al., 2015; reviewed in Copland et al., 2017; Figure 1.1b), thickness measurements (i.e., Petersen Ice Shelf; White et al., 2015) and changes (Milne Ice

Shelf; Mortimer et al., 2012), and surface mass balance (e.g., Ward Hunt Ice Shelf; Braun, 2017). Despite these advances, the mass balance processes and stability of the ice shelves remain poorly understood. Although surface mass balance data are available from the Ward Hunt Ice Shelf, they are temporally and spatially restricted (Braun, 2017).

Motivated by these knowledge gaps, this thesis presents the first comprehensive, integrated study of the recent changes to both land-terminating and marine-terminating glaciers across Northern Ellesmere Island. It has three primary objectives:

1. Generate an updated inventory that includes the area and characteristics of every individual glacier and ice shelf on Northern Ellesmere Island for ~1999 and ~2015. Using a variety of optical satellite imagery and the ArcticDEM, each glacier basin is defined and the ice extent delineated. Each glacier is visually classified by ice type using the optical satellite imagery, and terrain parameters (i.e., elevation, aspect, slope and flow length) are derived using the ArcticDEM to understand physical controls on glacier area losses.
2. Examine the changes to ice tongues in the Yelverton Bay region, and understand the factors that influence their stability and long-term variability (Figure 1.1b). This region contains the largest concentration of ice tongues on Northern Ellesmere Island, with a combination of aerial photographs and optical satellite imagery used to measured their changes since 1959. This includes a documentation of changes in surrounding marine ice types (i.e., sea ice, sikussak, and mélange), and an evaluation of connections between ice tongue changes and changes in ocean and air temperatures.
3. Examine the spatial and temporal variability in surface mass balance and climatology across the Milne Ice Shelf, the most stable remaining ice shelf on Northern Ellesmere Island. A total of 10 years of surface mass balance measurements are analysed and compared with automatic weather station data. GPR measurements are used to identify areas of long-term accumulation and ablation and compared with synthetic aperture radar satellite imagery to examine long-term (since the early 1990s) surface mass balance patterns across the ice shelf, and implications for its stability.

These objectives address the above knowledge gaps by providing area measurements that extend the previous 1959 and 2000 inventories (from Sharp et al., 2014) to 2015, and in addition

provide an analysis to better understand the spatial variability in area losses across Northern Ellesmere Island. The long-term change in ice tongues in the Yelverton Bay region, in relation to atmospheric and oceanographic factors, quantifies ice tongue area changes and identifies the factors that impact their stability. The 10-year record of surface mass balance on the Milne Ice Shelf provides a new mass balance record and examines the role of microclimatology on ice shelf stability. Together these three studies provide a more complete picture of how different glacier types are evolving as climate changes, and provide a comprehensive record of glacial change for all of Northern Ellesmere Island.

1.4 THESIS OUTLINE

This thesis follows a manuscript-style format and includes three articles. Chapter 1 provides a synthesis of the scientific literature motivating this thesis. Chapter 2 presents a complete inventory of glaciers across Northern Ellesmere Island, and the area changes for each glacier basin derived from optical satellite imagery in ~1999 and ~2017. Chapter 3 presents a description of the spatial and temporal changes to the ice tongues in the Yelverton Bay region on the northern coast of Ellesmere Island. Chapter 4 presents observations of surface mass balance of the Milne Ice Shelf and factors affecting the temporal and spatial variability in surface melt rates. Chapters 2-4 were written as stand-alone pieces of scientific literature, so some repetition (e.g., description of study area) is present between these. Chapter 5 summarizes the findings of these articles and discusses areas for future research. The references for each chapter are combined at the end of the thesis in Chapter 6.

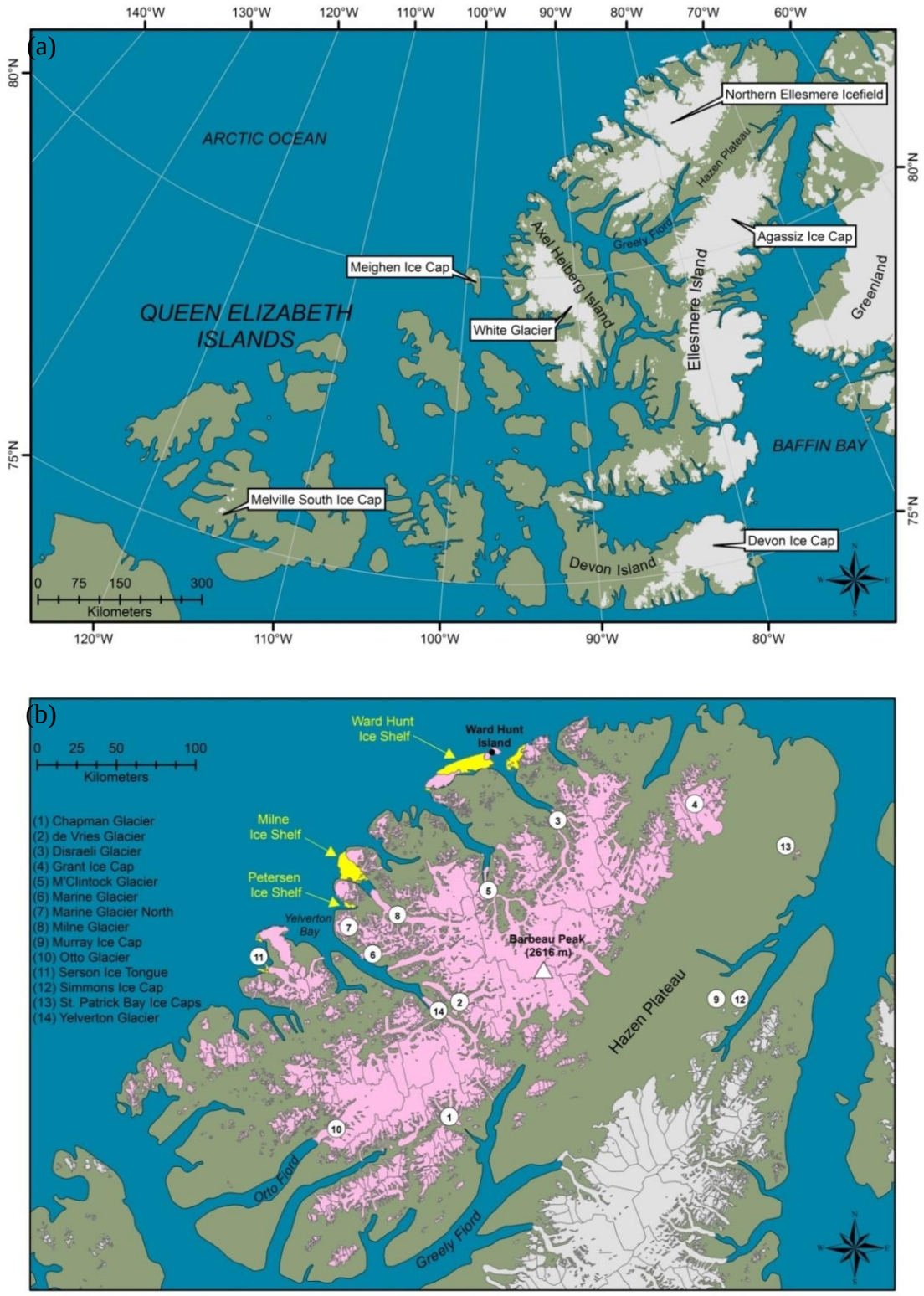

Figure 1.1: (a) Regional map of the Queen Elizabeth Islands; (b) Map of Northern Ellesmere Island showing the 1999 glacier extents from the Global Land Ice Measurements from Space (GLIMS) database (GLIMS and NSIDC, 2005), and the 2015 extents of the floating ice tongues and ice shelves derived by Mueller et al. (2017b).

CHAPTER 2: AREA CHANGE OF GLACIERS ACROSS NORTHERN ELLESMERE ISLAND, NUNAVUT, BETWEEN ~1999 AND ~2015

2.1 INTRODUCTION

The Canadian Arctic Archipelago (CAA) contains ~150,000 km^2 of glacier ice, making this region the most glaciated in the world outside of Greenland and Antarctica (Pfeffer et al., 2014). Based on satellite gravimetry measurements, this region has become the single largest contributor to eustatic sea-level rise outside of the major ice sheets since 2003 (Harig and Simons, 2016), during a period of rapid warming of glacier surface temperatures (Mortimer et al., 2016). The ice in this area can be separated into two groups, the southern area that spans Baffin (~36,839 km^2) and Bylot (~4,859 km^2) islands, and the northern area (107,488 km^2) that spans the Queen Elizabeth Islands (QEI), of which 27,556 km^2 (all ~1960 areas) is located on Northern Ellesmere Island (Figure 2.1; Andrews, 2002; Sharp et al., 2014).

The first detailed measurements of glacier thickness and volume change across Northern Ellesmere Island were conducted by Abdalati et al. (2004), who used repeat airborne altimetry measurements over the period 1995 to 2000 to calculate changes of -3.52 km^3 $year^{-1}$ (the highest rate of ice volume loss compared to all other ice caps in the CAA). Sharp et al. (2014) performed measurements of the area change of glaciers (excluding ice shelves) on Northern Ellesmere Island up to the year 2000, by using ice extents from 1956 to 1961 derived from aerial photography and 2000 extents delineated using an unsupervised classification of Landsat 7 Enhanced Thematic Mapper Plus (ETM+; 15-30 m resolution) and Advanced Spaceborne Thermal Emission and Reflection Radiometer (ASTER; 15 m resolution) imagery. Their study revealed that Northern Ellesmere experienced a reduction in glaciated area of 927 km^2 (3.4% of initial area) over this period, the greatest area loss of all regions measured across the CAA. The largest mean percentage area changes for Northern Ellesmere occurred from glaciers <1 km^2 in area, which lost an average of 29.2% of their initial ice area. Since 2000, a few studies have been conducted on Northern Ellesmere Island to assess changes in ice shelf area (e.g., Copland et al. 2007; Mueller et al., 2017a), and the changes of individual ice caps (Braun et al., 2004; Serreze et al., 2017), but no detailed regional assessment of glacier changes has been conducted.

Here I present a comprehensive inventory of the number and extent of all glaciers on Northern Ellesmere Island, using satellite data acquired between 1999 and 2016. This is the first study to present recent area change measurements for this region, and to analyse the spatial variability in glacier change in relation to terrain controls. Our data will be made available in the Global Land Ice Measurements from Space (GLIMS) database (http://www.glims.org).

2.1.1 Study area

Ellesmere Island is the largest island in the QEI, with an area of 196,236 km^2 and a length of 830 km (Figure 2.1). The island is the most mountainous in the CAA, and can be separated into different ice regions from north to south that include: Northern Ellesmere Icefield, Agassiz Ice Cap, Prince of Wales Icefield, Manson Icefield and Sydkap Icefield (Figure 2.1). The study area of Northern Ellesmere is separated from the rest of Ellesmere Island by the Hazen Plateau and Greely Fiord, and has a maximum elevation of 2,616 m at Barbeau Peak (Figure 2.2). Lake Hazen is a large inland lake, with a surface area of 537.5 km^2, which stretches in a southwest-northeast direction in the southeast part of Northern Ellesmere (Figure 2.2). The Northern Ellesmere Icefield spans the majority of the northern part of the island, while ice shelves and marine-terminating glaciers flow off the northern coastline. Smaller ice caps, such as Grant and Ad Astra, surround the main ice caps, but the majority are unnamed.

The climate regime of Northern Ellesmere varies between the coastal regions, interior lowlands and highlands. The coastal waters contain a mix of first- and multi-year ice. In summer, fall, and early winter (during the sea ice consolidation period), the varying coverage of sea ice and open water leads to high frequencies of fog and low cloud over the channels and along the coastlines (Maxwell, 1981). The interior lowlands are surrounded by mountains which cause a rain shadow that results in low mean precipitation, while exposed slopes at higher elevations receive >200 mm of precipitation per year (Maxwell, 1981). At Eureka weather station, ~100 km to the southwest of the Northern Ellesmere Icefield, mean monthly precipitable water ranged from 1.8 mm in late winter to 12 mm in July between 1961 and 2007, with a 10% increase in mean annual precipitable water over this period (Figure 2.1; Lesins et al., 2010). The increase in precipitable water has been dominated by increases during the spring, summer and fall, with the greatest increase occurring during summer at a rate of 0.3 mm $decade^{-1}$ since 1961. Over the 54-year period, the station recorded a mean air temperature of -19.1°C.

2.2 DATA AND METHODS

Area changes for each glacier were determined from optical satellite imagery within the periods ~1999 (period 1) and ~2015 (period 2) (Table 2.1). These periods were selected to provide the broadest temporal range with the highest resolution imagery, primarily from Landsat 7 (ETM+) and Landsat 8 (Operational Land Imager/Thermal Infrared Sensor; OLI/TIRS). The north coast of Ellesmere Island was beyond the orbit of Landsat 7 in 1999, so ASTER imagery from 2002 and 2003 was used instead, covering 5.2% of the total glaciated area. Glacier coverage for Ward Hunt Ice Shelf and for glaciers along the far north-east coast of Northern Ellesmere (comprising ~4.5% of the total glaciated area) was not available for 1999-2003, so Formosat-2 imagery from 2008 and ASTER imagery from 2009 was used in its place for period 1. Due to the lack of satellite coverage over the Markham Ice Shelf for period 1 (Figure 2.2), the extent (from 2003) was obtained from Mueller et al. (2017a). In the second period, Landsat 8 imagery from 2015 and 2016 provided complete coverage of the study area.

2.2.1 Basin boundaries

The ice cover across Northern Ellesmere Island was divided into individual drainage basins using a combination of elevation data and optical satellite imagery. Basins were delineated using a pre-release version of the ArcticDEM, a digital elevation model with 8 m resolution constructed by the Polar Geospatial Center (University of Minnesota) from in-track, high-resolution (~0.5 m) Digital Globe imagery from 2012-2015. A polygon shapefile was delineated for each drainage basin by using the Basin tool in ESRI ArcGIS 10.3.1. To create the basins, sinks were filled and an eight-direction (D8) flow model was used, which determines the flow direction of each raster cell based on the steepest path of the eight surrounding cells (Jenson and Domingue, 1988). The automated basin outlines were verified visually against the 2015/2016 Landsat 8 mosaic using visible features such as flow lines, and adjusted as necessary.

2.2.2 Glacier outlines

An outline of the ice extent was delineated for each glacier and nunatak from orthorectified ASTER (15 m resolution) and Landsat imagery (30 m resolution enhanced with the 15 m panchromatic band), and georeferenced Formosat-2 imagery (8 m resolution) (Table 2.1). Images with little to no cloud cover acquired during late summer were preferentially selected due to their minimal snow cover. Pan-sharpened Landsat 8 images acquired in 2015/2016 were mosaicked

and used as the master image against which all other satellite images were aligned (Figure 2.2; bolded scenes in Table 2.1). Eight ASTER images and one Formosat-2 image were georeferenced to the Landsat mosaic using 13 to 20 ground control points (GCPs), depending on the amount of flat and stable bedrock available in the scene. Georectification was completed using a zero-order polynomial shift in ESRI ArcGIS 10.3.1, which resulted in root mean square errors (RMSE) ranging from 15.02 to 21.80 m (Table 2.1). One Formosat-2 image was transformed using a first-order polynomial transformation and had an RMSE of 21.81 m. All other imagery was well-aligned and did not require modification.

During the digitization process, pan-sharpened Landsat scenes were displayed in both true colour and false colour; the false colour composites were represented with bands 4, 3 and 1 (for both Landsat 7 and Landsat 8) in the red, green and blue (RGB) channels. ASTER scenes were represented with bands 3, 2 and 1 in the RGB channels. To avoid misclassification, only glaciers >0.1 km^2 in area (in 1999) were digitized in this study, although glaciers that shrank to areas <0.1 km^2 during the second period of study were included for continuity of the dataset.

Once the ice extents and ice divides had been defined, nunataks were subtracted from these outlines so that each polygon represented only the area of ice and not internal rock. The image acquisition dates were used to convert measured area (in km^2) of the two time periods into standardized rates of percentage change per decade. Each glacier was assigned a unique ID following the format outlined by GLIMS, which incorporates centroid coordinates of each glacier (Raup and Khalsa, 2010). The official name was included for glaciers with a name assigned in the Canadian Geographical Names Data Base of Natural Resources Canada (http://www4.rncan.gc.ca/search-place-names/search).

2.2.3 Terrain variables

In total, 11 terrain variables were derived for the glaciers (in ~2015) measured in this study to examine the influence of physiography on area losses. The coordinates of the centroid of each glacier were calculated in ArcGIS 10.3.1 to determine location. The minimum, maximum and mean elevation, mean slope, flow length and mean aspect for each glacier were extracted from the ArcticDEM using the Spatial Analyst extension in ArcGIS 10.3.1. The statistics for each terrain parameter were calculated from all cell values within each glacier basin. The east-west and north-south scalar aspects were derived from the sine and cosine to calculate the mean aspect

(Copland, 1998). The main terminus for each glacier was visually assessed and classified into one of five types:

a) *Land-terminating glaciers* refers to all outlet glaciers and ice caps that terminate on land, and in this study includes glaciers with proglacial lakes or glaciers that calve into the proglacial lakes of neighbouring glaciers.
b) *Tidewater glaciers* are marine-terminating ice masses that are grounded on the sea floor (Dowdeswell and Jeffries, 2017). These glaciers were distinguished by their lack of extension away from the coastline and lack of tidal cracks. This category also includes glaciers flowing into ice shelves but without visual evidence of becoming incorporated into the ice shelf. Also included are coastal ice caps that flow into the sea. Note that if any land is apparent between the terminus and the coastline, the glacier is classified as land-terminating.
c) *Ice tongues* are the floating extensions of single valley glaciers over the ocean (Mueller et al., 2017a). In this study, ice tongues are classified as floating termini that extend into a bay or fiord and include ice fragments clustered together and frozen in place by sea ice around the terminus.
d) *Ice shelves* comprise extensive, permanent floating landfast ice features that are >20 m thick (Dowdeswell and Jeffries, 2017). In this study, ice shelves were identifiable by their characteristic undulating surface topography and their infilling of bays and fiords along the northern coastline.
e) *Ice shelf-terminating* refers to glaciers that flow into ice shelves. Although these glaciers contribute directly to the ice shelves, they are separated from the ice shelf as per the GLIMS procedure (Raup and Khalsa, 2010).

A linear regression model was used to quantify the relationship between the terrain variables (physiography) and glacier area loss between ~1999 and ~2015. The terminus environment for each glacier was classified as 1 if it terminated off the coast and 0 if it terminated on land. Glaciers that underwent considerable change prior to the acquisition of the 2012-2015 satellite imagery used to generate the ArcticDEM, such as Serson Ice Shelf, were excluded from the analysis. The assumptions of the linear regression model include linearity, statistical

independence, homoscedasticity, and normality. A principal component analysis (PCA) was used to determine the relationship between terrain variables and remove collinearity between them.

2.2.4 Changes in accumulation area ratio

To provide an estimate of the changes in accumulation area ratio (AAR) of the ice cover of Northern Ellesmere Island, the hypsometry of this region was compared to estimates of the changes in equilibrium line altitude (ELA) over the study period. The ELA across Northern Ellesmere Island at the start of period 1 was determined from digitizing the map of Wolken et al. (2008), which in turn was recreated from Miller et al. (1975). Wolken et al. (2008) describe this map as representing the ELA in 1960, and we assume that this ELA provides a conservative estimate of the conditions at the start of period 1. This is based on mass balance measurements on other QEI ice caps which show generally weak trends between 1960 and 2000 (Koerner, 2005; Thomson et al., 2017), and the observation that average glacier mass balance was five times more negative between 2005-2009 than 1963-2004 (Sharp and others, 2014). Since 1999, we estimate that the ELA on Northern Ellesmere has risen by ~100-300 m, based on measurements at White Glacier (Figure 2.1) (mean ELA 1960-1998 = 1022 m; mean ELA 1999-2014 = 1205 m; Thomson et al., 2017), and measurements on northern Agassiz Ice Cap that indicate that the 2014-2015 ELA was 300 m above the 1977-2015 mean (Burgess, 2017).

2.2.5 Error analysis

To calculate error associated with the alignment and resolution of the satellite imagery, we used the method defined by Hall et al. (2003). The uncertainty in the change of the ice extent in the linear dimension (*d*) between two satellite images was calculated from (after Williams et al., 1997):

$$\boldsymbol{d = \sqrt{r_1^2 + r_2^2} + RMSE} \tag{2.1}$$

where r_1 is the cell size of the first image, r_2 is the cell size of the second image, and RMSE is the error calculated during the georectification process (Table 2.1). The finest resolution (15 m) and the highest RMSE value (21.81 m) were used in this calculation. The linear uncertainty was converted to area uncertainty (*a*) using (after Hall et al., 2003):

$$\boldsymbol{a = 2dx} \quad (2.2)$$

where x = linear side dimension of the pixel (15 m). This calculation produced an error of ±0.0013 km^2.

To calculate human error that may occur during the digitization process, the same operator digitized three different glaciers from the data set for Northern Ellesmere, of differing sizes, environments, and locations, at a consistent scale of 1:10,000. Each glacier was digitized five times for each time period using imagery from the study. The G85164W81925N, G75159W81335N, and G69499W82211N glaciers were selected based on their range in size, distribution and terminal environment: G85164W81925N (5.99 km^2 in 1999) is a marine-terminating glacier in the northeast of the study region, G75159W81335N (1.00 km^2 in 1999) is a small ice cap in the southern region, and G69499W82211N (254.52 km^2 in 1999) is a large land-terminating glacier in the western region (Figure 2.2). The mean error for both time periods varied between 0.004 km^2 (0.07%) for G85164W81925N, 0.004 km^2 (0.69%) for G75159W81335N, and 0.136 km^2 (0.05%) for G69499W82211N. The largest of these errors (0.14 km^2) was summed with the satellite error (0.0013 km^2) to provide a total error. Based on these error calculations, glacier area changes were considered detectable if they were >0.14 km^2.

2.2.6 Climate data

To examine climate conditions since 1950, National Center for Environmental Prediction/National Center for Atmospheric Research (NCEP/NCAR) Reanalysis monthly mean data was downloaded from the NOAA Earth System Research Laboratory website (http://www.esrl.noaa.gov/psd/data/reanalysis/reanalysis.shtml). These data were drawn from an assimilated gridded (2.5° × 2.5° grid) dataset, based on observations from the land surface, ship, rawinsonde, piloted balloon, aircraft, satellite and other data (Kalnay et al 1996). It should be noted that NCEP/NCAR data prior to 1979 are of lower quality to the lack of assimilation data, although this is considered to be of minor significance as this study is primarily concerned with changes in conditions since ~1999. For this study, mean monthly surface air temperatures from 1948 to 2016 were analyzed for grid cells centered on Northern Ellesmere Island from 80.587-83.190°N and 60.678-92.296°W. This climate dataset was verified by comparing observations collected by an automatic weather station (AWS) in Purple Valley (Figure 2.2) over the period

2008-2016 to the NCEP/NCAR data grid cell centered on this region (82.500°N, -80.999°W). The close resemblance between these datasets (Figure 2.3) suggests that the reanalysis data is suitable for assessing trends in air temperature across Northern Ellesmere.

2.3 RESULTS

2.3.1 Regional glacier inventory

For period 2 (~2015) a total of 1768 glaciers were identified, comprising 1702 land-terminating glaciers, 45 tidewater glaciers, 8 marine-terminating glaciers with ice tongues, 6 ice shelf terminating glaciers and 7 ice shelves or remnant ice shelves (Table 2.2; Figures 2.2b and 2.4a). Land-terminating glaciers made up the highest proportion of the total ice area (63.4%), followed by tidewater glaciers (18.2%) (Table 2.2; Figure 2.4a). Glaciers between 0.1 and 1 km^2 in size made up 43.3% of the total number of glaciers, but only 1.2% of their total area (Figure 2.4b). In contrast, the majority (40.8%) of glaciers were between 100 and 1000 km^2 in size (Figure 2.4b). The largest single ice mass is M'Clintock Glacier (G75759W82147N), a marine-terminating glacier with an ice tongue, measuring 1468.4 km^2 in area and with a centreline flow length of ~44 km (Figure 2.2). The majority of individual glaciers had a north-east facing aspect, while the majority of the total ice area had a north-facing aspect (Figure 2.4c).

Mean glacier elevation ranged from 19 m a.s.l. (M'Clintock Ice Shelf; G77428W83023N) to 1519 m a.s.l. (G73513W81780N). Turnstone Glacier (G74388W81792N) had the highest maximum elevation (2603 m a.s.l.). Overall, 54.1% of glaciers had a mean elevation between 500 and 1000 m a.s.l., with <1% having a mean elevation <100 m a.s.l. (Figure 2.4d). There was a moderate positive relationship (r=0.323, p=3.23 × 10^{-44}) between maximum elevation and glacier area (Figure 2.4e), with the highest elevations concentrated from east to west along the main spine of the icefields. Glaciers with ice tongues had the highest mean difference in the highest and lowest points of elevation: 1595.0 m, compared to ice shelves with the lowest mean relief of 33.4 m. Glacier slope varied inversely with glacier area (r=-0.210, p=5.53 × 10^{-19}), with smaller glaciers tending to be steeper (Figure 2.4f). By glacier type, ice shelves tended to have the lowest gradient (mean slope of 2.0°) which is reflected in their large flat structure. The steepest glaciers, with a mean slope of >30°, were land-terminating with areas <1 km^2.

The central part of the Northern Ellesmere Icefield comprises the largest contiguous ice mass in the study region, with an area of 19,445 km^2 in 2015 (outlined in black on Figure 2.2) and length of up to ~300 km and width of ~160 km, located between 81°N to 83°N. It had a mean elevation of 1203 m a.s.l. This icefield contained 360 glaciers in 2015, of which 344 were land-terminating, 12 were tidewater-terminating, and 4 were marine-terminating with ice tongues. Land-terminating glaciers made up the majority of the icefield and had a total area of 11,294 km^2. All of the marine-terminating glaciers drained along the northern coast, with the exception of one tidewater glacier (Otto Glacier/G82716W81419N) flowing off the west coast (Figure 2.2).

2.3.2 Changes in glacier area, ~1999-2015

Over the study period, changes in glacier area primarily occurred due to the calving of ice shelves and ice tongues, changes in the position of land-terminating glacier termini, narrowing of glacier trunks and tributary branches, and increases in the area of nunataks. In general, there was a widespread decrease in glacier area for almost all glaciers in the study area (Table 2.2; Figure 2.5). Out of the 1773 glaciers present in the first period, 1353 (76.3%) of them lost >0.14 km^2 (the limit of uncertainty) of their area. The remaining 420 glaciers all decreased in area, but not beyond the error limits of this study, and are therefore classified as stationary. No glaciers increased in area over the period ~1999-~2015.

2.3.2.1 Land-terminating glacier change

A total of 1703 land-terminating glaciers were outlined across Northern Ellesmere Island for ~1999 (Table 2.2). Between ~1999 and ~2015, 416 were considered stationary and 1287 shrank beyond the limits of uncertainty. For the 1287 glaciers that shrank, there was a total area loss off 844.7 km^2 (4.8% of their initial area), and 150 of these glaciers (11.7%) lost >50% of their initial area. Separated by size class, the highest mean losses occurred from glaciers that measured <1 km^2 in the first time period, at a mean rate of 30.4% $decade^{-1}$ (Figure 2.6). With each increase in size class the mean rate of area loss decreased, with the lowest mean area losses (7.15 km^2) belonging to glaciers >1000 km^2. The greatest total area loss of 11.9 km^2 (14.3%) occurred from G89730W81726N, a medium-sized (83 km^2 in 1999) ice cap on the northwest coast of Northern Ellesmere Island (Figure 2.2). Relative to initial area, the greatest losses came from G74438W81359N, G76500W81203N and G76132W82570N, that all disappeared (Figure 2.7).

These small glaciers were all <1.5 km^2 in initial area and distributed north and south of the Northern Ellesmere Icefield (Figure 2.2).

2.3.2.2 Tidewater glacier change

A total of 28 glaciers were classified as tidewater in ~1999, with a total area of 1894.8 km^2 (Table 2.2). By ~2015, 24 tidewater glaciers had shrunk and lost a total area of 61.9 km^2, 3.3% of the initial ice area, at a mean rate of 8.7% $decade^{-1}$. Four glaciers did not lose area beyond the limit of uncertainty and were therefore classified as stationary. According to size class, the smallest tidewater glaciers (three glaciers measuring 1-5 km^2) had the greatest mean area loss of 22.9% $decade^{-1}$ (Figure 2.6). Similar to land-terminating glaciers, as the size class increased the mean rate of ice loss decreased with the exception of tidewater glaciers between 500-1000 km^2 that had a higher mean loss (2.7% $decade^{-1}$) than glaciers 100-500 km^2 (1.8% $decade^{-1}$). The greatest total area loss occurred from Otto Glacier (G82716W81419N), the largest tidewater glacier on Northern Ellesmere, which lost 19.5 km^2, 1.6% of its initial ice area. However, this glacier is a known surge-type glacier (Hattersley-Smith, 1969; Copland et al. 2003), which may explain some of these losses. The highest relative rate of area loss occurred from G74911W83042N and G91546W81713N which both lost ~27% $decade^{-1}$. Two glaciers (Bent Glacier/G78692W81412N, and G85628W82087N) retreated to the point of becoming land-terminating.

2.3.2.3 Ice tongue change

In the first period, 27 marine-terminating glaciers with ice tongues were identified along the northern coast of Ellesmere Island, covering an area of 7843.7 km^2 (Table 2.2). All 27 glaciers shrank by the year ~2015, with a total loss of 313.98 km^2, or 3.6% of their initial area at mean rate of 6.1% $decade^{-1}$. Classed by size, glaciers with ice tongues between 1-5 km^2 had the highest mean area loss of 11.4% $decade^{-1}$ (Figure 2.6). Only eight of the 27 glaciers with ice tongues remained by the second period: G79570W82808N, Ayles (G80489W82741N), Serson (G84958W82170N), G79117W82870N, G80481W81907N, Disraeli (G72723W82423N), Milne (G78878W82327N), and M'Clintock (G75759W82147N) glaciers. The remaining 19 retreated toward their grounding lines, causing the glaciers to lose their ice tongues and become classified as tidewater glaciers instead (Figure 2.8). The greatest total area loss occurred from Disraeli

Glacier, with a loss of 35.6 km^2, equivalent to 2.7% of its initial area. The greatest rate of area loss, relative to its area, occurred from G80169W82886N at 15.5% $decade^{-1}$.

2.3.2.4 Ice shelf change

Between 1999 and 2009, nine ice shelves and/or ice shelf remnants were identified along the northern coastline of Northern Ellesmere Island with a total area of 1028.7 km^2 (Table 2.2). From west to east, these comprise the Serson (G86130W82356N), Wooton (G84583W82434N), Petersen (G82050W82526N), Milne (G81511W82702N), Ayles (G80719W82854N), East Ayles (G79679W82827N), M'Clintock (G77428W83023N), Ward Hunt (G74723W83074N) and Markham (G71378W83067N) ice shelves. By ~2015, the ice shelves lost 436.1 km^2 of ice area, 42.4% of their original area. The greatest total area loss occurred from the Serson Ice Shelf (G86130W82356N), which lost 137.58 km^2, leaving behind a small ice shelf fragment on the northeast coast of Serson Bay. The Markham (G71378W83067N; 49.1 km^2) and Ayles (G80719W82854N; 75.4 km^2) ice shelves lost their entire area.

2.3.2.5 Ice shelf terminating

In ~1999, six glaciers terminating into ice shelves occurred along the northern coast of Ellesmere Island, contributing mass to the Petersen, Milne, and East Ayles ice shelves. By ~2015, these glaciers continued to flow into these ice shelves, but had lost a total area of 10.3 km^2, at a mean rate of 4.2% $decade^{-1}$. The greatest total area loss of 3.5 km^2 occurred from G81767W82616N, a glacier flowing into the south-west region of the Milne Ice Shelf (G81511W82702N). The greatest loss relative to initial size occurred to G81776W82542N, a glacier flowing into the north-east side of Petersen Ice Shelf, which lost 15.4% at a rate of 9% $decade^{-1}$.

2.3.3 Relationship between area changes and terrain

The PCA identified four components with eigenvalues >1 (Table 2.3). Component 1 is primarily an altitude factor that describes glaciers with high minimum, maximum and mean elevations, which tend to have steeper slopes and terminate on land. Component 2 is primarily a size factor that describes glaciers with longer flow lengths and larger areas, which also tend to reach to higher maximum and mean elevations. Component 3 is a location factor, dominated by glaciers that are located in areas that are further north and east than average. Component 4 is a north-facing aspect factor.

Components 2 and 3 were significantly (p<0.0001) correlated with the % decade^{-1} area changes (Table 2.3; Figure 2.9). Component 2 had the highest correlation with area change rate (r=-0.461), which indicates that the biggest % decade^{-1} changes occurred on relatively short and small glaciers at lower elevations. The correlation between area change and component 3 (r=0.205) suggests that greater area losses occurred in the north-east. When the terrain factors for component 2 are plotted against area changes (Figure 2.10), this reaffirms the fact that the terrain factors that are prominent in component 2 (i.e., mean elevation, maximum elevation, flow length and initial glacier area; Figure 2.10) are significantly correlated with area loss (p<0.0001). These relationships violate the assumption of homoscedasticity, which means that coefficient estimates are less precise and will produce a smaller p-value, but this does not change our main conclusions as the p-value is still highly significant.

From these analyses, it is apparent that glacier size, elevation and flow length were the dominant topographic controls on glacier shrinkage over the period ~1999-2015. In this case, the highest shrinkage rates occurred on small, short, low elevation glaciers. This is consistent with our results that show higher area changes from the small isolated remnant ice caps that surround the main icefields (Figures 2.6 and 2.7). For example, ice masses that lost >50% decade^{-1} (with the exception of ice shelves) had initial areas <5.4 km^2, maximum elevations <1676 m and flow lengths <4745 m.

2.3.4 AAR changes

In 1999, 35.2% of the ice area was in the ablation zone (AAR = 0.648) (Figure 2.11). If the ELA rose by a conservative 100 m, the ablation zone would comprise 47.1% of the total glacier cover (AAR = 0.529). If it rose by 200 or 300 m, as seems plausible based on measurements on nearby ice caps (Burgess, 2017; Thomson et al., 2017), the ablation zone area would then comprise 60.2% (AAR = 0.398) or 72.3% (AAR = 0.277) of the overall glacier cover, respectively.

2.3.5 Climate analysis

Mean annual surface air temperatures across Northern Ellesmere Island increased by 3.6°C (0.5°C decade^{-1}) between 1948 and 2016 (r^2 = 0.59, p=9.01 × 10^{-15}; Figure 2.12a). A shift seems to have occurred in the mid-1990s when the mean annual surface air temperature became consistently above -19°C (with the exception of 2004), and increases accelerated from a rate of +0.12°C decade^{-1} from 1948-1994 to +0.78°C decade^{-1} from 1995-2016. Since 1948, fall

(September, October, November) has shown the greatest overall increase in mean monthly surface temperature by 0.74°C decade^{-1} (p=1.45 × 10^{-13}), followed by winter (December, January, February) at 0.65°C decade^{-1} (p=7.75 × 10^{-10}) and spring (March, April, May) at 0.46°C decade^{-1} (Figure 2.12). Summer (June, July, August) had the weakest rate of warming at 0.24°C decade^{-1} (p=3.86 × 10^{-05}), although there has been a regime shift from mean negative to mean positive summer surface air temperatures since the year 2000. Of the 20 warmest mean annual surface air temperatures since 1946, 16 have occurred since 2000. Every summer since 2000 has exceeded the climatological summer mean temperature (-0.7°C) by 0.6 to 2.7°C. Compared to the climatological mean from 1981-2010, mean monthly temperature anomalies have been consistently above the 30-year average since 2000.

2.4 DISCUSSION

From the above results, it is clear that the ice cover of Northern Ellesmere Island has been undergoing widespread loss since 1999, with two trends standing out amongst the observations: (1) The dominance of the shrinkage of relatively small, low elevation glaciers in terms of relative area loss; (2) The substantial loss of floating ice from ice shelves and ice tongues along the northern coast. In the following analysis, we begin by comparing our inventory with others of the study region. We then examine the relationships between large area changes and small land-terminating glaciers, together with changes in the ELA and AAR. To gain a better understanding the rapid loss of floating ice termini, we then examine the influence of oceanographic factors.

2.4.1 Comparison against previous glacier inventories

One previous complete glacier inventory for Northern Ellesmere Island includes the outlines in the GLIMS database. These outlines were provided to GLIMS by the Randolph Glacier Inventory 6.0, a global inventory of glacier outlines (https://www.glims.org/RGI/). According to the inventory metadata these outlines provide coverage for 1999 and were completed by several analysts using a semi-automated glacier classification. Our 1999 inventory differs from the GLIMS inventory in several ways, including total area values and basin delineations. According to the GLIMS database, Northern Ellesmere glaciers had an area of 27,377 km^2, some 1569 km^2 less than the area calculated in our study. The main reason for this difference is because the GLIMS dataset does not include all the floating termini extending from the northern coastline: ice shelves and ice tongues. For example, the area covered by ice shelves in our inventory

amounts to >1050 km^2. In addition, our inventory incorporates more small ice caps (along the northern coastline) and outlines nunataks better across the region. Our basin delineations also differ from those of the GLIMS database, because our delineations were first generated with the recently released, high resolution ArcticDEM, and then manually corrected by examining glacier flow features (i.e., moraines and flowlines) in the Landsat and ASTER imagery.

A comprehensive inventory (from 1959 to 2015) of the floating portion of ice shelves and ice tongues along the northern coast of Ellesmere Island was produced by Mueller et al. (2017a). These outlines were digitized manually using anecdotal/survey data (1906), aerial photographs/maps (1959), optical satellite imagery (1963-1992) and synthetic aperture radar satellite imagery (2003-2015). The outlines include only floating ice that ends at the grounding line (i.e., excluding any land ice). In contrast, our ice tongue measurements include the entire drainage basin for each glacier, making direct comparison with our dataset difficult. However, both datasets for the ice shelves are comparable because they both only include floating ice. For 2015, the ice shelf inventory by Mueller et al. (2017a) calculated a total area of 532.2 km^2, whereas our inventory calculated a total area of 592.6 km^2. The greatest difference between the two datasets is in the outlines of Ward Hunt Ice Shelf, where the discrepancy between the two datasets was 53.4 km^2. Unlike the inventory by Mueller et al. (2017a), our outlines of Ward Hunt do not exclude any of the small ice rises on the eastern half of the ice shelf. In comparing the remaining ice shelf extents, the difference in area measurements does not exceed 4.3 km^2.

An inventory describing the distribution of surge-type glaciers across the Canadian High Arctic was generated by Copland et al. (2003), which included Northern Ellesmere. Copland et al. (2003) used 1959/60 aerial photographs and 1999/2000 Landsat 7 imagery to visually identify potential surging glaciers based on the presence of surface features (e.g. looped medial moraines, intense folding, heavy crevassing and rapid advance) consistent with surge activity. The findings identified eight possible surge-type glaciers across Northern Ellesmere, four likely surge-type glaciers, and one observed surge. The observed surge was from Otto Glacier (G82716W81419N), a glacier that was reported to have surged between 1950 and 1959 (by Hattersley-Smith, 1969) and continued to surge or surge again by 1999 (Copland et al., 2003). An active surge was also reported for the Milne Glacier from 1966-1983, when the glacier advanced by 4.25 km at a rate of 250 m $year^{-1}$ (Jeffries, 1984). Based on the recent surge activity

of the Otto and Milne glaciers, it is possible that the losses reported in our study (22.54 km^2 and 19.48 km^2, respectively) may be linked to the quiescent phase of their surge cycles. If all 13 of the glaciers identified by Copland et al. (2003) as being surge-type retreated solely as a result of surge behaviour, then this would account for 10.9% of the area changes determined across Northern Ellesmere in our study. However, the actual area changes attributable to surging are likely much less than this as only Otto and Chapman glaciers are known to have surged during the period 1999-2015 (Van Wychen et al., 2016).

2.4.2 Loss of small ice caps

Based on the terrain analysis presented in section 2.3.3, the largest area changes occurred from small, low elevation glaciers. Separated by size class, the largest area changes occurred from land-terminating glaciers that were <1 km^2, with a mean loss of 30.4% $decade^{-1}$ (Figure 2.6). Based on the results from Sharp et al. (2014), this trend was also apparent on Northern Ellesmere between ~1960 and ~2000, when 218 glaciers <1 km^2 and 1-5 km^2 in size had the highest mean losses of 29.2% (0.73% $decade^{-1}$) and 25.6% (0.64% $decade^{-1}$), respectively. For the other size classes described by Sharp et al. (2014), losses ranged from 22.2% for glaciers 5-10 km^2 in area, decreasing to 2% for glaciers >10,000 km^2. Sharp et al. (2014) also noted this trend on Agassiz Ice Cap, Prince of Wales Icefield, South Ellesmere Island, Axel Heiberg Island, and Devon Island. Similarly, Thomson et al. (2011) described a trend of significant retreat of small independent ice masses on Axel Heiberg Island, which included ice caps <25 km^2, along with the complete disappearance of 90% of ice masses smaller than 0.2 km^2 over the period 1958-2000.

Braun et al. (2004) examined the mass balance and area fluctuations of four ice caps on the Hazen Plateau of Northern Ellesmere from 1959-2002, including the St. Patrick Bay (also in our study; Figure 2.2), Murray and Simmons ice caps. In their study, the substantial loss observed from these small ice caps was attributed to low winter snow accumulation, the absence of ice flow and small vertical relief. Braun et al. (2004) described these small ice masses as relicts of the Little Ice Age, no longer sustainable in the current climate as the ELA rises above their summits (>1103 m). Rising ELAs have also been observed in the mass balance records of White Glacier, Axel Heiberg Island, the nearest long-term mass balance monitoring site to Northern Ellesmere (Figure 2.1). If the ELA at the start of our study period in ~1999 ascended as much as the ~200 m rise in ELA recorded at White Glacier since 1999 (Thomson et al., 2017), then

60.2% of the regional glacier cover across Northern Ellesmere would be in the ablation zone (AAR = 0.398), and 589 (33.3%) glaciers would be completely below the regional ELA. According to Dyurgerov et al. (2009) most glaciers with balanced regimes will have an AAR of ~0.40 to 0.80, which would suggest that Northern Ellesmere is out of balance with the current climate. If the ELA were to rise 300 m, 940 (53.2%) glaciers would be completely below the ELA and the regional AAR would only be 0.277 (Figure 2.11).

Serreze et al. (2017) described the continued loss of the Hazen Plateau ice caps up to 2016, and revealed that the St. Patrick Bay Ice Caps only had 5% of their 1959 area remaining (10.42 km^2 in 1959 vs. 0.50 km^2 in 2016). The authors noted that the ice caps even shrank noticeably between 2014 and 2015, in direct response to the particularly warm summer of 2015. The rapid loss of these ice caps was also attributed to the more pronounced appearance of dirt layers on the ice surface, leading to a decrease in summer surface albedo. In 2016 the Murray and Simmons ice caps still had 39% and 25% of their 1959 ice areas remaining, respectively, which was linked to their higher mean elevations (up to ~290 m higher), thus providing relatively cooler summer conditions.

2.4.3 Loss of floating glacier termini

Between 1999 and 2015, there was a marked loss in floating glacier termini, including the loss of 19 ice tongues, the complete loss of the Ayles and Markham ice shelves, and substantial decreases in the Serson and Ward Hunt ice shelves. Unlike land-terminating glaciers that typically shrink gradually under atmospheric forcing, marine-terminating glaciers and ice shelves are subject to oceanographic forcing and can lose mass rapidly through calving.

Detailed studies have been conducted on several Arctic ice shelves, including the Petersen and Ayles, that document the events leading up to calving events (Copland et al., 2017). In the study by White et al. (2015), the Petersen Ice Shelf is shown to have undergone a series of calving events between 2005 and 2012, during record high summer temperatures, that resulted in a ~61% loss in ice area. The calving events were initiated by the loss of >50-year-old multi-year landfast sea ice (MLSI) that fringed the ice shelf front in 2005, and by open water events in 2008, 2011 and 2012. White et al. (2015) also reported that in-situ thinning and pre-existing fractures in the ice shelf would have weakened it, thus allowing ice islands to separate from the ice shelf during open water events and drift away. Copland et al. (2007) described the conditions leading to the

complete collapse of the Ayles Ice Shelf in August 2005 that resulted in it calving within the space of a few hours and producing an 87.1 km^2 ice island. Similar to the Petersen, Copland et al. (2007, 2017) reported that this collapse was initiated by record high summer temperatures in 2005, and by the loss of landfast sea ice that had previously fringed the ice shelf. Copland et al. (2007) also reported that high offshore winds occurred during the event.

For marine-terminating glaciers with floating termini, the presence of ice mélange and sea ice provides a seasonally dependent stabilizing mechanism that allows the termini to remain intact and possibly advance (Reeh et al., 2001; Pimentel et al., 2017). This has been evident with ice tongues composed of agglomerated ice blocks such as at the front of Jakobshavn Isbrae, Greenland (Amundsen et al., 2010). During winter, sea ice forms and binds the ice mélange and prevents glacier calving, while the retreat of sea ice in spring causes the mélange to weaken and calving to recommence. Todd and Christoffersen (2014) examined the calving dynamics of Store Glacier in West Greenland and found that the presence of ice mélange was principally responsible for the observed seasonal advance of the terminus.

These factors may have also played an important role in the loss of the floating ice tongues observed in this study, particularly in Yelverton Inlet and Bay where several ice tongues disappeared over the study period. According to Pope et al. (2012), 932.6 km^2 of MLSI occupied Yelverton Inlet and Bay, including Kulutingwak Fiord in 1959 (locations in Figure 2.5). By August 2005, ~330 km^2 of MLSI broke away from Yelverton Bay and was soon followed by the fragmentation of 690 km^2 of older MLSI from Yelverton Inlet. In summer 2008 fragments of MLSI in Yelverton Bay and Kulutingwak Fiord broke apart and drifted away. In summer 2010, the last remaining plug of MLSI in Yelverton Inlet broke away, along with sections of MLSI from Kulutingwak Fiord. The loss of MLSI from this region means that the glaciers flowing into this system would then be exposed to an entirely new environment consisting of open water and young, thinner sea ice. It is likely that the loss of the floating ice tongues was a direct response to the loss of the back pressure previously provided by the thick and semi-permanent MLSI cover.

2.5 SUMMARY AND CONCLUSIONS

According to our observations between ~1999 and ~2015, regional ice coverage has decreased by 5.89% (3.68% $decade^{-1}$) over the 16-year study period. This equates to an area loss of 822

km^2 $decade^{-1}$. From 1948-2016, the highest rate of warming occurred during fall and winter at 0.74 and 0.65°C $decade^{-1}$, respectively. Although summer showed the lowest rate of temperature increase (0.24°C $decade^{-1}$), the change in the mean summer temperature over time has resulted in a change from mean negative temperatures to mean positive temperatures since 2007 (with the exception of 2014). There is evidence for a small increase in precipitation over time on Ellesmere Island at Eureka (~10% between 1961 and 2007; Lesins et al., 2010), but this is insufficient to compensate for the rapid recent increase in air temperatures.

Recent area losses from some glaciers, such as the Milne (G78878W82327N) and Otto (G82716W81419N), could be explained by retreat during quiescent periods after potential surge-type behaviour observed over past decades (Hattersley-Smith, 1969; Jeffries, 1984; Copland et al., 2003), but this is likely much less than 10% of the regional total. Two main trends for the remaining glaciers include: the rapid loss of small, low elevation land-terminating glaciers, and the loss of floating glacier termini in the form of ice tongues and ice shelves. The loss of small glaciers is a trend that has continued since the 1950s, and has been observed in other regions across the CAA as well (Braun et al., 2004; Serreze et al., 2017; Sharp et al., 2014; Thomson et al., 2011). Our analysis also revealed the complete loss of three small ice caps. The increased loss of small ice caps on Northern Ellesmere can be attributed to their increased sensitivity to the accelerated warming in the region, and the decrease in their surface albedo due to the accumulation of surface debris (Serreze et al., 2017). Small glaciers with relatively higher mean elevation are slightly less sensitive due to their cooler summer temperatures at high altitudes (Serreze et al., 2017). This is apparent in our study, where for land-terminating glaciers <10 km^2, glaciers with mean elevations <700 m had a mean loss of 25.7% $decade^{-1}$ whereas glaciers with mean elevations >700 m had a mean loss of 16.0% $decade^{-1}$.

Over our 16-year study period, there was a substantial change in the amount of floating ice. Ice shelves lost ~42.4% of their initial ice area, including the complete loss of the Ayles Ice Shelf (-75.4 km^2) and nearly the complete loss of the Serson Ice Shelf (-137.6 km^2). Our inventory also identified the loss of 18 floating ice tongues, causing these marine-terminating glaciers to retreat to their grounding lines. Past studies have linked the loss of ice shelves to warmer summer temperatures, offshore winds, and the loss of the protective barrier created by MLSI (Copland et al., 2007; White et al., 2015; Copland et al., 2017). These factors may have also played an

important role in the loss of floating ice tongues observed in this study, particularly in Yelverton Inlet and Bay where several ice tongues have disappeared since the loss of MLSI in this region in summers 2008 and 2009 (Pope et al., 2012).

This study demonstrates that the icescape of Northern Ellesmere is changing and, if current temperatures persist or continue to increase, small ice caps will be the first to vanish and coastal zones will become free of floating glacier termini and ice shelves. If the ELA has risen by 300 m since 1960 levels, which seems possible given the rapid recent changes recorded by mass balance programs on other nearby ice caps, then >50% of glaciers are currently completely in the ablation zone. It is important that regional inventories such as this one continue to be created and updated to monitor changing glacial landscapes in a warming climate.

Table 2.1: Satellite scenes used to delineate glacier extents in this study. Landsat and ASTER images were obtained from the U.S. Geological Survey Earth Explorer (https://earthexplorer.usgs.gov/). Formosat-2 image obtained from Planet Action (http://www.planet-action.org/#). Images used in the 2015/16 mosaic (Fig. 2.2; the master image against which all other imagery was georeferenced) are shown in bold.

Sensor	Scene ID	Acquisition date	Resolution (m)	Number of GCPs	RMSE (m)
ASTER	AST_L1T_00306212002211846	30-Jul-02	15	15	20.21
ASTER	AST_L1T_00308142002222030	10-Aug-02	15	23	15.02
ASTER	AST_L1T_00308142002222039	10-Aug-02	15	15	19.13
ASTER	AST_L1T_00308142002222021	10-Aug-02	15	15	21.80
ASTER	AST_L1T_00307182003220559	08-Aug-03	15	13	17.99
ASTER	AST_L1T_00307182003220550	08-Aug-03	15	-	-
ASTER	AST_L1T_00307182003220541	08-Aug-03	15	15	18.63
ASTER	AST_L1T_00307162009204046	23-Jul-09	15	20	18.62
ASTER	AST_L1T_00307102009211741	30-Jul-09	15	-	-
ASTER	AST_L1T_00307102009211750	30-Jul-09	15	15	17.94
Landsat ETM+	LE70462481999202EDC00	21-Jul-99	15	-	-
Landsat ETM+	LE70622471999202EDC00	21-Jul-99	15	-	-
Landsat ETM+	LE70442471999204EDC00	23-Jul-99	15	-	-
Landsat ETM+	LE70442481999204EDC00	23-Jul-99	15	-	-
Landsat ETM+	LE70512461999205EDC01	24-Jul-99	15	-	-
Landsat ETM+	LE70512471999205EDC01	24-Jul-99	15	-	-
Landsat ETM+	LE70512481999205EDC01	24-Jul-99	15	-	-
Landsat ETM+	LE70612461999211EDC00	30-Jul-99	15	-	-
Formosat-2	FS2_20080828_171027_MS_124580000	28-Aug-08	8	13	21.81
Landsat OLI	**LC80512472015193LGN00**	12-Jul-15	15	-	-
Landsat OLI	**LC80492472015195LGN00**	14-Jul-15	15	-	-
Landsat OLI	LC80492482015195LGN00	14-Jul-15	15	-	-
Landsat OLI	LC80402482015196LGN00	15-Jul-15	15	-	-
Landsat OLI	**LC80562472015196LGN00**	15-Jul-15	15	-	-
Landsat OLI	LC80522472015200LGN00	19-Jul-15	15	-	-
Landsat OLI	LC80482482015204LGN00	23-Jul-15	15	-	-
Landsat OLI	LC80462472015222LGN00	10-Aug-15	15	-	-
Landsat OLI	LC80462482015222LGN00	10-Aug-15	15	-	-
Landsat OLI	LC80442472015224LGN00	12-Aug-15	15	-	-
Landsat OLI	LC80512472015225LGN00	13-Aug-15	15	-	-
Landsat OLI	**LC80422472015226LGN00**	14-Aug-15	15	-	-
Landsat OLI	**LC80422482015226LGN00**	14-Aug-15	15	-	-
Landsat OLI	LC80582472015226LGN00	14-Aug-15	15	-	-
Landsat OLI	**LC80580012015226LGN00**	14-Aug-15	15	-	-
Landsat OLI	LC80602472015240LGN00	28-Aug-15	15	-	-
Landsat OLI	**LC80402472016199LGN00**	17-Jul-16	15	-	-

Table 2.2: Overview of glacier inventory, with details as a total area and percentage of each glacier type. Note: glaciers classified as an ice tongue type become tidewater glaciers if the tongue is lost, and tidewater glaciers become land-terminating if the terminus retreats onto land.

Type	Period 1 (~1999)			Period 2 (~2015)		
	Total area (km^2)	% of total area	Count	Total area (km^2)	% of total area	Count
Land Terminating	17960.3	62.2	1703	17254.0	63.4	1702
Tidewater Glacier	1894.8	6.6	28	4948.5	18.2	45
Ice tongue	7843.7	27.2	27	4237.4	15.6	8
Ice Shelf Terminating	218	0.8	6	207.7	0.8	6
Ice Shelf	1028.7	3.6	9	592.6	2.2	7
Total	**28945.4**		**1773**	**27240.1**		**1768**

Table 2.3: Factor loadings for each significant principal component (eigenvalue >1) identified in the PCA. Bolded values indicate dominant terrain parameter(s) for each principal component.

Principal component	1	2	3	4
Latitude	-0.248	-0.015	**0.898**	-0.102
Longitude	0.333	0.263	**0.799**	-0.225
Minimum elevation	**0.839**	-0.134	0.000	-0.055
Maximum elevation	**0.540**	**0.750**	-0.013	0.082
Mean elevation	**0.831**	**0.512**	-0.065	0.044
Mean slope	**0.590**	-0.244	0.139	0.407
Flow length	-0.325	**0.891**	-0.077	0.048
Area (1999-2003; period 1)	-0.263	**0.807**	-0.038	0.153
Mean east-west aspect	-0.003	-0.155	0.248	0.162
Mean north-south aspect	-0.114	-0.141	0.201	**0.845**
Land or water terminating	**-0.541**	0.331	0.139	0.134
Eigenvalue	2.687	2.569	1.598	1.022

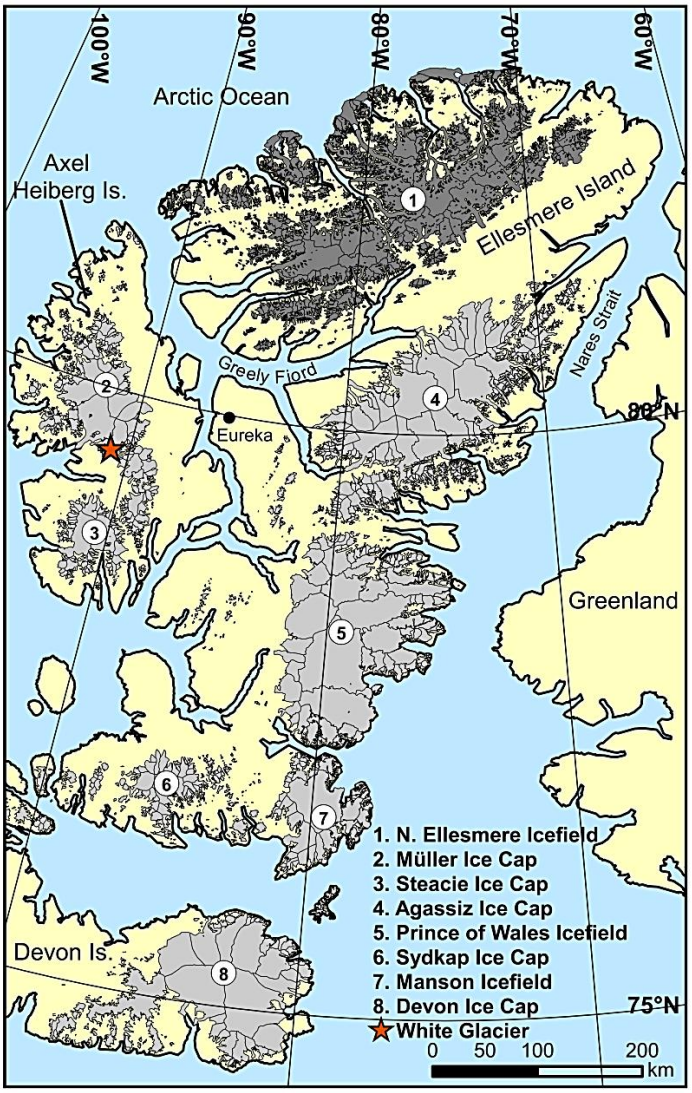

Figure 2.1: Queen Elizabeth Islands, Canada. Study region is shown by the dark grey area on Northern Ellesmere Island. Ice outlines (in light grey) from 1999 for Axel Heiberg, Devon, and Southern Ellesmere Island were acquired from GLIMS (http://www.glims.org/maps/glims).

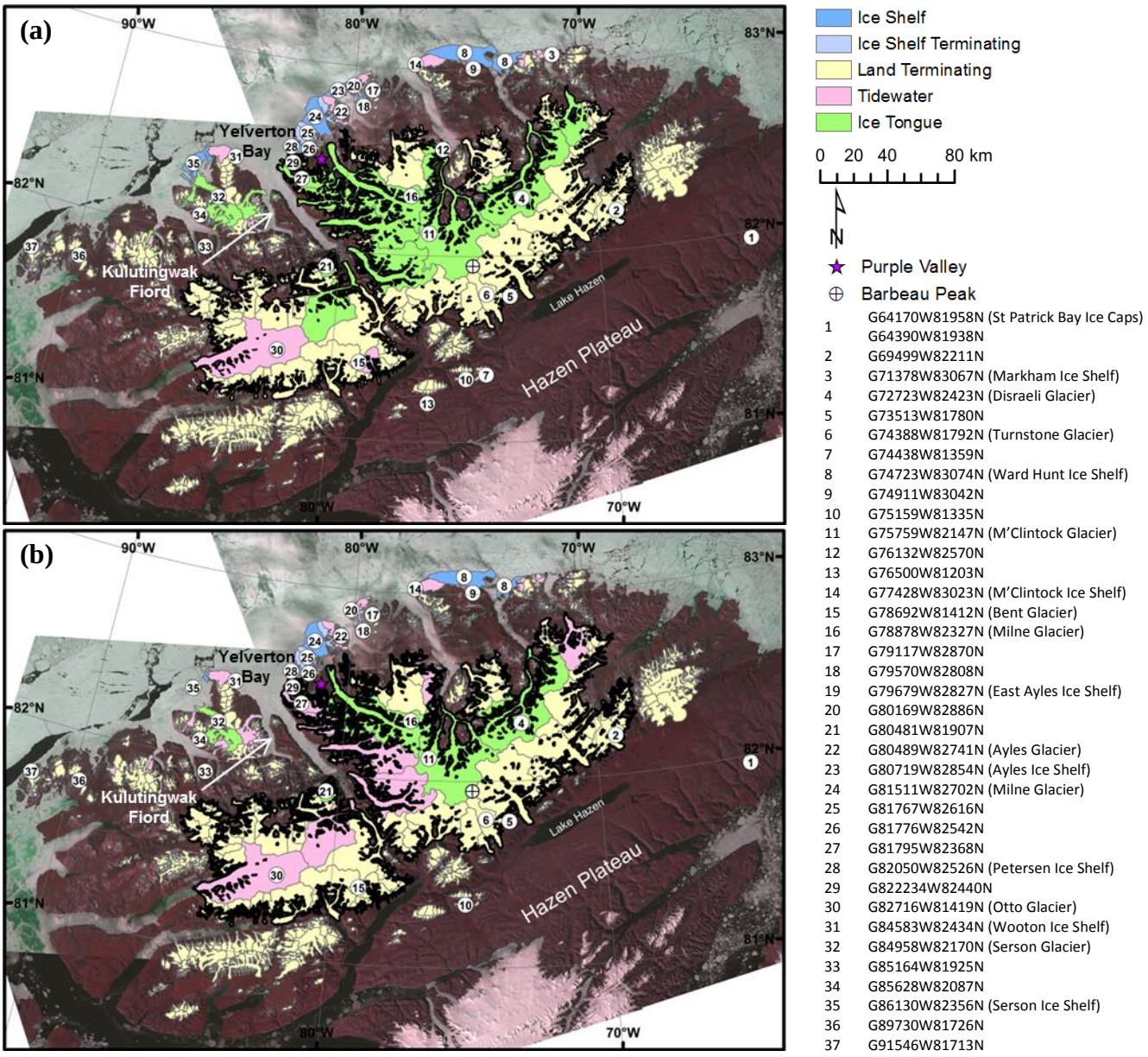

Figure 2.2: Landsat OLI/TIRS mosaic (Table 2.1) of Northern Ellesmere Island showing the outlines classified by terminating environment in: (a) 1999-2008; (b) 2015-2016. Labels show the locations of the basins referred to throughout the study. Note: Northern Ellesmere Icefield is outlined with a thick black line.

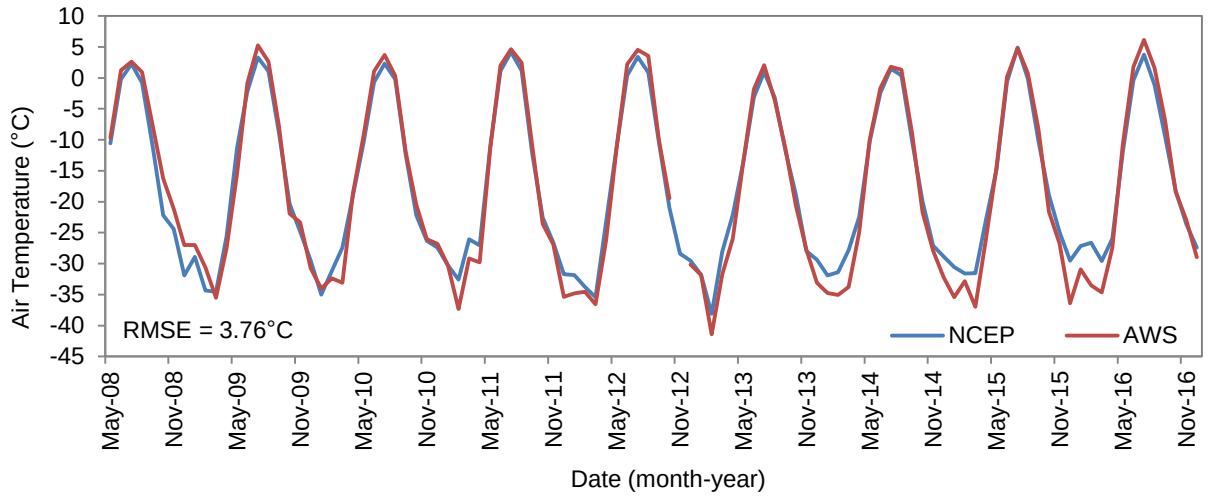

Figure 2.3: Comparison of NCEP/NCAR Reanalysis and AWS mean monthly surface air temperature datasets from May 2008 to November 2016 for Purple Valley, Northern Ellesmere Island. November 2012 AWS data omitted due to sensor error.

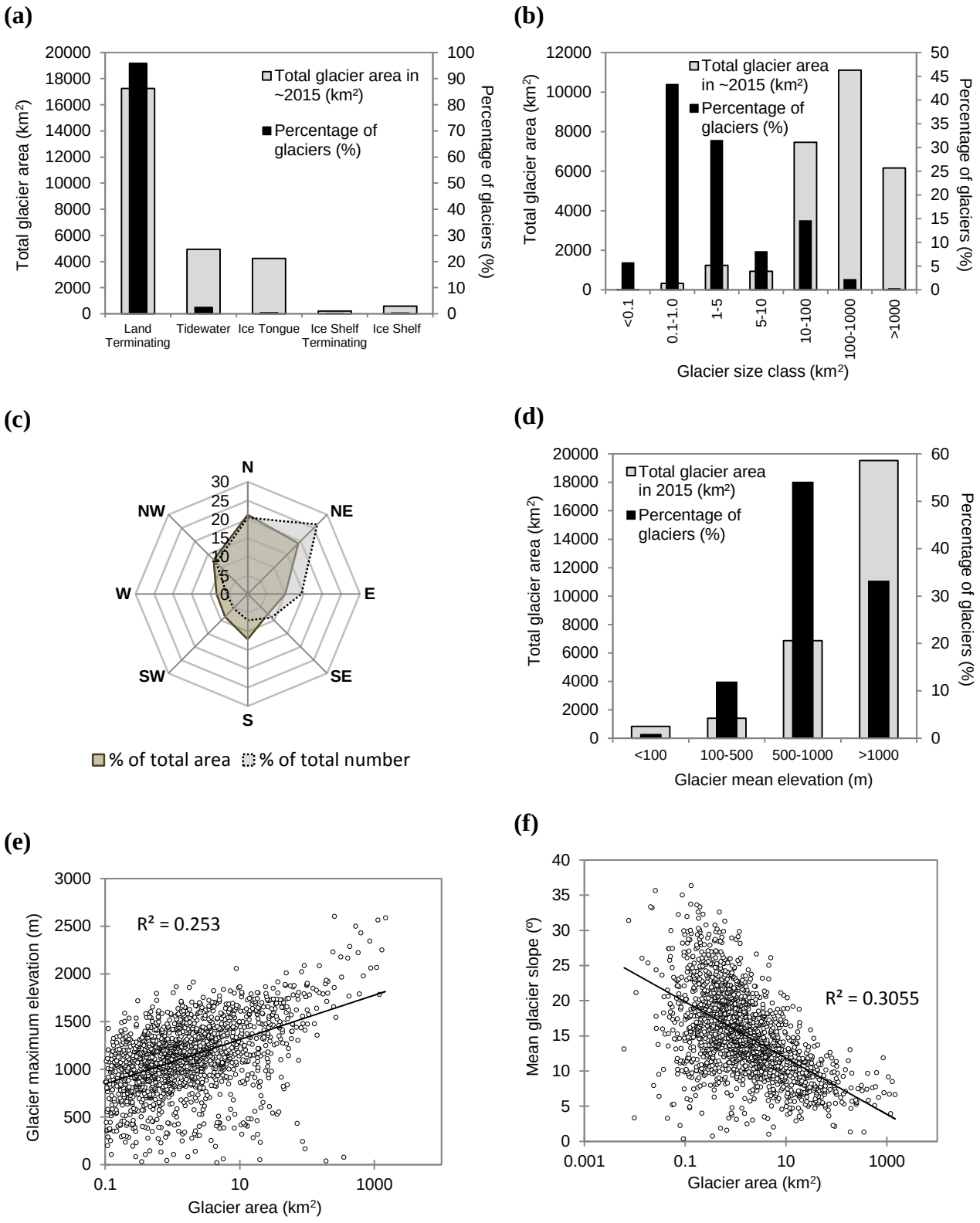

Figure 2.4: Glacier inventory characteristics for ~2015: Total glacier area (km^2) and number of glaciers in each: (a) terminus environment; (b) size class; (c) aspect class; (d) elevation class, and relationship between glacier area and (e) maximum elevation; (f) mean glacier slope. Note logarithmic scales on (e) and (f).

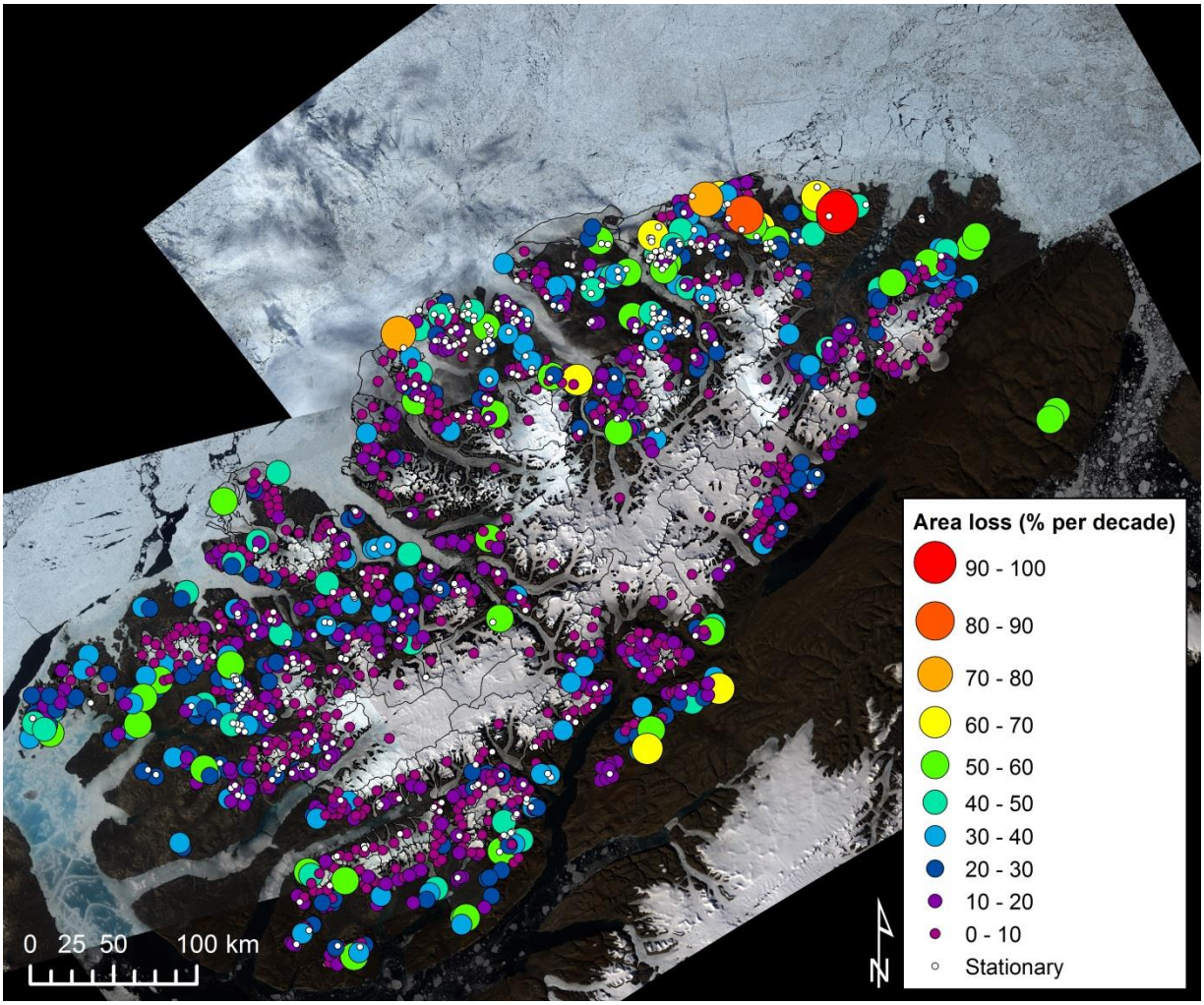

Figure 2.5: Magnitude of area loss for each glacier basin between 1999 and 2016, overlaid on a Landsat OLI/TIRS mosaic from 2015/2016 (Table 2.1). Basin delineations are for ~1999. Stationary results refer to glaciers with area loss within the limits of uncertainty.

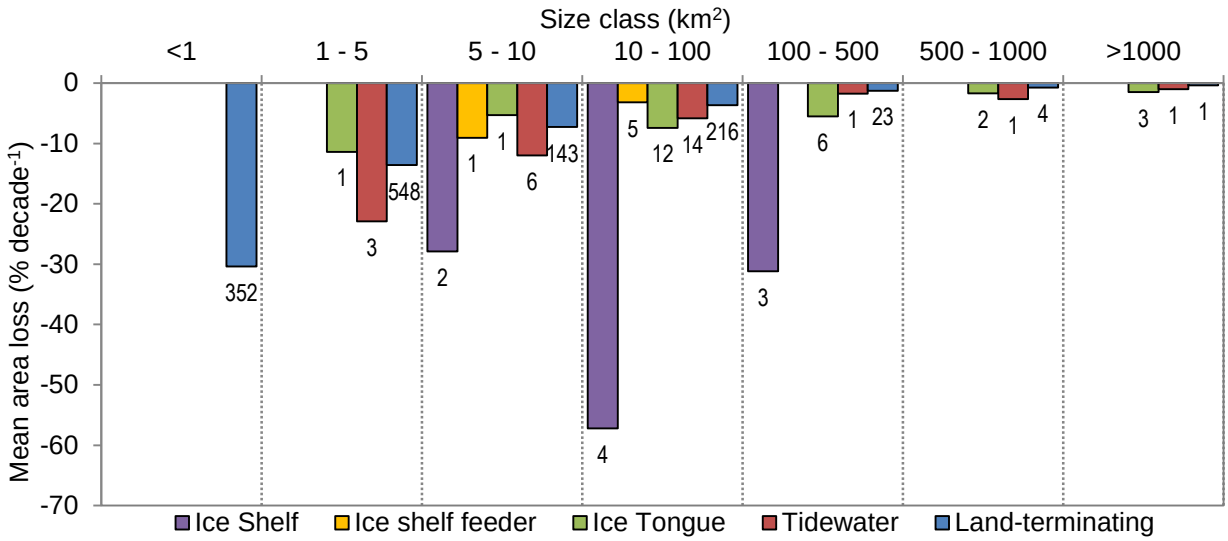

Figure 2.6: Mean rate of glacier loss (% decade^{-1}) for glaciers that lost mass between ~1999 and ~2015 for each glacier type (as classified initially), separated into size classes.

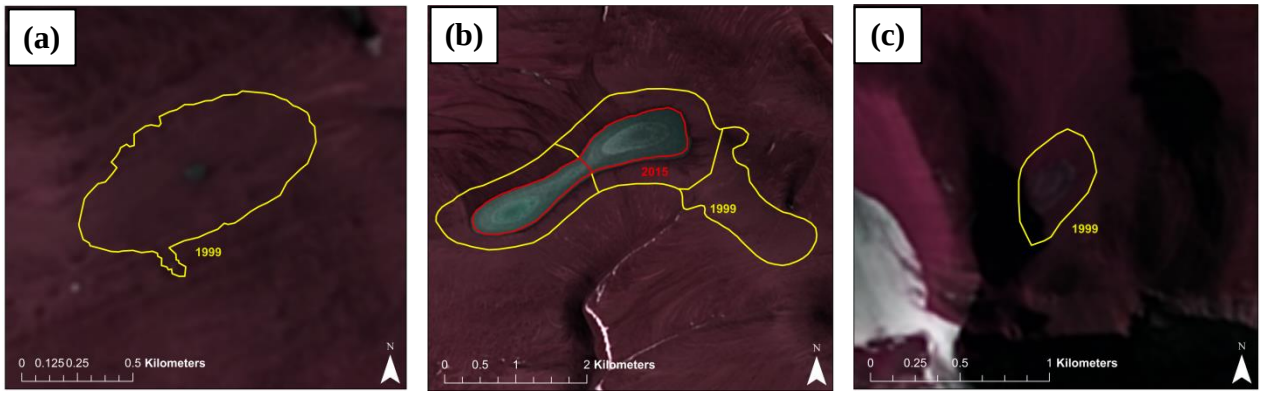

Figure 2.7: Outlines from 1999 of small ice caps that lost 100% of their area: (a) G74438W81359N overlaid on Landsat 8 image from July 12, 2015 (#7 on Fig. 2.2a); (b) G76500W81203N (eastern-most basin) overlaid on Landsat 8 image from July 14, 2015 (#13 on Fig. 2.2a); and (c) G76132W82570N overlaid on Landsat 8 image from July 12, 2015 (#12 on Fig. 2.2a).

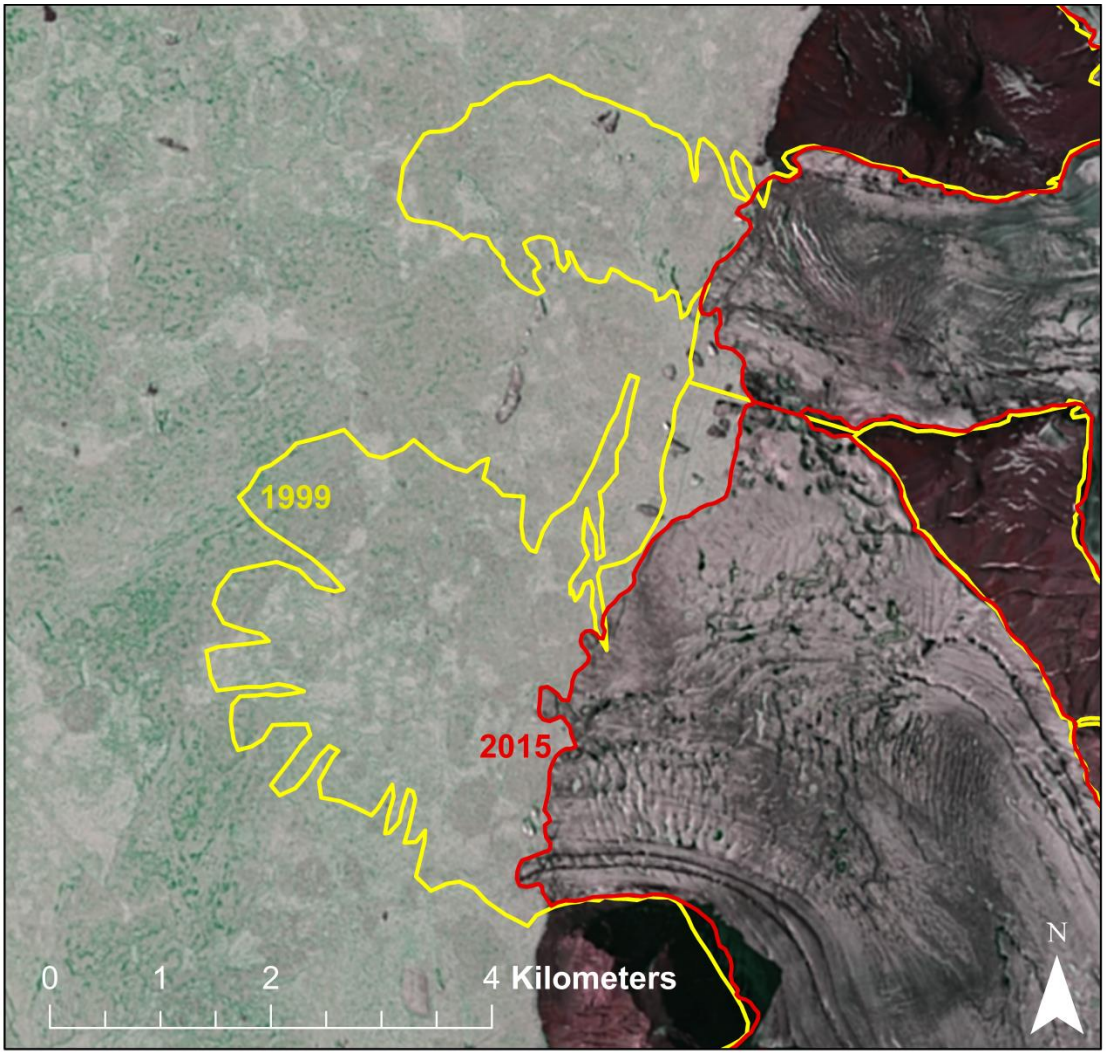

Figure 2.8: Outlines showing the loss of floating ice tongues between 1999 and 2015 from glaciers entering Yelverton Bay, Northern Ellesmere Island: (a) G81795W82368N (south; #27 on Fig. 2.2); and (b) G822234W82440N (north; #29 on Fig. 2.2), overlaid on Landsat 8 image from July 12, 2015.

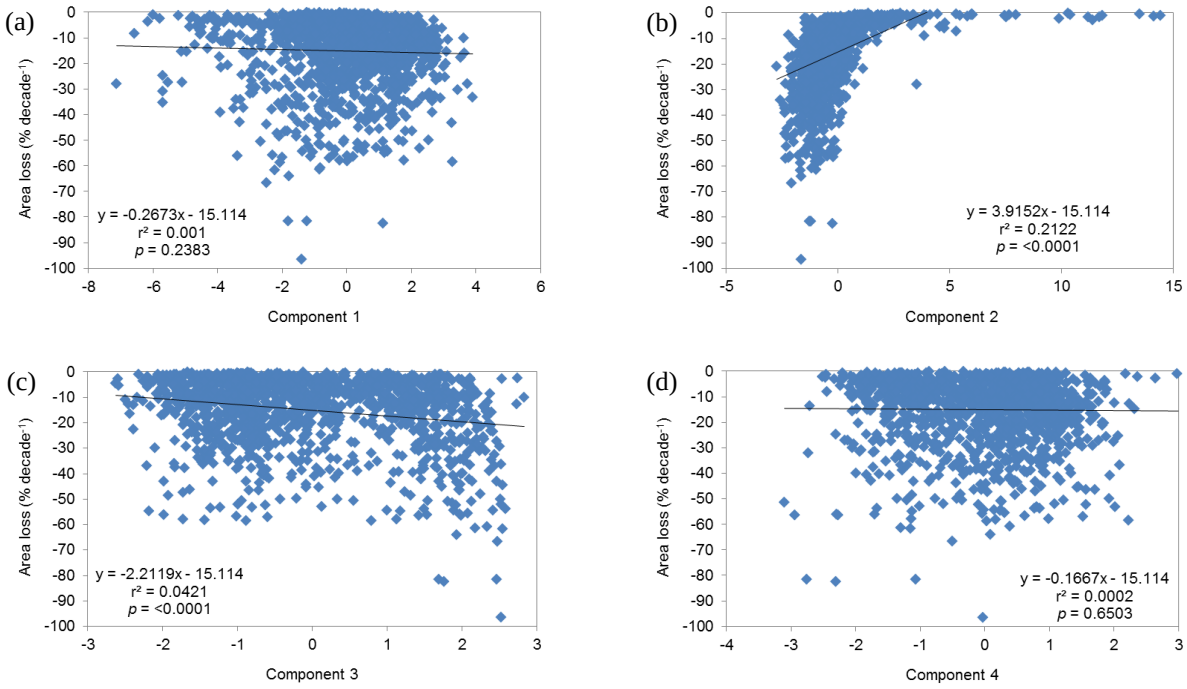

Figure 2.9: Relationship between loss (% decade^{-1}) and each significant principal component (Table 2.3) identified in the PCA: (a) component 1; (b) component 2; (c) component 3; and (d) component 4.

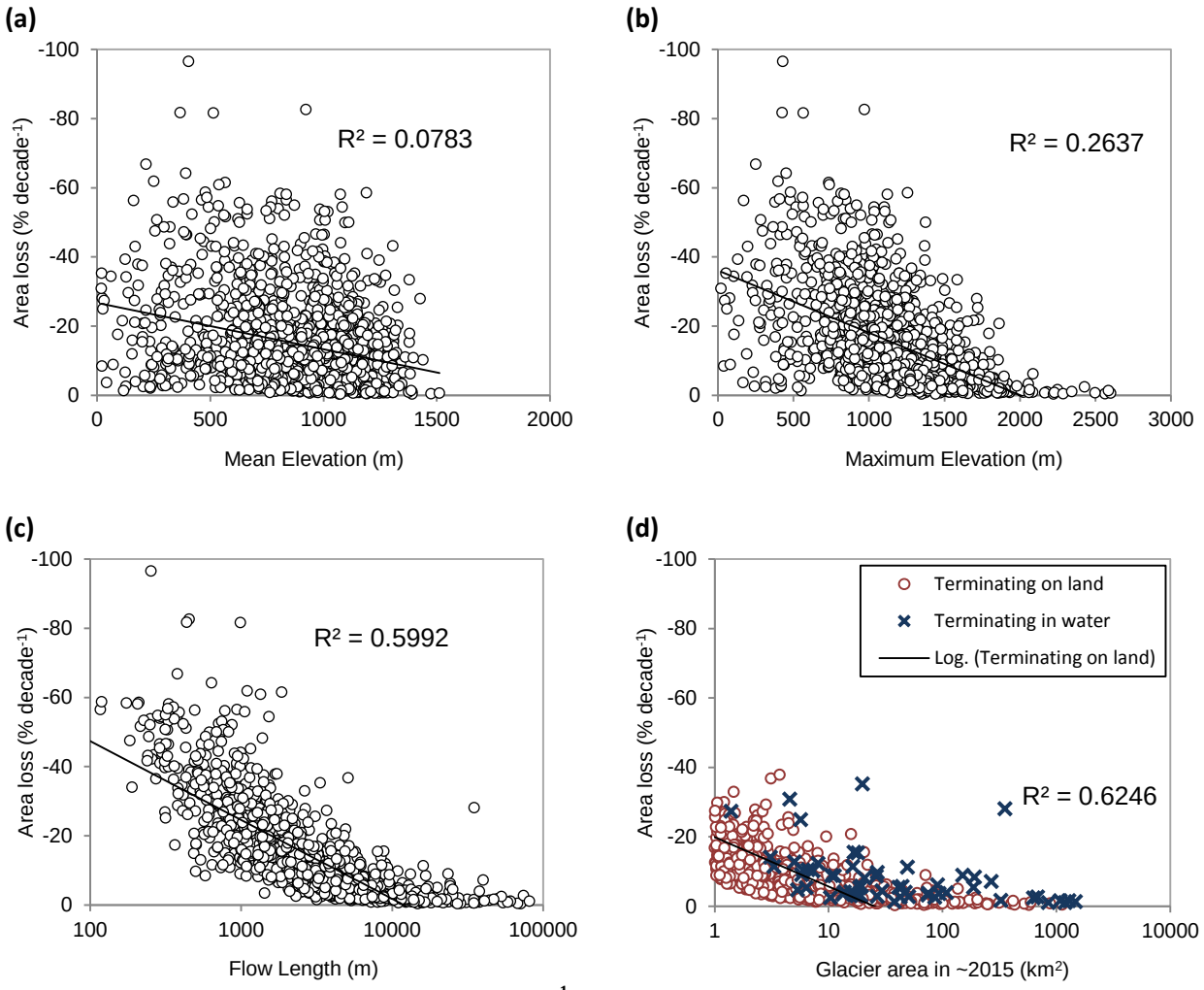

Figure 2.10: Relationship between loss (% decade^{-1}) and: (a) mean elevation; (b) maximum elevation; (c) flow length (note log scale on x-axis) and; (d) glacier area (note log scale on x -axis).

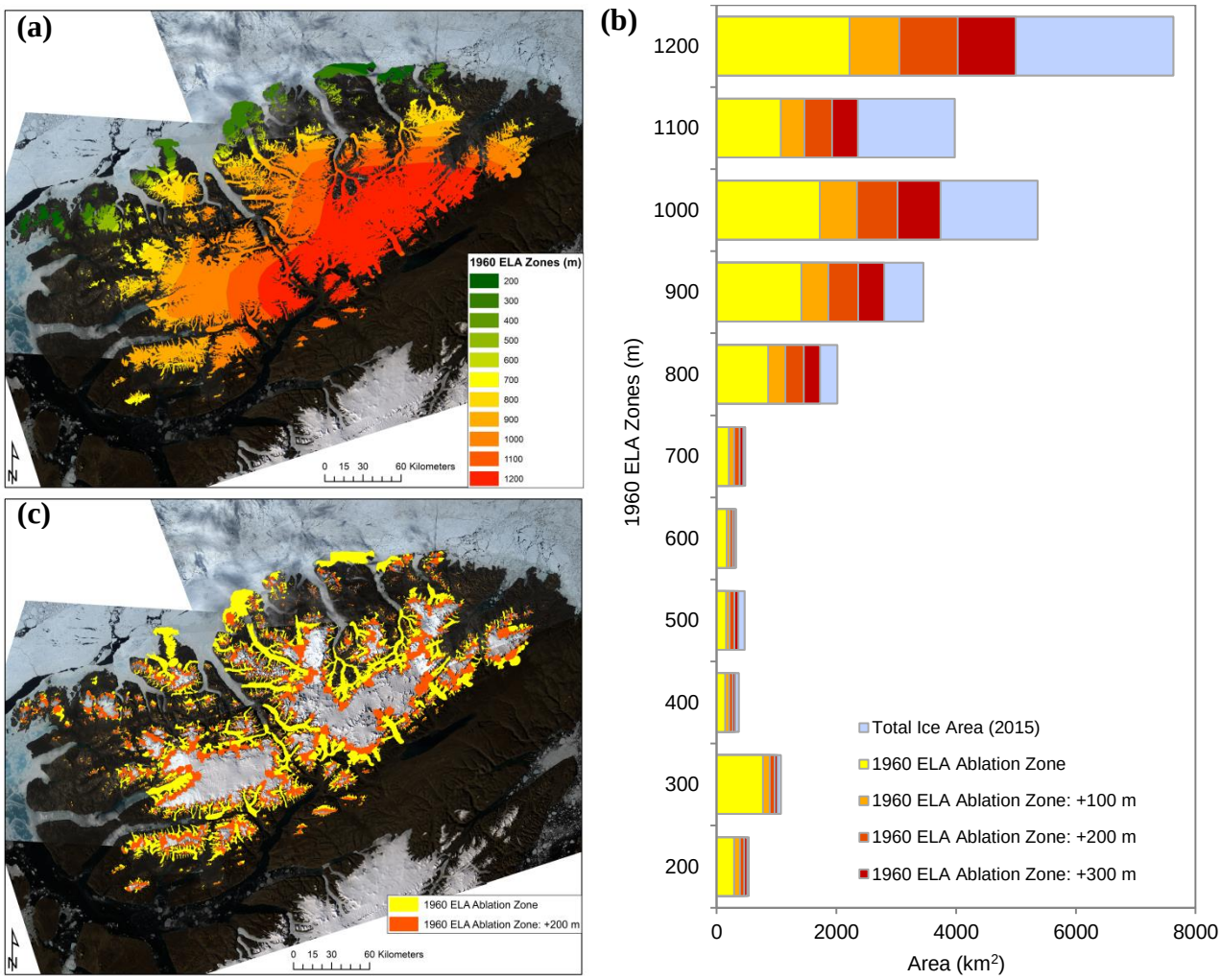

Figure 2.11: (a) 1960 ELA trend surface digitized from Wolken et al. (2008), assumed to represent conditions at the start of the study period, overlaid on a Landsat 8 mosaic from 2015/2016 (Table 2.1); (b) Total ablation area (as a proportion of total ice area) for 1960 ELA and at 100 m increments (c) Total ablation area based on the 1960 ELA zones and with a 200 m increment, overlaid on a Landsat OLI/TIRS mosaic from 2015/2016 (Table 2.1).

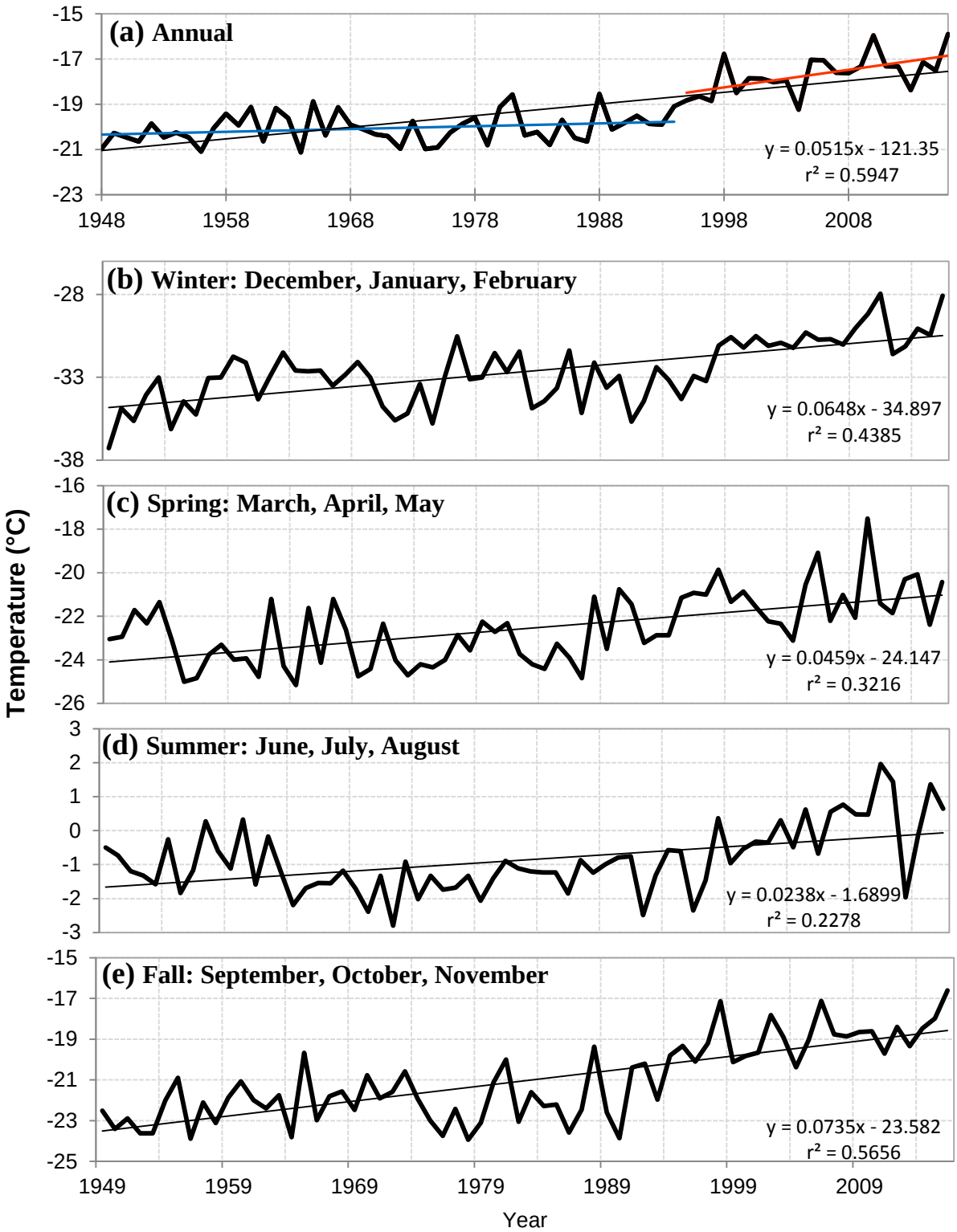

Figure 2.12: Time series of: (a) mean annual surface air temperatures (1948-2016). The linear trend from 1948-1994 is represented in blue, while the linear trend from 1995-2016 is shown in red; (b-e) seasonal surface air temperatures (1949-2016). Data derived from NCEP/NCAR Reanalysis, averaged across the region 80.587-83.190°N, 60.678-92.296°W.

CHAPTER 3: LOSS OF FLOATING GLACIER TONGUES FROM THE YELVERTON BAY REGION, ELLESMERE ISLAND, CANADA

3.1 INTRODUCTION

In the Canadian Arctic Archipelago (CAA), the northern coast of Ellesmere Island is unique for having a coastline characterized by tidewater glaciers that include floating glacier tongues (hereafter referred to as ice tongues) and ice shelves, typically fringed by multi-year landfast sea ice (MLSI). The ice shelves are remnants of a 500 km long ice shelf (unofficially named the Ellesmere Ice Shelf) that fringed the northern coast of Ellesmere Island at the start of the 20th century, which initially formed through the thickening of MLSI and sometimes glacial input (Vincent et al., 2001). Since 2005, the coastline has undergone rapid and extensive changes in its floating ice cover, including nearly complete loss of the Ayles, Markham and Serson ice shelves, and the complete loss of >70 year old MLSI from Yelverton Bay, Yelverton Inlet and Kulutingwak Fiord (Copland et al., 2007; Pope et al., 2012; White et al., 2015; Mueller et al., 2008, 2017a). Chapter 2 reported the loss of 19 out of 27 ice tongues between ~1999 and ~2015, located predominantly in the Yelverton Bay region. While numerous studies have been undertaken to analyse changes and identify the factors leading to ice shelf reductions (Copland et al., 2007; White et al., 2015; Copland et al., 2017; Mueller et al., 2017a) and MLSI loss (Pope et al., 2012; Pope et al., 2017) on Northern Ellesmere Island, there has never been a systematic analysis of how or why ice tongues in this region have responded to the dramatic changes in the marine ice environment.

Numerous studies from Greenland and Antarctica have highlighted several key controls on the dynamics, stability, and retreat of floating glaciers, including increasing air temperatures, increasing ocean temperatures, and the weakening or removal of fast ice or mélange (a conglomeration of icebergs and sea ice) from the glacier terminus. Warmer air temperatures increase surface melt, which can enhance water penetration into crevasses and drive their vertical expansion through floating termini via hydrofracturing (Sohn et al., 1998; van der Veen, 1998), or strengthen subglacial plumes that enhance submarine melt (Jenkins, 2011). Warmer ocean temperatures can lead to grounding line retreat, thinning and undercutting of the calving front through submarine melting (Vieli and Nick, 2011; Nick et al., 2012). Warming air and ocean

temperatures can both melt sea ice and mélange, which have been shown to suppress calving through mechanical buttressing (Sohn et al., 1998; Reeh et al., 2001; Massom, 2003; Amundson et al., 2010; Walter et al., 2012). Robel (2017) described the physical process where landfast sea ice supports a mélange which prevents glacier calving by exerting a buttressing force against the glacier terminus. When the sea ice thins, the buttressing force provided by the mélange is reduced or removed and the likelihood of a calving event is increased (Robel, 2017).

Given the rapid recent loss of floating glacier tongues on Northern Ellesmere Island (Chapter 2), this study examines controls on the long-term stability of 13 ice tongues in the Yelverton Bay region by quantifying area changes in the floating termini in relation to sea ice, atmospheric forcing, and oceanographic forcing between 1959 and 2017. The results contribute to the growing body of research regarding the mechanisms driving ice tongue disintegration, in a location not previously studied.

3.2 STUDY SITE

Yelverton Bay (82°23' N, 83°18' W) is situated on the northern coast of Ellesmere Island between Alert Point and Hansen Point, ~300 km west of Alert (Figure 3.1). Yelverton Bay is ~40 km wide at its widest point and was typically filled with MLSI (Jeffries and Serson, 1986; Pope et al., 2012). Yelverton Inlet and Kulutingwak Fiord are adjacent waterways divided by Mitchell Point at the southern end of Yelverton Bay, which have historically contained an extensive MLSI cover (Figure 3.1; Pope et al., 2012). These interconnected waterways, collectively referred to as the 'Yelverton Bay region' in this study, were selected for analysis because they contain the largest concentration of tidewater glaciers with ice tongues in the CAA, in a region that has experienced widespread glacier, ice shelf and sea ice changes in the recent past (Pope et al., 2012; Mueller et al., 2017a; Chapter 2). The 13 outlet glaciers that terminate in the ocean in this region ranged in basin size from 5.51 km^2 (Glacier C) to 852.37 km^2 (De Vries Glacier) in 2015 (Table 3.1; Chapter 2). Yelverton Glacier has become the dominant source of ice discharge to the ocean on Northern Ellesmere since 2010, with a mean discharge of 0.1118 Gt yr^{-1} between 2000 and 2015 (Table 3.1; Millan et al., 2017).

The only glacier with an official name in the study region, as defined by the Canadian Geographical Names Data Base (http://www4.rncan.gc.ca/search-place-names/search), is De

Vries Glacier, but several glaciers have been unofficially named on maps and in past research (e.g., Van Wychen et al., 2015; Mueller et al., 2017a). To ease identification we use unofficial names from previous studies where available, and for those glaciers without names, we have named them A through G from north to south (Figure 3.1; Table 3.1). The Global Land Ice Measurements from Space (GLIMS) ID (from Chapter 2) has also been included for each glacier in Table 3.1.

3.3 METHODS

3.3.1 Imagery and ice type measurements

To map changes in ice tongues and sea ice conditions over time, we delineated their ice extents using cloud-free, summer imagery from the period 1959-2017 (Table 3.2). To measure the change in the proportion of each ice type a box was delineated around the terminus of each glacier, extending beyond the maximum extent and width of the sikussak/mélange or ice tongue, and up-glacier beyond the glacier grounding line (Figure 3.1 and 3.2). For each glacier, the surrounding sea ice, open water, sikussak, mélange, ice tongue, and grounded glacier ice was outlined. The different floating ice types were defined as follows (and shown in Figure 3.2):

a) Ice tongues comprise the floating extension of single valley glaciers over the ocean (Mueller et al., 2017a), including all floating glacier ice beyond the grounding line.
b) Sikussak is a Greenlandic term (also spelled Sikussaq) used to describe ‘ice which resembles the ocean-ice’ (Rasmussen, 1921, p.331) and is comprised of a combination of MLSI and icebergs (Dowdeswell and Jeffries, 2017). If sikussak becomes thicker than 20 m through surface accumulation and basal accretion, it would be termed a composite ice shelf (Dowdeswell and Jeffries, 2017). In this study, sikussak is defined as a multi-year conglomeration of multi-year ice, brash ice, icebergs and/or ice islands that remains in position for more than one year.
c) Ice mélange refers to a mix of sea-ice floes and icebergs that forms and breaks out seasonally (Amundson et al., 2010; Dowdeswell and Jeffries, 2017). If ice mélange remains for more than one year, it would be termed sikussak.
d) Sea ice refers to any form of ice at sea which has formed from freezing water. If the sea ice has survived for at least two summers and is landfast, it is referred to as MLSI, whereas first-year ice (FYI) refers to sea ice from one winter's growth (Canadian Ice

Service, 2005). While MLSI and FYI are used to describe overall changes in the Yelverton Bay region, these types are not distinguished in the changing proportions of ice types for each glacier front (i.e., Tables 3.3 and 3.4).

The grounding line and grounded vs. ungrounded portions of a glacier were distinguished based on:

a) presence of longitudinal fractures in the ungrounded part, where floating glacier ice begins to spread in a digitate pattern
b) occurrence of tidal cracks at the grounding line, perpendicular to the glacier flow direction
c) presence of transverse crevasses, supraglacial streams and surface slopes on the grounded portion.

The earliest extent of each ice type (i.e., sea ice, sikussak, mélange, and ice tongue) was mapped using stereo aerial photographs from 1959, collected by the Royal Canadian Air Force and acquired from the National Air Photo Library (Natural Resources Canada), Ottawa, Canada. Satellite Pour l'Observation de la Terre (SPOT) satellite imagery was used to delineate ice types in 1987/88. Annual measurements were made from 1999 to 2017 (with the exception of 2006) using the Landsat Tier 1 collection, obtained from the United States Geological Survey Earth Explorer (https://earthexplorer.usgs.gov/), which consists of a level-1 precision and terrain corrected satellite image product that is consistently georegistered within tolerances of ≤12 m radial root mean square error (RMSE; U.S. Geological Survey, 2016). Aerial photographs and SPOT imagery were georeferenced to a 15 m pansharpened Landsat-8 image from July 2017 with complete coverage of the study area, using a minimum of 20 ground control points (GCPs) and a 1st order polynomial transformation, resulting in a RMSE of <15 m. In some instances, a 3rd order polynomial transformation was used where warp was necessary.

3.3.2 Open water analysis

To examine the spatial distribution and interannual frequency of open water events throughout the study area, Moderate Resolution Imaging Spectroradiometer (MODIS) Terra/Aqua satellite imagery (Corrected Reflectance, True Colour), with 250 m resolution was used for summer (June 1st to September 30th) observations from 2000-2017. The images were downloaded from

NASA WorldView (https://worldview.earthdata.nasa.gov/). Although MODIS data is acquired daily, observations were limited to mostly cloud-free imagery, which typically occurred at least once per week. Open water was only recorded when it extended across an inlet or fiord. The Yelverton Bay region was divided into sub-regions for the open water analysis to enable understanding of connections to individual glacier changes (Figure 3.3a).

3.3.3 Air temperature data

Due to the lack of long-term meteorological stations in the study area, we used the 2.5° National Center for Environmental Protection/National Center for Atmospheric Research (NCEP/NCAR) Reanalysis dataset (Kalnay et al., 1996; https://www.esrl.noaa.gov/psd/cgi-bin/data/timeseries/timeseries1.pl) to calculate mean summer (June, July, and August) surface (1000 mb) air temperatures since 1948. For this study, the air temperature data were downloaded for the grid point nearest to the Yelverton Bay region, at 82.5°N, 82.5°W. Recent studies have compared the NCEP/NCAR Reanalysis dataset with surface temperatures recorded since 2008 at an automatic weather station in Purple Valley, ~30 km east of Yelverton Bay (Figure 3.1), and found that although the reanalysis data has a positive bias in some winters the dataset is sufficient for understanding trends and variability in surface air temperature (White et al., 2015; Chapter 2). A linear regression between the reanalyzed and the observed temperature is highly significant (R^2=0.98, p<0.0001), with a RMSE of 3.97°C (White et al., 2015).

3.3.4 Ocean temperature data

In the absence of oceanographic measurements in the study region, we used the TOPAZ4 Arctic Ocean Reanalysis dataset, generated by the Copernicus Marine Environment Monitoring Service (CMEMS; http://marine.copernicus.eu/), to calculate mean monthly temperatures from 1999-2016. This dataset was derived from a 12.5 km resolution gridded dataset, based on *in situ* and satellite measurements, and assimilated using the HYCOM model. We downloaded the mean monthly product (ARCTIC_REANALYSIS_PHYS_002_003) from 1999-2016, at standard depths of 50 m, 100 m, and 200 m. From this data, we extracted the mean annual temperature at each depth for the grid cell (82°33.032’ N, 83°46.856’ W) nearest to the study region, in Yelverton Bay. The RMSE for ocean temperatures is stated as being between 0.34°C and 0.92°C for ocean depths of 0, 100, 300, 800 and 2000 m (http://cmems-resources.cls.fr/documents/QUID/CMEMS-ARC-QUID-002-003.pdf). There are no local

measurements available to verify the TOPAZ4 outputs, so it is difficult to use them to reconstruct detailed ocean temperatures for specific dates. However, it is the best available data for this region, and we expect it to provide a reasonable estimate of long-term changes.

3.4 RESULTS

3.4.1 Changes in ice types

Analysis of the proportion of each ice type at the front of the 13 glaciers in the Yelverton Bay region between 1959 and 2017 revealed a marked change in floating ice conditions (Figures 3.1 and 3.4; Tables 3.3 and 3.4). Sikussak fringed the front of 12 glaciers in 1959, but reduced in area in the early 2000s and had lost 86.24 km^2 (58.7%) of its area by 2003 (Figure 3.1 and 3.4). From 2003 onwards ice-free, open water conditions began to develop seasonally at the south end of both Yelverton Inlet and Kulutingwak Fiord, and eventually spread throughout the entire study area in summer 2010 (Figure 3.3). As individual glacier fronts became exposed to open water in one summer, the following summer would typically reveal the loss of sikussak and ice tongue area. Since 2010 sea ice now occurs almost exclusively at the fronts of the glaciers, with little of the other ice types left (Figure 3.4).

Despite the overall pattern of losses described above, there are several important variations based on location and/or initial morphology of the glacier environment. The first unique behaviour is shown by De Vries Glacier, which had the most extensive collection of sikussak (70.4 km^2) adjacent to a relatively short (~600 m long) ice tongue in 1959 (Figure 3.5a). Almost all of this sikussak was lost by 1987, much earlier than the other glaciers (Figures 3.1 and 3.5b). In the years following, the small amount of remaining sikussak (1.68 km^2 in July 1999; Figure 3.5cd) was lost and replaced by sea ice, and the ice tongue lost 0.46 km^2 (72.5%) between 1999 and 2007 (Figure 3.5d). By 2010, during an open water event, a tidal fracture formed ~240 m up-glacier, suggesting that the grounding line had retreated (Figure 3.5e). After 2010 the ice tongue was quasi-stationary, expanding slightly (0.06 km^2) between 2010 and 2013, then decreasing slightly (0.03 km^2) by 2017 (Figure 3.5f).

Another location which saw dramatic changes in the floating ice cover occurred at Yelverton Glacier which, in 1959, had an ice tongue ~23 km long, surrounded by sikussak which merged with the sikussak from neighbouring De Vries Glacier (Figures 3.5a and 3.6a). Between 1959

and 1987 the ice tongue reduced in area by 19.67 km^2 (58.5%), thus contributing to the surrounding sikussak. From 1987 to 1999 the ice tongue advanced by ~3.8 km along its centerline, increasing in area by 6.6 km^2 (47.4%), where it remained stable until 2004; however, the surrounding sikussak decreased by 19.26 km^2 (60%) between 1999 and 2004. Between 2008 and 2009 the once large ice tongue (20.96 km^2 in 2004; Figure 3.6d) underwent a dramatic collapse, losing 9.3 km of its centerline length, and became a 34.17 km^2 area of ice mélange (Figure 3.6e). The ice tongue then expanded 0.26 km^2 between 2009 and 2010 (Figure 3.6ef). The changes observed in 2009 and 2010 were preceded by open water in 2008 and 2009 (Figures 3.3 and 3.7ef). By 2013, Yelverton Glacier terminated at the grounding line and remained in this position through 2014. By 2015, the terminus had advanced ~220 m along its centerline and developed an ice tongue surrounded by calved icebergs bounded in sea ice (sikussak; Figure 3.6g). Further advance by 2016 caused the terminus to expand by 0.37 km^2 and calve icebergs into the surrounding sikussak, resulting in its expansion by 1.00 km^2 (Figure 3.6h). By 2017 all sikussak had drifted away from the glacier front, but the ice tongue had increased again by 0.54 km^2 after open water in 2016 occurred in the fiord in front of Yelverton Glacier (Figure 3.3 and 3.6i).

3.4.2 Open water events

The summer MODIS imagery provides information concerning the progression of open water events in the Yelverton Bay region from 2000 to 2017 (Figures 3.3 and 3.7). From 2000 to 2001, there was no evidence for open water throughout any part of the study region (Figures 3.3 and 3.7a). However, in 2002 sea ice was replaced by open water at the head (SE arm) of Kulutingwak Fiord and the head of Yelverton Inlet (Figure 3.3). By 2003, the areas of open water in the previous year again occurred in similar locations, with the addition of the area in the south-west of Kulutingwak Fiord (Figure 3.7b). There was no open water in any of the cloud-free MODIS imagery in 2004, but in 2005 open water was found across the entire southern half of Yelverton Inlet, the southeast arm at the back of Kulutingwak Fiord, and Yelverton Bay (Figure 3.7c). In 2006 and 2007 there was generally little open water, except for the southeast arm at the head of Kulutingwak Fiord and Yelverton Bay in 2007 (Figure 3.7d).

Summer 2008 marked the first year of widespread open water in the MODIS record, with the only sea ice that remained during this season occurring in the northern half of Kulutingwak Fiord

and Yelverton Inlet (Figure 3.7e). The sea ice that remained in 2008 appeared to act as a plug, preventing ice from escaping from these waterways into Yelverton Bay. There were some limited areas of open water in 2009 (Figures 3.3 and 3.7f), but from 2010 to 2012 open water was extensive and penetrated further towards Yelverton Glacier, replacing areas once occupied by the ice tongue (Figure 3.7g). Between 2013 and 2017 most open water was restricted to the southerly parts of Kulutingwak Fiord and Yelverton Inlet, except for 2016 when there was widespread open water in areas outside of Yelverton Bay (Figure 3.7hi). Overall, there was far more extensive open water over the past decade than in the years before it, with widespread open water in 2008, 2010, 2011, 2012 and 2016 (Figure 3.3).

3.4.3 Links between sea ice loss and glacier calving

Analysis of changes to ice types and frequency of open water between 1999 and 2017 reveals a strong link between the break out of sea ice (open water events) and the loss of sikussak/mélange and ice tongues. The timing and nature of this relationship differed somewhat between regions, so each is described separately below.

3.4.3.1 Yelverton Bay

In Yelverton Bay, Marine Glacier North-N and Marine Glacier North-S both had ice tongues extending 1.5 and 2.4 km (along their centerlines) away from their grounding lines in 1959, with a total combined area of 7.23 km^2 (Figure 3.1 and 3.8a; Table 3.3). These ice tongues were both surrounded by sikussak which was bounded by MLSI. In August 2005 open water occurred across Yelverton Bay (Figure 3.7c), which likely caused the ice tongues to collapse and the sikussak to be replaced with mélange, as seen by 2007 (Figure 3.8d). This collapse resulted in Marine Glacier North-N and Marine Glacier North-S losing 87.7% (2.80 km^2) and 79.2% (6.08 km^2) of their 1999 ice tongue areas. From August 30 to approximately September 12, 2007, open water occurred in Yelverton Bay which allowed the mélange to drift away from the glaciers and become replaced by sea ice. By August 2008 the glaciers had retreated to their grounding line, where they have remained in a quasi-stable position up to the present day, typically varying by <0.7 km^2 between years (Figure 3.8ef, Table 3.3).

3.4.3.2 Yelverton Inlet

The loss of sea ice from Yelverton Inlet occurred in stages. While Marine and Vanier glaciers are both located in the central part of Yelverton Inlet, the loss of sea ice surrounding their sikussak

zones occurred at different times (Figure 3.1). In 2005, the sea ice broke apart at the front of Vanier Glacier, which was followed by a 1.45 km^2 (29.6%) decrease in the extent of the mélange and a 0.42 km^2 (18.9%) loss in ice tongue area by 2007 (Figure 3.1; Table 3.3). In 2008 open water occurred across the majority of Yelverton Inlet, causing Marine Glacier to lose 81% of its surrounding mélange, and Vanier Glacier to lose all of its remaining mélange (Figures 3.3 and 3.7e). From 2008 to 2017 neither glacier experienced an ice tongue area change of >0.71 km^2 at Vanier Glacier or >0.30 km^2 at Marine Glacier, likely due to their lack of extension into the inlet and pinning by surrounding valley walls (Figure 3.1).

In south Yelverton Inlet, the sea ice broke up in 2002, creating an open water environment at the front of De Vries Glacier and Glacier G (Figure 3.3). This open water led to the complete loss of sikussak at both glaciers by 2003 (Figure 3.1). In the years that followed, some mélange (0.36-0.64 km^2) was recorded at the front of Glacier G in 2007, 2008, 2013 and 2014, but was removed in 2010 and 2016 when open water allowed it to drift away (Figure 3.8i). Following open water conditions at De Vries Glacier in 2005, the ice tongue retreated, losing 0.43 km^2 in area by 2007 (Figures 3.5d and 3.7c).

3.4.3.3 Kulutingwak Fiord

In 2008 the sea ice broke up at the front of Glacier A and Glacier B (Figures 3.3 and 3.7e). By 2009 all sikussak and the majority of the ice tongue at Glacier A was lost (-2.85 km^2; Figure 3.1). Although there was already no ice tongue at Glacier B, the sikussak at the ice front reduced by 0.04 km^2 between 2008 and 2009. In August 2010, when open water surrounded both termini, the remaining sikussak at the front of Glacier B drifted away, while the ice tongue at the front of Glacier A expanded slightly (by 0.29 km^2) and remained stable through 2017 (Figures 3.1 and 3.3; Table 3.4).

The break-up of sea ice occurred in south Kulutingwak Fiord in two stages; first at the head of the fiord in 2003, followed by the central portion of the fiord in 2009 (Figures 3.3 and 3.7bf). The open water in 2003 led to the complete loss of all sikussak (-0.52 km^2) and the entire ice tongue (-0.05 km^2) of Glacier E in 2004 (Figure 3.7b). This open water event had little effect on Glacier F, which had undergone the greatest losses to its ice tongue and sikussak before 1999 (Figure 3.1). Following the open water in the central portion of the fiord in 2009, Glacier C and Glacier D both lost 100% of their surrounding sikussak by 2010 (Figure 3.1). The small ice

tongue at the front of Glacier D in 1999 (0.03 km^2) had shrunk back to its grounding line by 2010. Between 2013 and 2015, an ice tongue began to expand at Glacier D and contribute to the surrounding mélange, although this tongue disappeared again by 2017 (Figure 3.1).

3.4.4 Ocean temperatures

The TOPAZ4 Arctic Ocean Reanalysis data from the grid cell in the center of Yelverton Bay showed distinct patterns at 50, 100 and 200 m depths (Figure 3.9 and 3.10b). Ocean temperatures at all three depths peaked in 2007, 2008, and 2009, with the mean annual temperature at 100 m and 200 m depths reaching above 0°C. The highest increase occurred at 100 m depth, with an increase in mean temperature from -0.68°C between 1999 and 2005 to 1.07°C between 2006 and 2010. At 200 m depth, the mean temperature was 0.10°C between 1999 and 2005, and increased to 0.95°C between 2006 and 2010. The lowest increases occurred at 50 m depth, where mean annual ocean temperatures exceeded -1°C in 2008 and 2009. From 2011 to 2016, however, mean annual ocean temperatures for all depths combined dropped to -0.95°C, 0.28°C cooler than the 1999-2005 levels.

3.4.5 Air temperatures

NCEP/NCAR reanalysis shows that mean annual summer surface air temperatures in the study region increased by ~1.0°C (0.15°C $decade^{-1}$, R^2=0.1247, p=0.003) between 1948 and 2016 (Figure 3.10a). The warmest summer on record occurred in 2011 when mean summer surface temperatures reached 4.10°C, followed by 3.65°C in 2012, and 3.52°C in 2015. Since the year 2000, mean summer surface temperatures have exceeded the long-term (1948-2017) mean of 1.68°C every year, except for 2013. In summer 2013 the mean temperature was 0.85°C, making it the 10th coldest summer on record.

3.5 DISCUSSION

Over the study period, we observed the nearly complete loss of ice tongues (>85% loss) from 8 glaciers, with most losses occurring since the start of the 21st century. Between 1959 and 1999 the ice tongues saw generally mixed changes (i.e., advances and retreats) in extent (up to ±65%), with sikussak remaining present around most of them (Figure 3.1). The main exceptions were Glacier C which lost all of its small tongue (0.06 km^2), and De Vries Glacier, which lost an extensive area of sikussak (~70 km^2) between 1959 and 1987 (Figure 3.1 and 3.5ab), which

could have been produced during a historical surge event as Copland et al. (2003) classified it as a possible surge-type glacier due to the presence of looped moraines. Between 1999 and 2003, marine ice losses were dominated by decreases in the area of sikussak, by a total of 11.02 km^2 along the front of several glaciers, where sikussak either disappeared or broke apart into a mélange (total mélange: 5.50 km^2; Figure 3.4; Table 3.3). From 2005 to 2010, sikussak losses accelerated (38.97 km^2), and the entire ice tongue area decreased by 33.13 km^2, including >90% of the ice tongue from Yelverton Glacier and Glacier D, and >~80% of the ice tongue area from Marine North N, Marine North S and Glacier A (Figure 3.4). The loss of sikussak, mélange and ice tongues from 2002 to 2010 occurred in tandem with open water events, which began to appear in isolated regions in 2002, became more common in 2005, and were widespread each summer from 2008 to 2012 (except for 2009; Figure 3.3).

From 2010 to 2017 there was a limited recovery in total ice tongue area for some glaciers due to terminus advance, although these gains were more than offset by ice tongue losses at other glaciers, resulting in a net decrease in area of 1.75 km^2 (Figure 3.4; Tables 3.3 and 3.4). These temporary gains could be linked to the unusually cold summer in 2013, when the mean summer temperature (-0.85°C) was 0.88°C below the 1981-2010 climatological mean (Figure 3.10), resulting in a lack of open water and presence of supportive sea ice adjacent to the glaciers in summers 2013 and 2014 (Figures 3.3 and 3.7h).

From these observations, it is apparent that the majority of ice tongue losses occurred in tandem with the loss of adjacent sea ice, resulting in the loss of buttressing of glacier termini. Without the backpressure of sea ice, sikussak/mélange breaks-up, causing the ice tongue to destabilize and calve. When sea ice is replaced by open water, the sikussak or mélange can destabilize and cause the ice tongue to collapse in place, becoming a new mélange at the glacier front. If offshore winds accompany the open water, the free-floating icebergs and ice islands produced from the destabilized sikussak/mélange and ice tongue can move away from the glacier front, leaving behind sea ice with dispersed icebergs the following summer. For instance, in 2008, sea ice was replaced by open water near Yelverton Glacier causing the sikussak and majority of the ice tongue to collapse, forming a new mélange visible in summer 2009 that later dispersed following open water in August 2010 (Figure 3.6e-f). While this sea ice buttressing mechanism has been widely documented for ice shelves and ice tongues in Greenland (Joughin et al., 2008;

Amundson et al., 2010; Carr et al., 2013; Carr et al., 2017; Robel, 2017), Russia (Carr et al., 2014), and Antarctica (Massom et al., 2010; Miles et al., 2016; Miles et al., 2017), it has only previously been described for ice shelves on northern Ellesmere Island (Copland et al., 2007; White et al., 2015).

3.5.1 Controls on MLSI stability in the Yelverton Bay region

Given the strong connection between the stability of ice tongues and surrounding MLSI in the Yelverton Bay region, the question remains of what has been the driver for MLSI losses there? The MLSI in Yelverton Bay originally formed in the 1950s, following the removal of a large ice shelf that occupied this area in the early 1900s (Koenig et al., 1952; Jeffries 1987). Pope et al. (2012) report that the main region of MLSI in Yelverton Bay remained stable between 1950 and 2005 based on analyses of ice cores, ice thicknesses and the presence of matching features (e.g., large cracks, ice islands) from imagery over this period. The only variation in MLSI extent occurred along the seaward edge (advancing ~3-5 km into the Arctic Ocean), and at the far southern end of Yelverton Inlet and Kulutingwak Fiord where the sikussak in front of De Vries Glacier was lost between 1959 and 1987 (Figure 3.5), and where open water was observed as early as 2002 and 2003 in the MODIS time series (e.g., Figure 3.7b).

Starting in 2005 the MLSI broke-up in two stages which began with the removal of the youngest and thinnest ice at the back of Yelverton Inlet and Kulutingwak Fiord, followed by the older and thicker ice in Yelverton Bay. In the first week of August 2005, 330 km^2 of the newer MLSI broke away from the outer portion of Yelverton Bay (Copland et al., 2007; Pope et al., 2012). This was followed by the loss of 690 km^2 of the older MLSI in Yelverton Bay, together with ~8 km^2 from the margin of the Petersen Ice Shelf and ~8 km^2 from the margin of the Wootton Peninsula Ice Shelf, the two remaining ice shelves which occupied Yelverton Bay at this time (Copland et al., 2007; Pope et al., 2012; White et al., 2015). In spring 2008, ice core and thickness measurements confirmed the presence of FYI at the back of Yelverton Inlet and the last remaining old MLSI at the head of Yelverton Inlet and Kulutingwak Fiord (Pope et al., 2012). The remaining old MLSI in Kulutingwak Fiord broke out in August 2009, while the remaining old MLSI broke out of Yelverton Inlet in August 2010 (Pope et al., 2012).

The timing and patterns of these MLSI losses, together with losses from associated ice tongues, can provide insight into factors controlling these changes, with several potential factors at play. These are discussed further below.

3.5.1.1 Air temperatures

From 1948 to 2016 mean summer air temperatures increased by 0.15°C decade^{-1} (p=0.003) (Figure 3.10a), but this rate has accelerated to 0.58°C decade^{-1} (p=0.107) since 1999 (Figure 3.10c). Over the 68 years there have been two periods (late 1940s to early 1960s, and late-1990s to 2016) of anomalously warm temperatures, with a particular cluster over the past decade (Figure 3.10b). These periods of anomalously warm summer air temperatures and the overall warming from 1948 to 2016 likely contributed to the weakening of ice tongues (e.g., through thinning and potentially hydrofracturing) and MLSI in the Yelverton Bay region. There are no long-term mass balance measurements in our study region to confirm this directly, but modelling by Noël et al. (2017) indicates that the average rate of mass loss across the northern CAA more than doubled between 1958-1996 (11.9 Gt yr^{-1}) and 1996-2015 (28.2 ±11.5 Gt yr^{-1}). The recent period of anomalously high summer air temperatures in the Yelverton Bay region was punctuated by record-breaking conditions in 2005, when mean summer air temperatures reached 3.1°C (1.4°C above the climatological mean). This resulted in the widespread occurrence of surface meltwater pools visible in July Landsat imagery, and when combined with long-term thinning caused by long-term warming, likely had a crucial role in the largest break-out of MLSI from the Yelverton Bay region ever recorded (1020 km^2; Pope et al., 2012).

Regarding the occurrence of open water observed at the head of Yelverton Inlet and Kulutingwak Fiord in some years before 2005 (e.g., Figure 3.7b), this likely relates to local microclimatology. Field and remote sensing observations indicate that ocean-derived fog and associated cooler air temperatures are common at the seaward margin of Yelverton Bay (similar to the Milne Fiord to the east; Chapter 4), with Pope et al. (2012) describing a trend of greater snow accumulation at the mouth of Yelverton Inlet due to its proximity to the Arctic Ocean, which acts as a moisture source. This is reflected in spatial gradients in sea ice thickness, which ranged from 3.71 m at the mouth of Yelverton Inlet to 1.19 m at the central (inland) part of Yelverton Inlet in spring 2008 (Pope et al., 2012). The thinner ice with less snow cover at the back of Yelverton Inlet, together with warmer air temperatures, could, therefore, be lost more

quickly due to atmospheric forcing. The open water may also be linked to subglacial discharge from the glaciers within this area (i.e., Yelverton and De Vries), which provides a source of buoyancy that drives convective motion at the glacier front that can break-up sea ice and move it away from the glacier termini (Jenkins, 2011). While there is limited data regarding subglacial processes in this region, field observations during a helicopter survey in July 2015 showed extensive upwelling of sediment-laden water from the front of Yelverton Glacier.

3.5.1.2 Sea ice convergence/divergence

The most negative glacier mass balance years between 2005 and 2012, including each summer between 2007 and 2012, have been characterized by frequent summer anti-cyclonic circulation over the CAA and West Greenland (Bezeau et al., 2015). Described by Alt (1978, 1987) as synoptic Type III (termed Island Circulation), this pattern brings clear, warm weather coupled with southerly wind flow, resulting in more melting degree days and divergence of sea ice from the northern coast of the CAA. Furthermore, well-developed mid-latitude frontal systems lead to strong winds in the Queen Elizabeth Islands and rapid wind reversals (Pope et al., 2017). Kwok (2015) also reported divergence across the Arctic Ocean in 2011 and negligible convergence in summer 2012, which would have increased the amount of open water along the northern coast of Ellesmere Island. This combination of high air temperatures and strong winds played an important role in repeatedly destabilizing the Nansen and Sverdrup ice plugs (Pope et al., 2017), and most likely facilitated the breakup of the MLSI and recovering landfast ice in the Yelverton Bay region between 2005 and 2012. For instance, Copland et al. (2007) reported that unusually persistent and strong offshore winds (up to 90 km hr^{-1}) in the first two weeks of August 2005 resulted in a large offshore lead and the associated removal of MLSI and the Ayles Ice Shelf from the northern coast of Ellesmere Island. The role of winds on MLSI removal has also been observed in the past, when persistent offshore winds (lasting four days) with speeds up to 10 m s^{-1} led to the detachment of the Milne Re-Entrant in February 1988 (Sackinger et al., 1991).

3.5.1.3 Oceanic forcing

It is unlikely that change in mid-depth ocean temperatures will affect sea ice, but glacier termini with deep grounding lines are susceptible to melt. The degree of oceanic control on glacier retreat will depend on the ice thickness and water depth along the glacier terminus. NASA Operation IceBridge measured ice thicknesses across the termini of six glaciers in the Yelverton

Bay region on April 1, 2014, using the airborne Multichannel Coherent Radar Depth Sounder (Leuschen et al., 2010). These were verified against single point measurements at the center of the terminus of Marine, Vanier, De Vries and Yelverton glaciers, made with a 10 MHz ground-penetrating radar system during a field campaign on July 18, 2014. Together, these measurements reveal centreline near-terminus thicknesses of up to ~150 m at Marine and Marine North-N glaciers, ~200 m at Marine North-S, Vanier and DeVries glaciers, and ~250 m at Yelverton Glacier. Based on these ice thicknesses, the increase in mean ocean temperatures to depths of 200 m from 2006-2010 are likely to have impacted the stability of these ice tongues. For example, when 20-60 m ocean temperatures at the front of four glaciers in Svalbard reached >0°C, there was a strong and linear relationship between increasing ocean temperature and frontal ablation (Luckman et al., 2015). The warmer ocean temperatures are thought to encourage submarine melt, leading to undercutting and eventual collapse.

Recent studies also suggest that oceanic warming has been a primary driver of thinning and mass loss at ice tongues such as Jakobshavn Isbrae in west Greenland (Thomas et al., 2003; Holland et al., 2008; Motyka et al., 2011). Thinning due to submarine melting averaged 228 ±49 m a^{-1} between 1984 and 1985, due to the circulation of warm seawater with a thermal forcing up to 4.2°C (Motyka et al., 2011). The rate of basal melt along its 15 km long floating tongue later increased by ~25%, following a 1.1°C warming of ocean water in the fiord after 1997, which is thought to have led to its destabilization (Motyka et al., 2011). According to the TOPAZ4 dataset, only 100 and 200 m ocean depths had mean annual temperatures >0°C between ~2004 and 2010, but most of the larger glaciers in the Yelverton Bay region would have felt these changes due to the ice thicknesses at their grounding lines of up to 250 m, resulting in their increased basal melt and undercutting. Assuming a salinity of 32 psu (measured from 2011 to 2015 in nearby Milne Fiord; Hamilton, 2016) in Yelverton Inlet, the pressure melting point at the base of 150 to 250 m thick glaciers would be -1.85 to -1.92°C, respectively. The maximum thermal forcing would therefore be 3.0°C for 150 m thick glaciers in 2008 and 3.1°C for glaciers ≥200 m thick in 2007 (>1°C less than the maximum thermal forcing linked to thinning at Jakobshavn Isbrae; Motyka et al., 2011).

3.6 SUMMARY AND CONCLUSIONS

The northern coast of Ellesmere Island is unique because it contains the only region with marine-terminating glaciers with ice tongues in the CAA, which drain a significant area of the Northern Ellesmere Icefield and a neighbouring ice cap (Chapter 2). This study conducted the first detailed analysis of changes to these ice tongues in relation to proglacial conditions since 1959, oceanographic factors since 1999, and atmospheric factors since 1948. Overall, the ice tongues have dramatically shrunk and have retreated to their grounding lines recently, particularly since 2005 (Figure 3.4). Except for surge-type De Vries Glacier, most ice tongues were relatively stable between 1959 and 1999, when the tongues and surrounding sikussak were held in place by MLSI that had been in place for decades (Pope et al., 2012). This semi-permanent configuration remained until ~2005 when MLSI began to break out of Yelverton Bay, a catalyst for the rapid changes that followed. Anomalously high summer temperatures and strong, offshore winds led to the loss of MLSI (Pope et al., 2012). The loss of supporting MLSI from within our study region began a cascade of changes that led to the break-up of the sikussak and ice tongues. The replacement of MLSI throughout the Yelverton Bay region with FYI, in combination with longer melt seasons, resulted in sea ice that was more easily destabilized the following summer, facilitating a positive feedback loop that allowed open water to continue in later years (Howell et al., 2009; Figures 3.3, 3.9 and 3.10b).

Unlike ice shelves that take hundreds of years to form, tidewater glaciers need only to flow to replenish their ice tongues (Mueller et al., 2017a). However, it is unlikely that the ice tongues in the Yelverton Bay region will be able to recuperate in the future. The recovery and re-stabilization of these ice tongues are dependent on the sustained presence and back-stress provided by MLSI, which is unlikely to reform as a long-term feature under current and future climate change. Further research is necessary to examine the role of sub-surface ocean temperatures along the bays and fiords in areas such as Northern Ellesmere Island, along with the resulting changes in glacier fronts and proglacial environments.

Table 3.1: Key data on the 13 tidewater glaciers described in this study.

Glacier Name	GLIMS ID[a]	2017 Grounding line width (km)	2015 Drainage area (km^2)[a]	Ice discharge ($Gt\ yr^{-1}$)	Surge-type[d]
YELVERTON BAY					
Marine North-N	G82234W82440N	1.83	49.22	-	-
Marine North-S	G81795W82368N	4.86	150.76	2000: 0.02±0.01[b] 2011: 0.01±0.01[b] 2012: 0.00±0.01[b] 2013: 0.01±0.01[b] 2014: 0.01±0.01[b] 2015: 0.02±0.01[b]	-
YELVERTON INLET					
Marine Glacier	G80929W82271N	3.42	187.82	2000: 0.01±0.01[b] 2011: 0.01±0.01[b] 2012: 0.01±0.01[b] 2013: 0.01±0.01[b] 2014: 0.01±0.01[b] 2015: 0.01±0.01[b]	-
Vanier Glacier	G78855W82142N	2.85	631.29	2000: 0.01±0.01[b] 2011: 0.01±0.01[b] 2012: 0.01±0.01[b] 2013: 0.01±0.01[b] 2014: 0.01±0.01[b] 2015: 0.01±0.01[b]	Possible
De Vries Glacier	G77854W81941N	1.53	852.37	1991: 0.005±0.002[c] 2000: 0.002±0.002[c] 2006: 0.003±0.002[c] 2007: 0.006±0.002[c] 2011: 0.01±0.01[b] 2012: 0.01±0.01[b] 2013: 0.001±0.002[c]; 0.01±0.01[b] 2014: 0.002±0.002[c]; 0.01±0.01[b] 2015: 0.005±0.006[c]; 0.01±0.01[b]	Possible
Glacier G	G80481W81907N	1.04	74.88	-	-
Yelverton Glacier	G80268W81677N	3.22	683.99	2000: 0.114±0.029[c]; 0.12±0.02[b] 2006: 0.119±0.03[c] 2007: 0.110±0.028[c] 2011: 0.06±0.01[b] 2012: 0.07±0.01[b] 2013: 0.105±0.027[c]; 0.08±0.02[b] 2014: 0.117±0.029[c]; 0.08±0.02[b] 2015: 0.106±0.028[c]; 0.08±0.02[b]	-
KULUTINGWAK FIORD					
Glacier A	G83760W82186N	1.88	108.86	-	-
Glacier B	G82817W82252N	0.37	6.37	-	-
Glacier C	G83429W82201N	0.41	5.51	-	-
Glacier D	G83314W82175N	0.31	10.64	-	-
Glacier E	G83297W82136N	0.37	18.71	-	-
Glacier F	G83504W82091N	0.79	29.49	-	Possible

[a]Chapter 2; [b]Van Wychen et al., 2015; [c]Surveyed ice discharge values from Millan et al., 2017; [d]Copland et al., 2003

Table 3.2: List of imagery used to delineate the different ice types measured in this study.

Dataset	Product Identifier[1]	Acquisition Date (yyyy-mm-dd)	Resolution (m)	Number of GCPs	Transformation	RMSE (m)
Stereo Aerial Photography	A16690_100	1959-07-28	5.59	22	1st order polynomial	14.80
	A16688_25	1959-07-29	3.08	23	1st order polynomial	12.69
	A16688_27	1959-07-29	3.24	21	1st order polynomial	14.80
	A16785_201	1959-08-17	2.79	23	1st order polynomial	14.70
	A16734_6	1959-08-17	3.15	20	1st order polynomial	13.87
	A16734_8	1959-08-17	2.75	20	1st order polynomial	13.70
	A16785_56	1959-08-17	2.98	21	1st order polynomial	13.03
	A16785_91	1959-08-17	2.86	23	1st order polynomial	6.58
	A16785_193	1959-08-17	3.06	38	3rd order polynomial	14.88
	A16785_196	1959-08-17	3.01	23	1st order polynomial	14.75
	A16785_197	1959-08-17	2.73	21	1st order polynomial	14.42
SPOT	SPOT1086124870705225806 1P0	1987-07-05	10	21	1st order polynomial	14.64
	SPOT1085125870705225806 2P0	1987-07-05	31.77	20	3rd order polynomial	13.84
	SPOT1086126870820195240 1P0	1987-08-20	10.02	23	1st order polynomial	14.67
	SPOT1086122880808194439 1P0	1988-08-08	10.65	29	3rd order polynomial	12.60
Landsat-7 (ETM+), Level 1, Tier 1	LE07_L1TP_051247_19990724_20170218_01_T1	1999-07-24	15	-	-	≤ 12.00
	LE07_L1TP_049247_20030721_20170125_01_T1	2003-07-21	15	-	-	≤ 12.00
	LE07_L1TP_047247_20030723_20170125_01_T1	2003-07-23	15	-	-	≤ 12.00
	LE07_L1TP_047248_20030723_20170124_01_T1	2003-07-23	15	-	-	≤ 12.00
	LE07_L1TP_054247_20030724_20170124_01_T1	2003-07-24	15	-	-	≤ 12.00
	LE07_L1TP_044248_20040720_20170120_01_T1	2004-07-20	15	-	-	≤ 12.00
	LE07_L1TP_049247_20050726_20170113_01_T1	2005-07-26	15	-	-	≤ 12.00
	LE07_L1TP_054247_20070719_20170102_01_T1	2007-07-19	15	-	-	≤ 12.00
	LE07_L1TP_052247_20070721_20170103_01_T1	2007-07-21	15	-	-	≤ 12.00
	LE07_L1TP_053247_20070728_20170103_01_T1	2007-07-28	15	-	-	≤ 12.00
	LE07_L1TP_051247_20080630_20161228_01_T1	2008-06-30	15	-	-	≤ 12.00
	LE07_L1TP_049247_20080702_20161228_01_T1	2008-07-02	15	-	-	≤ 12.00
	LE07_L1TP_055247_20080728_20161228_01_T1	2008-07-28	15	-	-	≤ 12.00
	LE07_L1TP_054247_20090708_20161219_01_T1	2009-07-08	15	-	-	≤ 12.00
	LE07_L1TP_052247_20090710_20161221_01_T1	2009-07-10	15	-	-	≤ 12.00
	LE07_L1TP_049247_20090721_20161220_01_T1	2009-07-21	15	-	-	≤ 12.00
	LE07_L1TP_047248_20090723_20161220_01_T1	2009-07-23	15	-	-	≤ 12.00
	LE07_L1TP_046248_20100719_20161213_01_T1	2010-07-19	15	-	-	≤ 12.00
	LE07_L1TP_046248_20100820_20161213_01_T1	2010-08-20	15	-	-	≤ 12.00
	LE07_L1TP_053247_20100821_20161213_01_T1	2010-08-21	15	-	-	≤ 12.00
	LE07_L1TP_044248_20100822_20161213_01_T1	2010-08-22	15	-	-	≤ 12.00
	LE07_L1TP_043248_20100831_20161213_01_T1	2010-08-31	15	-	-	≤ 12.00
Landsat-8 (OLI), Level 1, Tier 1	LC08_L1TP_052247_20130830_20170502_01_T1	2013-08-30	15	-	-	≤ 12.00
	LC08_L1TP_059246_20140818_20170304_01_T1	2014-08-18	15	-	-	≤ 12.00
	LC08_L1TP_052247_20150719_20170406_01_T1	2015-07-19	15	-	-	≤ 12.00
	LC08_L1TP_053247_20160712_20170323_01_T1	2016-07-12	15	-	-	≤ 12.00
	LC08_L1TP_051247_20170717_20180202_01_T1	2017-07-17	15	-	-	≤ 12.00
	LC08_L1TP_052247_20170724_20170809_01_T1[2]	2017-07-24	15	-	-	≤ 12.00

[1]The product identifier for aerial photography includes the film roll number and ID number.
[2]Master image against which all aerial photographs and SPOT imagery was georeferenced.

Table 3.3: Area of each ice type for 7 glaciers in Yelverton Bay and Inlet between 1959 and 2017.

Glacier Name	Date	Area (km^2)					
		Grounded ice	Ice tongue	Sikussak	Mélange	Sea ice	Open water
YELVERTON BAY							
Marine North-N	1959	1.63	1.93	1.96	0.00	11.32	0.00
	1988	1.64	2.24	3.02	0.00	9.98	0.00
	1999	1.60	3.19	2.32	0.00	9.77	0.00
	2007	1.50	0.39	0.00	4.11	10.87	0.00
	2008	1.58	0.37	0.00	0.00	14.90	0.00
	2010	1.29	0.71	0.00	0.00	0.00	15.03
	2013	1.06	0.38	0.00	0.00	15.83	0.00
	2017	1.06	0.29	0.00	0.00	15.85	0.00
Marine North-S	1959	2.83	5.31	7.75	0.00	16.41	0.00
	1988	3.01	7.28	8.25	0.00	13.83	0.00
	1999	3.37	7.68	8.32	0.00	12.90	0.00
	2007	3.48	1.60	0.00	6.63	20.59	0.00
	2008	2.85	1.65	0.00	0.30	27.40	0.00
	2009	3.24	0.98	0.00	0.00	28.14	0.00
	2010	3.26	0.77	0.00	0.00	0.00	28.33
	2013	3.12	0.27	0.00	0.00	29.19	0.00
	2017	2.92	0.23	0.13	0.00	29.34	0.00
YELVERTON INLET							
Marine	1959	2.38	2.45	2.54	0.00	2.24	0.00
	1987	1.54	1.90	1.27	0.00	4.94	0.00
	1999	1.14	2.21	1.99	0.00	4.26	0.00
	2005	1.19	1.98	0.00	1.86	4.60	0.00
	2008	1.29	2.08	0.00	1.43	4.90	0.00
	2009	1.50	1.81	0.00	0.27	6.10	0.00
	2010	1.08	1.98	0.00	0.00	0.00	6.57
	2013	1.15	1.68	0.00	0.00	6.83	0.00
	2015	1.04	1.86	0.00	0.00	6.66	0.06
	2016	1.25	1.75	0.00	0.00	6.59	0.05
	2017	1.24	1.52	0.00	0.00	6.86	0.00
Vanier	1959	1.50	2.22	15.12	0.00	7.21	0.78
	1987	1.58	1.75	5.15	0.00	18.42	0.00
	1999	2.22	1.20	5.25	0.00	18.33	0.00
	2003	0.81	2.23	0.00	5.50	17.77	0.69
	2005	0.93	2.20	0.00	4.90	17.82	1.16
	2007	1.13	1.79	0.00	3.45	19.81	0.90
	2008	1.57	1.08	0.00	4.33	19.57	0.51
	2009	1.85	0.73	0.00	0.00	24.40	0.00
	2010	1.29	1.28	0.00	0.00	0.00	24.48
	2013	1.00	1.33	0.00	0.00	24.74	0.00
	2016	0.86	1.19	0.00	0.00	24.33	0.67
	2017	0.90	0.90	0.00	0.00	24.98	0.29
De Vries	1959	2.39	1.33	70.42	0.00	6.98	1.01
	1987	1.27	1.49	0.70	0.00	79.34	0.00
	1999	0.85	0.63	1.68	0.00	79.60	0.00
	2003	0.81	0.60	0.00	0.00	81.40	0.00
	2007	0.81	0.17	0.00	0.00	81.81	0.00
	2010	0.55	0.38	0.00	0.00	0.00	81.84
	2013	0.43	0.43	0.00	0.00	81.99	0.00
	2016	0.40	0.42	0.00	0.00	81.68	0.35
	2017	0.41	0.41	0.00	0.00	82.03	0.00
Glacier G	1959	0.50	0.40	7.89	0.00	0.00	0.00
	1987	0.33	0.35	3.35	0.00	4.66	0.00
	1999	0.43	0.29	4.10	0.00	3.88	0.00
	2003	0.34	0.44	0.00	0.00	7.88	0.00
	2005	0.31	0.35	0.00	0.00	7.99	0.00
	2007	0.32	0.35	0.00	0.47	7.53	0.00
	2008	0.34	0.31	0.00	0.64	7.37	0.00
	2010	0.29	0.36	0.00	0.00	0.00	8.05
	2013	0.25	0.23	0.00	0.36	7.85	0.00
	2014	0.21	0.52	0.00	0.40	7.53	0.00
	2016	0.28	0.28	0.00	0.00	7.94	0.11
	2017	0.33	0.35	0.00	0.00	7.95	0.00
Yelverton	1959	1.16	33.64	28.52	0.00	0.00	0.00
	1987	1.01	13.97	38.31	0.00	9.99	0.00
	1999	1.27	20.58	32.09	0.00	9.46	0.00
	2004	0.50	22.15	12.36	0.00	6.21	0.00
	2009	1.41	0.78	0.00	34.17	27.03	0.00
	2010	1.76	0.36	0.00	0.00	0.00	61.59
	2013	1.10	0.00	0.00	0.00	62.89	0.00
	2014	1.18	0.00	0.00	0.00	62.78	0.00
	2015	1.26	0.31	8.54	0.00	53.79	0.00
	2016	0.85	0.99	9.53	0.00	52.31	0.00
	2017	1.43	0.96	0.00	0.00	61.49	0.00

Table 3.4: Area of each ice type for 6 glaciers in Kulutingwak Fiord between 1959 and 2017.

Glacier Name	Date	Area (km^2)					
		Grounded ice	Ice tongue	Sikussak	Mélange	Sea ice	Open water
Glacier A	1959	1.02	7.01	10.53	0.00	14.04	0.27
	1987	1.10	1.56	13.20	0.00	17.08	0.00
	1999	1.02	3.44	13.71	0.00	14.63	0.00
	2009	1.12	0.59	0.00	0.00	31.28	0.00
	2010	0.58	0.88	0.00	0.00	0.00	31.47
	2013	0.56	0.89	0.00	0.00	31.74	0.00
	2017	0.56	0.74	0.00	0.00	31.77	0.00
Glacier B	1959	0.04	0.00	0.00	0.00	0.00	0.07
	1987	0.05	0.00	0.06	0.00	0.00	0.00
	1999	0.05	0.00	0.05	0.00	0.00	0.00
	2009	0.04	0.00	0.01	0.00	0.05	0.00
	2010	0.04	0.00	0.00	0.00	0.00	0.07
	2015	0.04	0.00	0.00	0.01	0.06	0.00
	2016	0.03	0.02	0.00	0.00	0.05	0.00
	2017	0.03	0.02	0.00	0.00	0.05	0.00
Glacier C	1959	0.06	0.06	1.17	0.00	1.07	0.00
	1987	0.09	0.00	0.53	0.00	1.74	0.00
	1999	0.06	0.00	0.82	0.00	1.47	0.00
	2010	0.05	0.00	0.00	0.00	0.00	2.32
	2013	0.05	0.00	0.00	0.00	2.31	0.00
	2014	0.05	0.00	0.00	0.03	2.27	0.00
	2015	0.04	0.00	0.00	0.05	2.22	0.00
	2016	0.05	0.00	0.00	0.03	2.25	0.00
	2017	0.05	0.00	0.00	0.05	2.26	0.00
Glacier D	1959	0.03	0.04	0.67	0.00	1.07	0.00
	1987	0.04	0.03	0.51	0.00	1.24	0.00
	1999	0.03	0.03	0.87	0.00	0.89	0.00
	2010	0.05	0.00	0.00	0.00	0.00	1.76
	2013	0.03	0.02	0.00	0.08	1.77	0.00
	2014	0.03	0.08	0.00	0.03	1.67	0.00
	2015	0.03	0.03	0.00	0.13	1.62	0.00
	2017	0.02	0.00	0.00	0.00	1.80	0.00
Glacier E	1959	0.08	0.12	0.26	0.00	0.66	0.00
	1987	0.10	0.04	0.61	0.00	0.38	0.00
	1999	0.13	0.05	0.52	0.00	0.43	0.00
	2004	0.14	0.00	0.00	0.00	0.99	0.00
	2005	0.14	0.04	0.07	0.00	0.89	0.00
	2007	0.13	0.04	0.18	0.00	0.76	0.00
	2009	0.13	0.04	0.08	0.00	0.89	0.00
	2010	0.08	0.02	0.00	0.00	0.00	1.02
	2013	0.04	0.07	0.00	0.00	1.02	0.00
	2016	0.08	0.00	0.00	0.06	0.97	0.00
	2017	0.07	0.00	0.00	0.07	0.98	0.00
Glacier F	1959	0.39	0.37	0.08	0.00	0.35	0.00
	1987	0.36	0.21	0.25	0.00	0.39	0.00
	1999	0.37	0.20	0.00	0.00	0.62	0.00
	2009	0.35	0.18	0.00	0.00	0.66	0.00
	2010	0.32	0.12	0.00	0.00	0.00	0.77
	2013	0.32	0.04	0.00	0.00	0.86	0.00
	2014	0.29	0.06	0.00	0.00	0.70	0.12
	2016	0.28	0.04	0.00	0.00	0.83	0.00
	2017	0.24	0.03	0.00	0.00	0.88	0.00

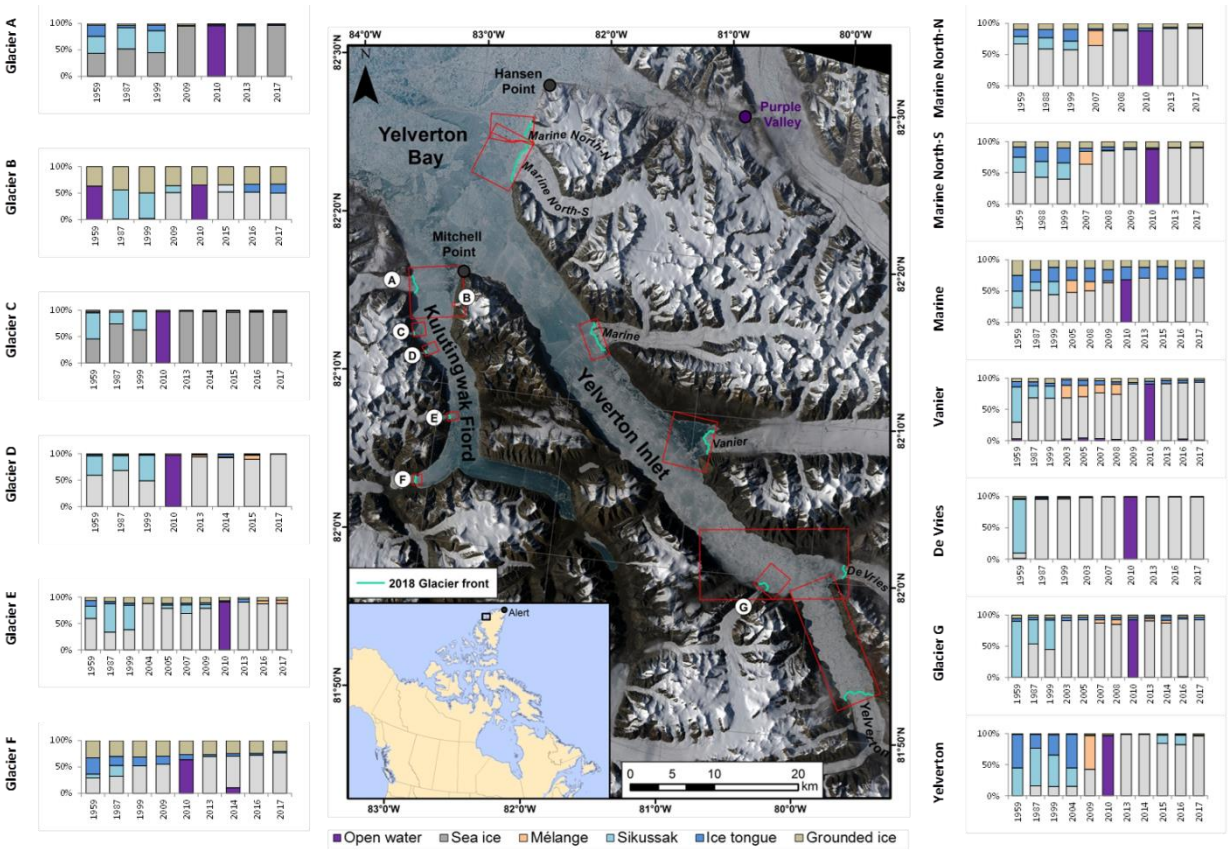

Figure 3.1: Change in the proportion of each ice type (in summer) at the terminus of 13 marine-terminating glaciers in the Yelverton Bay region between 1959 and 2017 (note the different scales on x-axes). Boxes used for area measurements shown in red. Base image: Landsat-8, June 29, 2018.

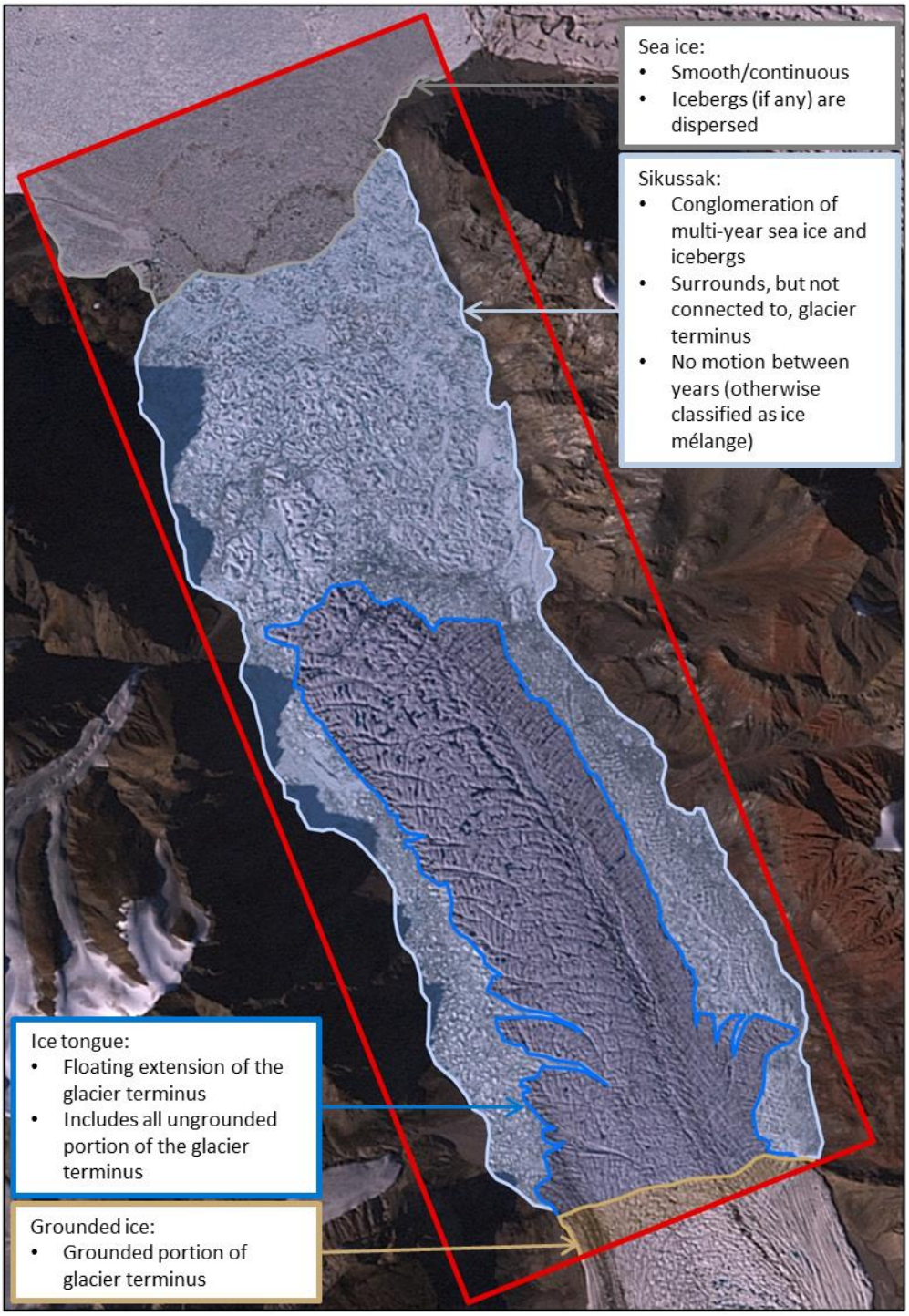

Figure 3.2: Landsat-7 (July 24, 1999) of Yelverton Glacier (see Fig. 3.1 for location), illustrating the difference between ice types delineated in this study.

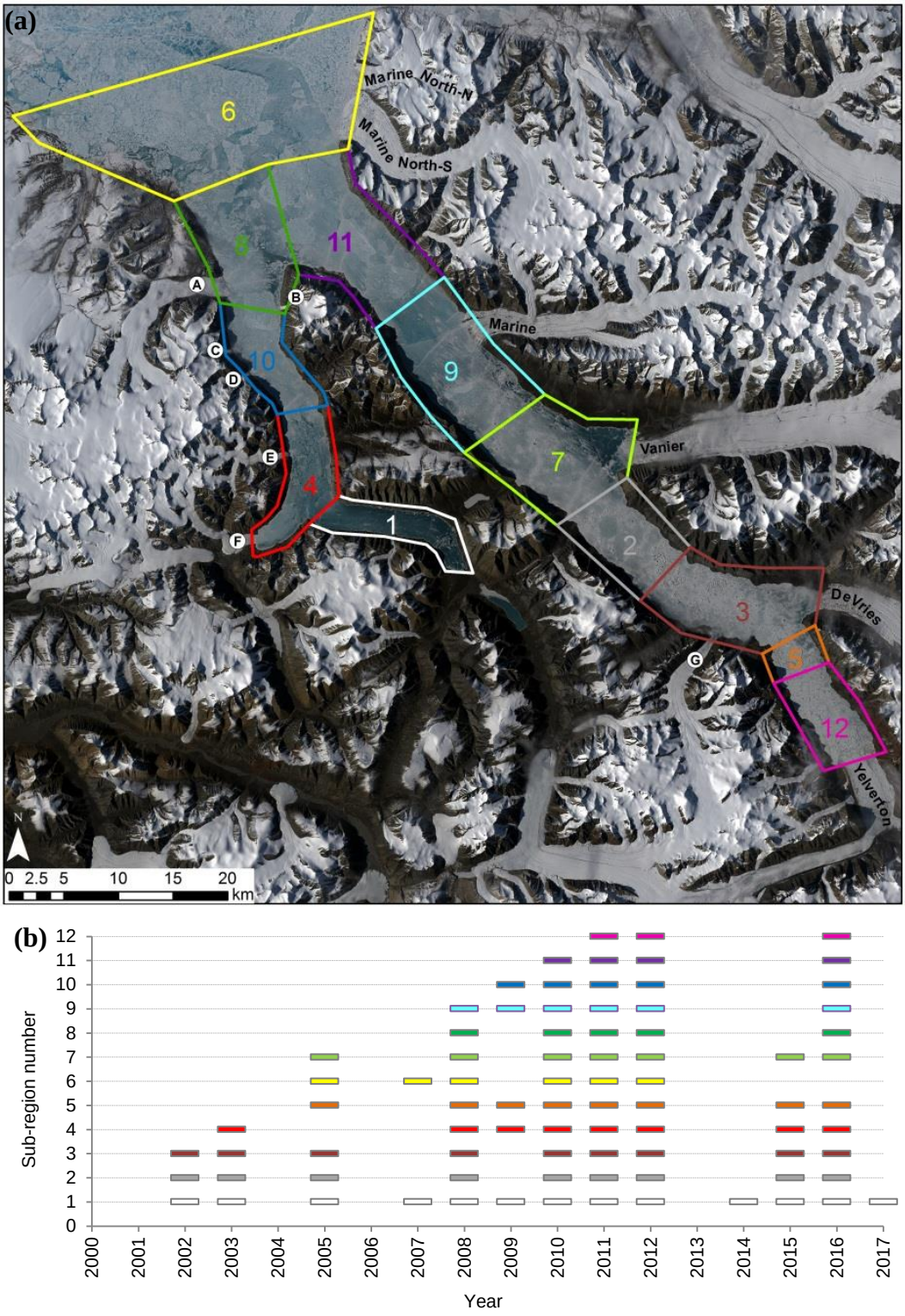

Figure 3.3: Summer open water years between 2000 and 2017 determined from MODIS imagery: (a) Sub-regions used to track open water areas, labelled by the order in which each region became ice-free (base image: Landsat-8, June 29, 2018); (b) Summers with open water for sub-regions identified in part a. Note: the sub-regions in part (a) contain the location of the open water but do not necessarily represent the total extent of the open water.

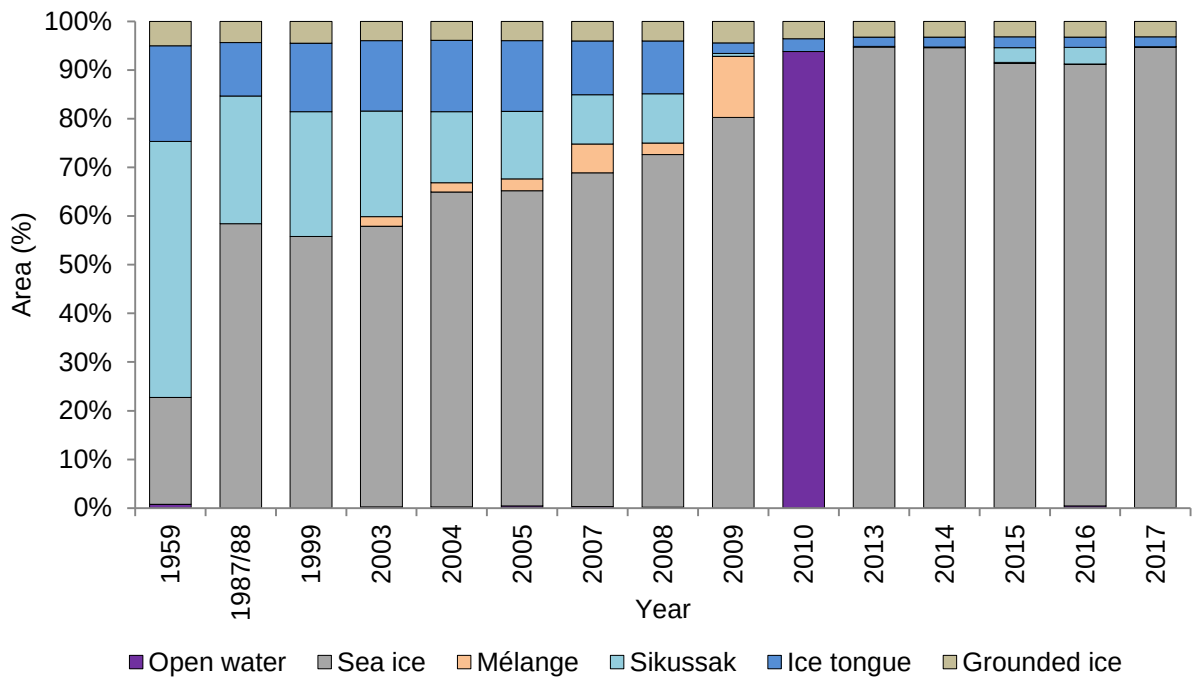

Figure 3.4: Total change in the relative proportion of each ice type (in summer) for all 13 marine-terminating outlet glaciers in the Yelverton Bay region from 1959 to 2017. Boxes used for area measurements are shown in red in Fig. 3.1.

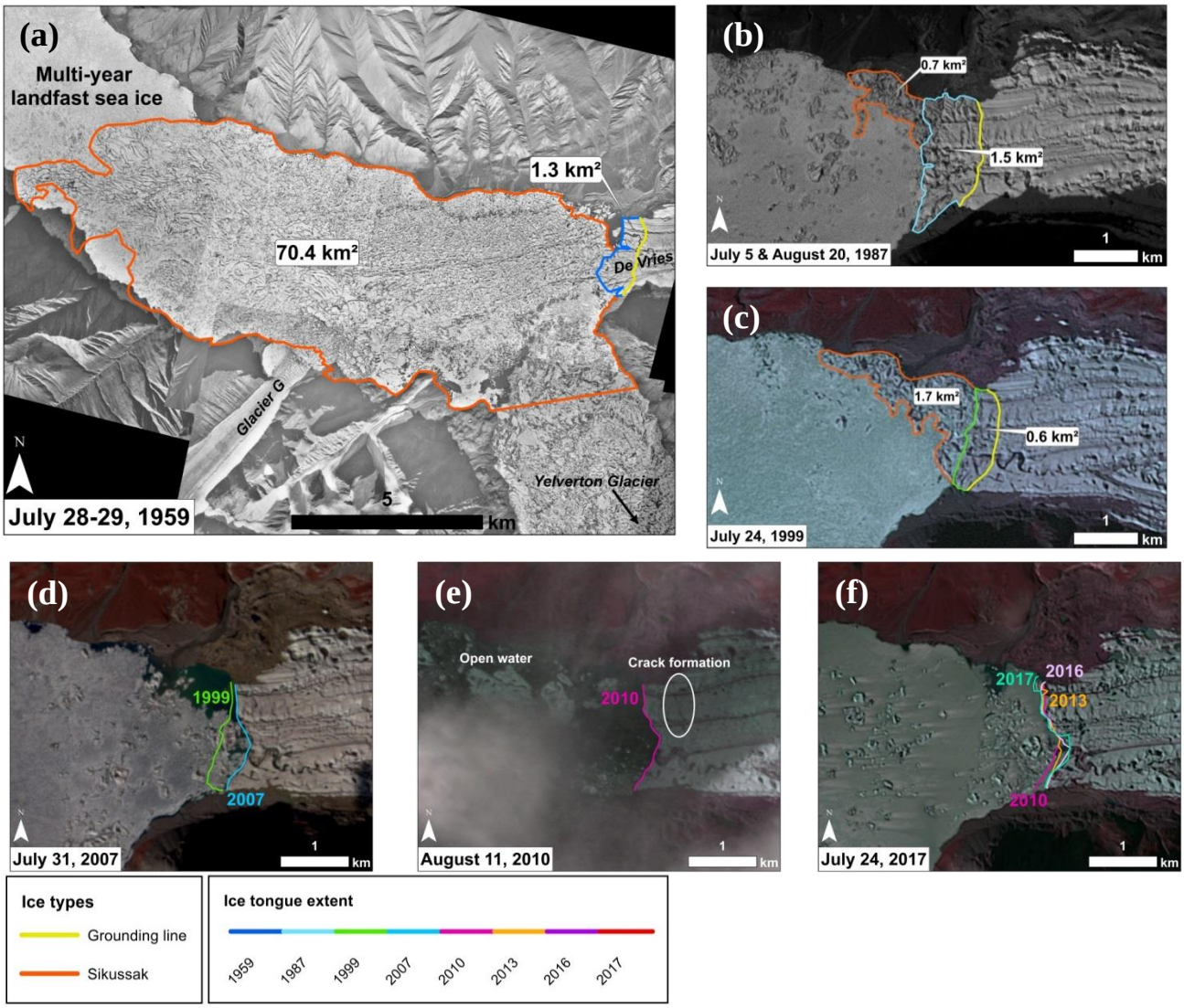

Figure 3.5: Imagery of De Vries Glacier showing: (a, b, c) ice type changes between 1959 and 1999; (d, e, f) changes in the glacier front position between 1999 and 2017. See Table 3.2 for image details.

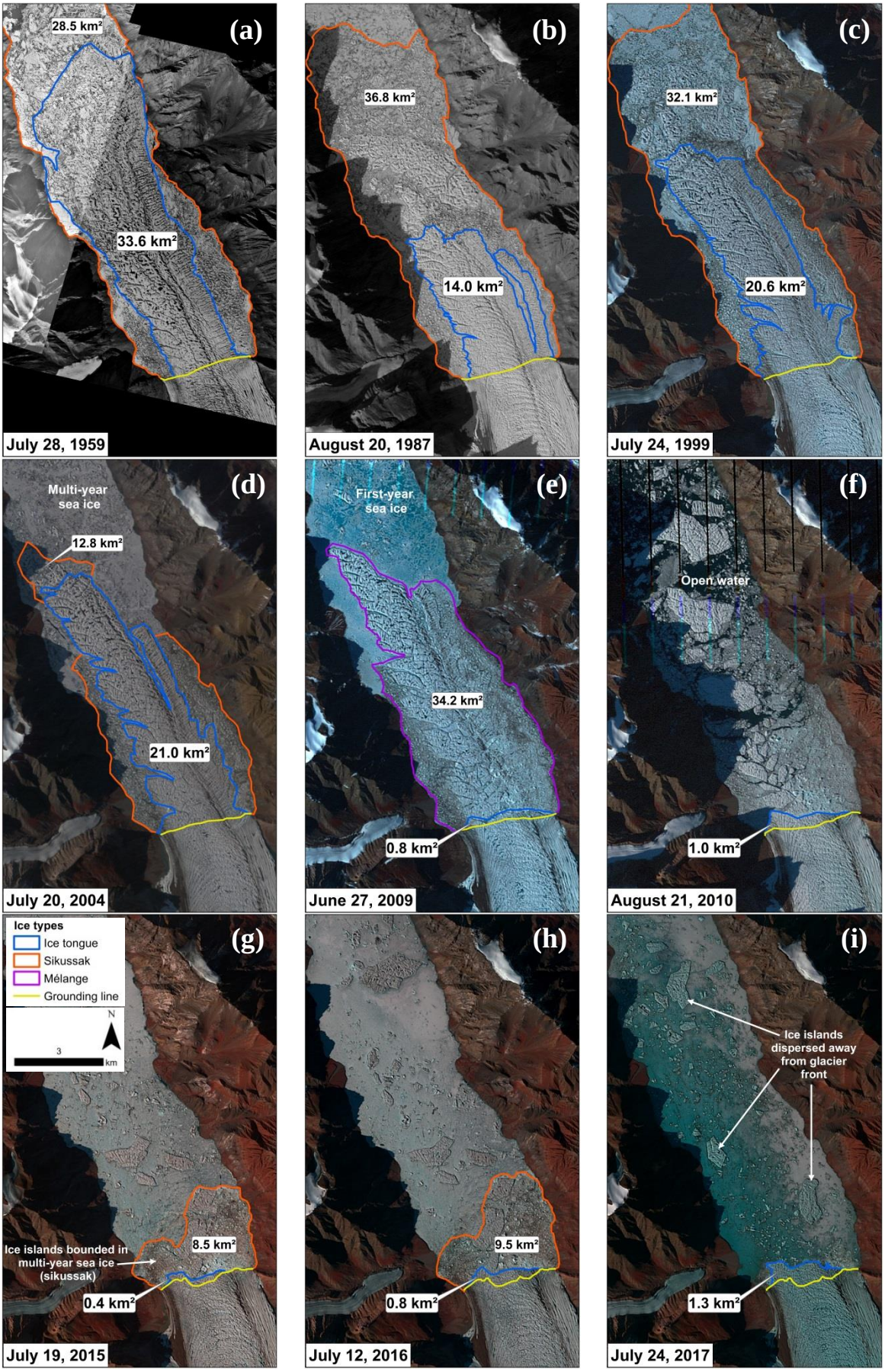

Figure 3.6: Progression of ice tongue loss at Yelverton Glacier between 1959 and 2017. See Table 3.2 for image details.

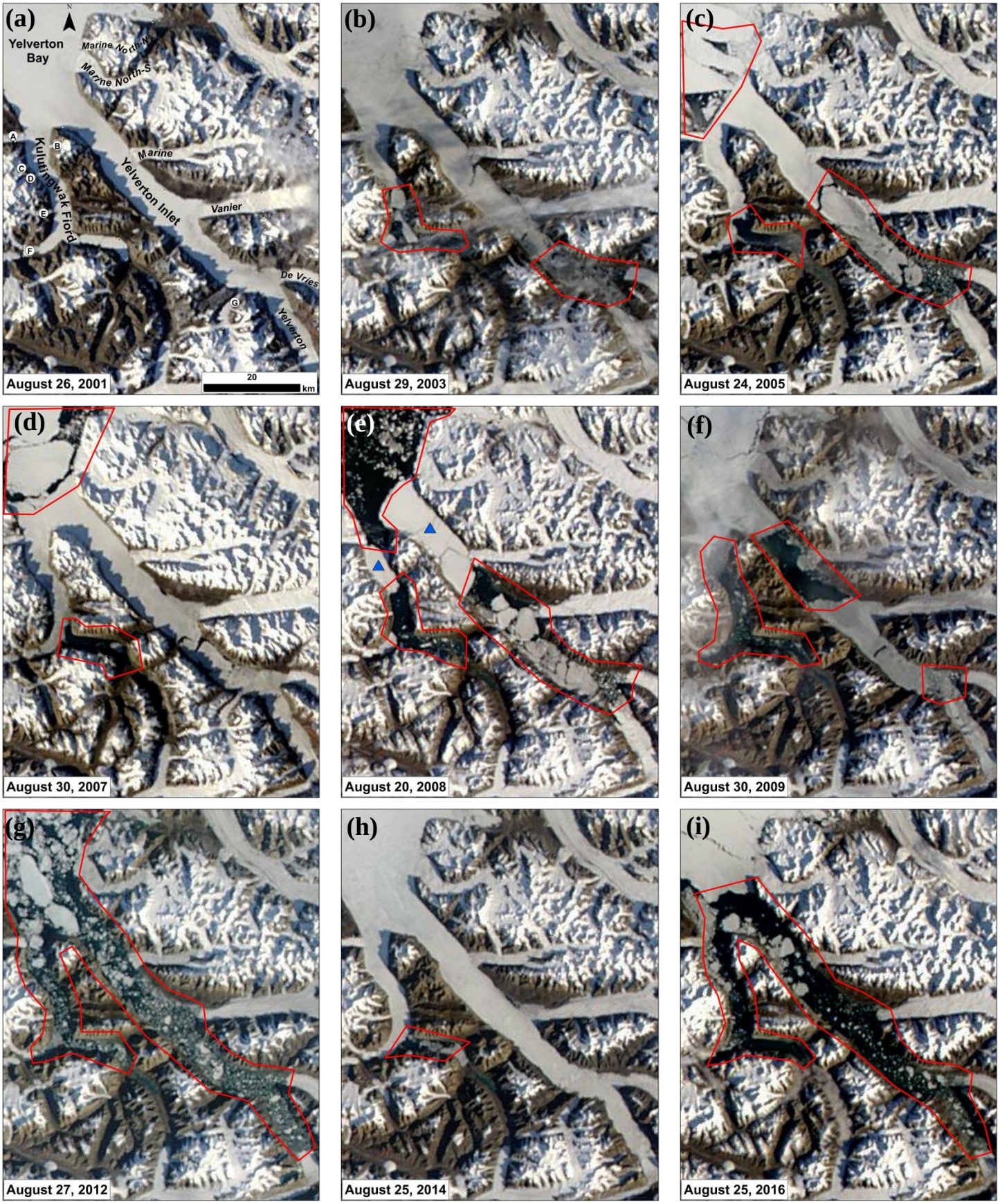

Figure 3.7: Late summer MODIS Terra imagery of the Yelverton Bay region for selected years between 2001 and 2016, illustrating the distribution of open water. Red polygons indicate regions of open water and blue triangles in (e) show ice plugs that remained in 2008, but broke out in subsequent years. Place names indicated on panel (a).

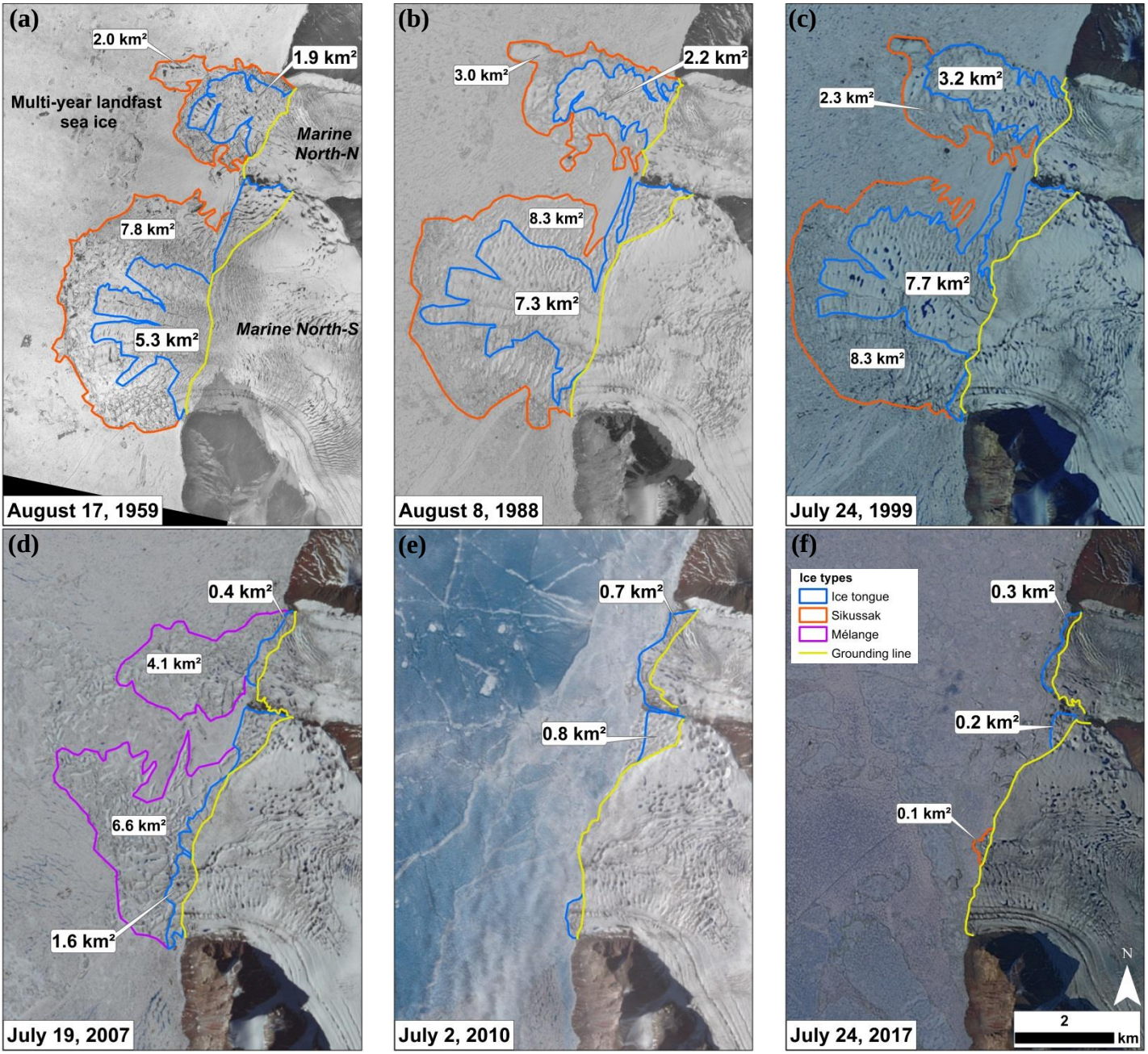

Figure 3.8: (a, b, c) Progression of ice tongue loss at Marine Glacier North-N and Marine Glacier North-S between 1959 and 1999 when the floating ice tongues were intact and abutted by sikussak and multi-year sea ice; (d) ice tongues break apart from both glaciers in 2007 and a mélange forms at the ice fronts; (e) both glaciers are stable in 2010; and (f) both glaciers have retreated by 2017. See Table 3.2 for image details.

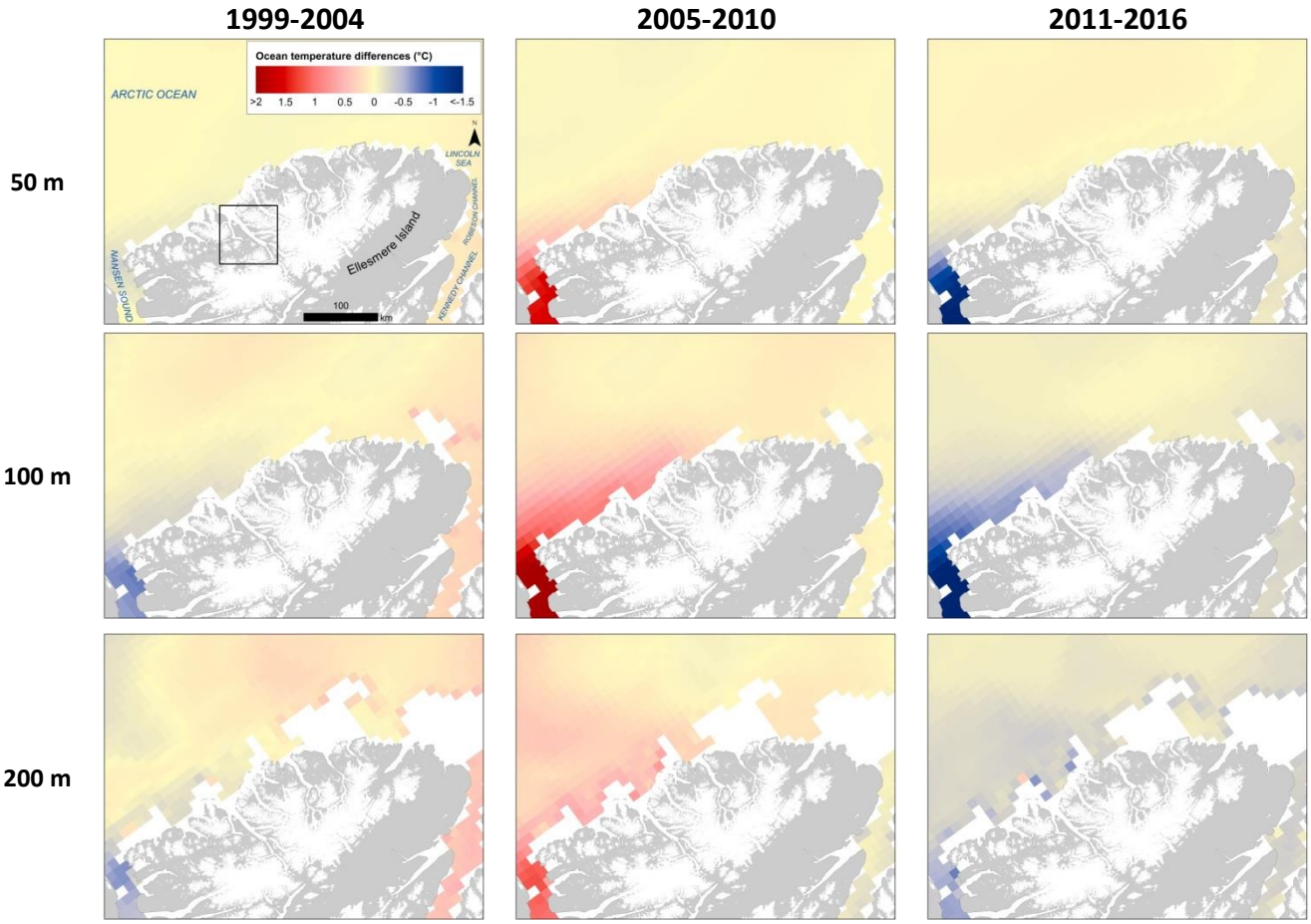

Figure 3.9: Difference in mean annual ocean temperature (from TOPAZ4 Arctic Ocean Reanalysis supplied by CMEMS) for the periods 1999-2004, 2005-2010, and 2011-2016, relative to the long-term mean (1999-2016), at standard depths of 50, 100 and 200 m. Study region is indicated by a black box in the first panel.

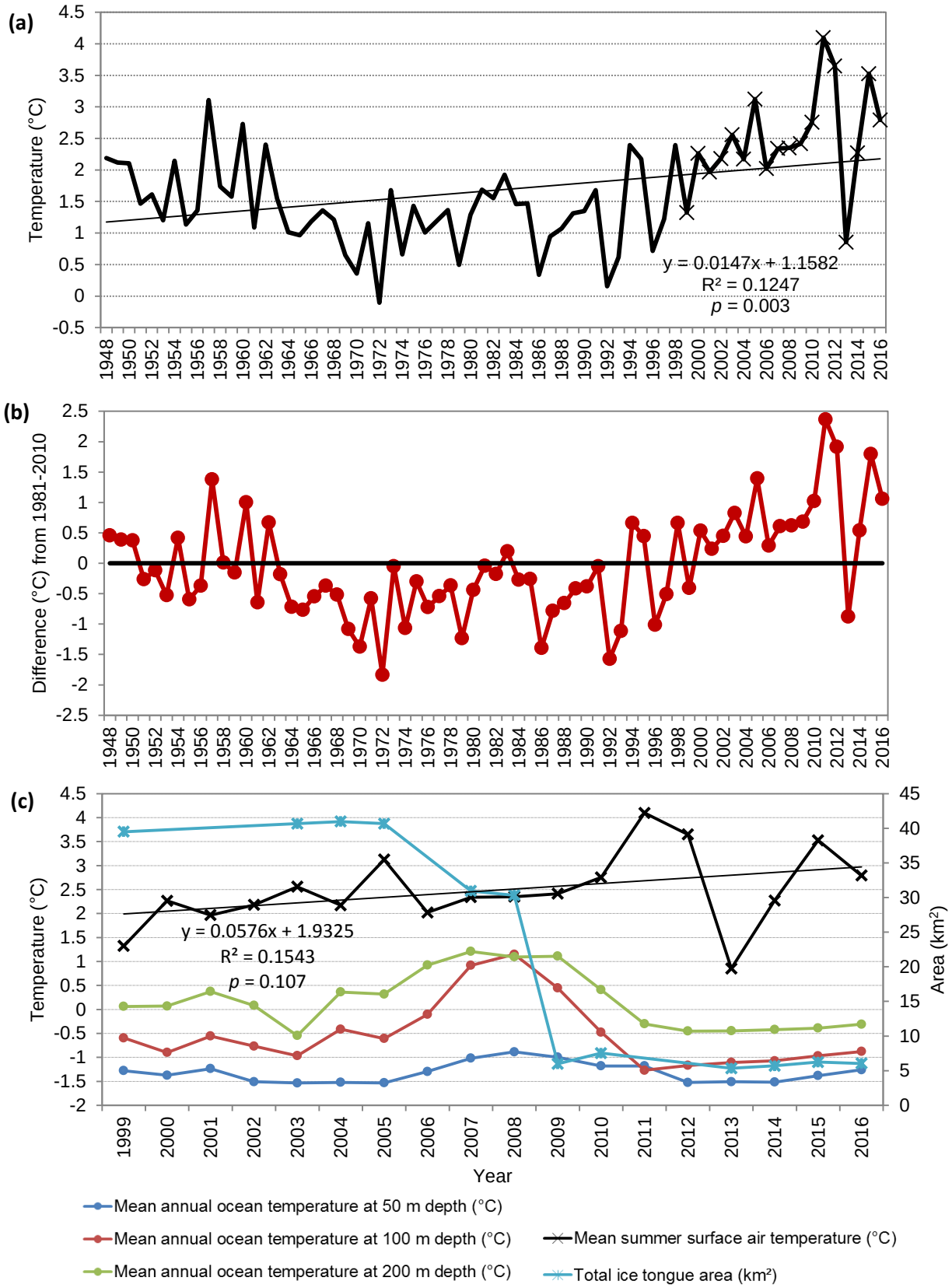

Figure 3.10: (a) Time series of mean summer (June, July, August) surface air temperatures (1948-2017) derived from NCEP/NCAR Reanalysis. Markers represent the mean summer surface air temperatures plotted from 1999 to 2016 in part c; (b) Air temperature anomalies (relative to 1981-2010 climatology); and (c) Time series of mean summer surface air temperatures, sub-surface ocean temperatures at 50, 100 and 200 m depths (left axis), and total area of floating glacier tongues (right axis) within the Yelverton Bay region from 1999 to 2016. Ocean temperatures derived from TOPAZ4 Arctic Ocean Reanalysis supplied by CMEMS.

CHAPTER 4: CONNECTIONS BETWEEN CLIMATE, MASS BALANCE AND STABILITY OF THE MILNE ICE SHELF, NORTHERN ELLESMERE ISLAND

4.1 INTRODUCTION

The ice shelves of northern Ellesmere Island currently occupy an area of ~535 km^2, approximately half of the area that they occupied at the start of the 21st century (Mueller et al., 2017a). Some ice shelves have been lost completely during this period, such as the Ayles in 2005 (Copland et al., 2007) and the Markham in 2008 (Mueller et al., 2017a), while others have lost significant area, such as the Petersen (31.0 km^2 loss, 61.6%, 2003-2012; White et al., 2015) and the Serson (187.1 km^2 loss, 95.5%, 2003-2015; Mueller et al., 2017a). These losses have resulted in ice-free fiords for the first time in ~3500-5500 years (England et al., 2017) and have occurred in tandem with a period of rapidly rising air temperatures and significant reductions in the age and thickness of sea ice fringing northern Ellesmere Island (Maslanik et al., 2011; Yu et al., 2013; Kwok, 2018). Despite the extensive fracturing that is apparent across the Milne Ice Shelf (Figure 4.1c), it has remained relatively stable compared to the other ice shelves on northern Ellesmere Island during this period, reducing in area from 200.6 km^2 in 1998 to 187.4 km^2 in 2015, a loss of only 6.6% (Mueller et al., 2017a).

Based on previous research, it would appear that unlike the other Northern Ellesmere ice shelves, the Milne is unique in its apparent structural stability. Some have suggested that the lack of calving events, aside from a major calving event from its seaward coastline in the 1960s and a 3 km^2 loss in 2012/13 (near Cape Evans; Mueller et al., 2017a), could be linked to the supportive physiography of Milne Fiord (Jeffries, 1986a; Veillette et al., 2008). However, little is currently known about the surface mass balance of the ice shelf, its spatial and temporal variability, and the factors that control it. This limits understanding of the causes of recent thinning observed by Mortimer et al. (2012), such as the importance of basal vs. surface melt, and hinders predictions of how the ice shelf may evolve in the future.

This study evaluates the hypothesis that a surface mass balance gradient occurs along the length of the Milne Ice Shelf due to variations in the microclimate with proximity to the ocean edge. Accordingly, the objective of this study is to use a combination of field measurements and

remote sensing to examine the spatial patterns of accumulation and ablation across the ice shelf to identify the factors controlling surface mass balance processes and patterns, and assess whether they have varied over time in response to a warming climate. Results of this study contribute to our knowledge of the factors that control mass balance without varying altitude. An understanding of these processes may provide insight into the stability of the other remaining ice shelves on Ellesmere Island and perhaps in other coastal regions with a semi-permanent floating ice cover (i.e., multi-year landfast sea ice and outlet glaciers).

4.2 STUDY AREA

The Milne Ice Shelf is located in Milne Fiord (82°41'N, 81°25'W), situated on the northern coast of Ellesmere Island, approximately ~275 km west of Alert, and ~310 km north of Eureka (Figure 4.1). After the Ward Hunt Ice Shelf, measuring 224.3 km^2, the Milne has the second largest surface area of the remaining Canadian ice shelves, measuring 187.4 km^2 in March 2015 (Mueller et al., 2017a). The surface of the ice shelf is characterized by surface undulations or rolls that consist of a series of ridges separated by melt-pond filled troughs (Hattersley-Smith, 1957). Jeffries (1986a) divided the ice shelf into individual units based upon the differing geometry of the undulating surface topography. The rolls across the Outer Unit are oriented parallel to the coastline (i.e., southwest to northeast) with a longer wavelength (~300 m) and become increasingly disorganized and shorter towards the Central Unit (~150-180 m; Figure 4.1c). The Inner Unit described by Jeffries (1986a) is currently recognized as an epishelf lake, composed of a layer of buoyant freshwater overlying sea water, developed from summer melt of snow and glacier ice that is dammed by the ice shelf (Veillette et al., 2008). Jeffries (1986a) associated the variation in surface topography with ice thickness variations derived by Prager (1983); the more developed ridges occurred in the Outer Unit where thicker ice (up to 90 m) was more widespread. Thickness measurements in 2008/2009 by Mortimer et al. (2012) showed that the ice shelf had a mean thickness of 55 ±1.1 m, with the thickest ice (70 – 80 m) located across the Outer Unit and considerably thinner ice (~50 m) in the Central Unit, except for thicker areas (up to 94 m) where glaciers enter (Figure 4.1; Mortimer et al., 2012).

The first accurate measurement of the area of the Milne Ice Shelf is from 1959, when air photos indicate that it was 287.6 km^2 (Jeffries, 1986b; Mueller et al., 2017a). Since then, the only significant loss from the seaward (front, northern) edge of the ice shelf occurred between 1959

and 1963, when 27 km^2 broke away. However, this area was replaced by multi-year landfast sea ice (MLSI), named the Milne Re-entrant, which thickened in situ to reach a thickness of 7.24 to 9.80 m by spring 1985 (Jeffries, 1986b). The Milne re-entrant remained in place until February 1988, when the large MLSI floe separated from the ice shelf during a brief episode of strong offshore winds (Jeffries, 1992; Jeffries 2002). With the exception of 2012/13, all area losses since 1963 have occurred from the landward (rear, southern) side of the ice shelf, where ice shelf ice has been replaced by epishelf lake ice with thicknesses that decreased from a maximum of 3.19 m in 1983 (Jeffries, 1985) to 0.65 m in summer 2010 (Hamilton et al., 2017). Mortimer et al. (2012) compared terrestrial ground-penetrating radar (GPR) measurements collected in 2008/2009 with airborne radio-echo sounding measurements collected in 1981 to determine that mean ice shelf thickness decreased by ~13 m over this period. The measurements revealed spatial variability in the thinning rate, with a higher rate of loss in the Central Unit compared to the Outer Unit (Figure 4c of Mortimer et al., 2012).

Richer-McCallum (2015) examined shallow ice cores (~2 m long) from both the Central and Outer units of the Milne Ice Shelf to identify the source of ice based on salinities and structural characteristics (i.e. bubble shape, size and density). This study confirmed that meteoric ice (i.e., originating from atmospheric precipitation; Jeffries, 2017) was present across the Outer Unit, while meteoric ice and old sea ice were identified across the Central Unit. Although past studies described the Milne Ice Shelf as having originated from glacier ice (Jeffries 1986a), the results presented by Richer-McCallum (2015) suggest that it is more likely a composite-type, being composed of both sea ice and glacier ice (Lemmen et al., 1988). Composite ice shelves can accumulate mass via glacier inflow, surface snowfall, basal freeze-on and sea ice accretion, while ablation occurs via surface runoff, basal melt and calving. Although five tributary glaciers currently terminate along the sides of the Milne Ice Shelf, since 2011 glacial input has been limited to Glacier 2 (Mortimer et al., 2012; Figure 4.1).

4.3 METHODS

4.3.1 Mass balance

The surface mass balance of the Milne Ice Shelf was measured from a network of eight ablation stakes established in early April 2008, spanning the ice shelf length and width (Figure 4.1c). With the exception of 2010, mass balance measurements were made annually between 2008 and

2018, to produce data for the full mass balance years 2008 to 2017. No field measurements were made in 2010, so the 2009 and 2010 results are presented as the annual average from the combined 2 year period (Table 4.1). All eight ablation stake sites couldn't be visited each year due to logistical constraints, but a minimum of four stakes across the length of the ice shelf were visited each year. Each year the stake height above the ice and the snow depth was measured, and a new stake was installed if the previous stake was near to melting out. The location of the ablation stake was recorded using a GPS.

The mass balance was measured using the conventional glaciological method as described by Østrem and Brugman (1991). The summer balance (b_s) was determined as the mean change in surface height for all available stakes. The winter balance (b_w) was calculated as the mean snow cover (snow water equivalent) remaining at all accessible sites in spring 2008, 2009, 2011 and 2013, and in summer 2012, 2014, 2015, 2016 and 2017. With mass gains regarded as positive and mass losses regarded as negative, the annual net surface mass balance (b_n) was then calculated as:

$$b_n = b_w + b_s \tag{4.1}$$

In this study, the balance year represents accumulation from the previous winter with ablation that occurred by the following spring. For example, the 2008 balance year combined accumulation from fall 2007 and winter 2008 (measured as the snow depth in spring 2008) with ablation from summer 2008 (measured as the difference in stake height above the ice between spring 2008 and spring 2009). This method was used for mass balance measurements collected in spring 2008, 2009, 2011 and 2013, but in all other years mass balance measurements were conducted in early to mid-summer, so some adjustments were made to maintain the same balance year. In most of these cases, winter snow was still present at each stake site and it was assumed that ablation had not yet begun. However, in years when no snow remained at a stake site, the summer ablation that had already occurred had to be accounted for. Automatic snow depth sounders installed at study sites M1, M3 and M5 (Figure 4.1c), were used to estimate this in order to remove it from the current mass balance year and include it in the subsequent balance year.

During spring field seasons in April-May 2008, 2009, 2011 and 2013, snow depth and density were measured in snow pits at each ablation stake site to determine the winter balance in snow water equivalence. In 2009, measurements were limited to snow depths, so the mean snow densities collected from each site in 2008, 2011 and 2013 were weighted by individual layer thickness and applied to the snow depths measured from May 31 to June 3, 2009. In 2012, 2014, 2015, 2016, 2017 and 2018, the study sites were only visited in summer (between June 28 and July 24), and therefore there was not enough snow to conduct snow pit measurements. Instead, snow densities typical of mid-summer (i.e., 300 to 700 kg m^3) were assumed, based on summer measurements at other low elevation locations across the Canadian Arctic Archipelago (e.g., White Glacier, Axel Heiberg Island), and used to quantify any remaining winter accumulation at the time of measurement. Therefore the winter balance for these years is provided with an error that accounts for the range in assumed densities of the snow.

4.3.2 Microclimatology

To examine the climate and its link to surface mass balance across the ~20 km length of the Milne Ice Shelf, three automated weather stations (AWS; M5-AWS, M3-AWS and M1-AWS) were installed on the ice shelf surface in June 2012, with an additional AWS installed in May 2009 in Purple Valley (PV-AWS), located ~1 km inland from the Milne Glacier (Figure 4.1). The stations were set up to record how the climate might vary with distance from the coast. Each AWS was installed on a steel pole and contained sensors to record incoming solar radiation (Hobo Silicon Pyranometer Smart Sensor S-LIB-XXXX), air temperature and relative humidity (Hobo 12-bit temperature/RH sensor S-THB-XXXX), and snow depth (Judd Communications Depth sounder on M1-AWS and M5-AWS; Senix ToughSonic TS-15S on M3-AWS) on an hourly basis. The M3-AWS and PV-AWS also recorded wind speed and direction (Hobo wind speed smart sensor S-MSA-XXXX and Hobo wind direction smart sensor S-WDA-XXXX on M-3 AWS; Hobo wind speed & direction smart sensor S-WCA-XXXX on PV-AWS). PV-AWS recorded air temperature at two sensors installed 1 m and 2 m above the surface, with the mean of these values used in this study. M3-AWS and M1-AWS recorded almost continuously from June 2012 to December 2017 (Figure 4.2). M5-AWS only recorded data from June 2012 to August 2013 due to an instrumentation failure after water damage to the sensors. PV-AWS has recorded almost continuously since 2009.

4.3.3 Distribution of ice facies

To examine the spatial distribution of ice facies, GPR surveys were conducted in May 2013 to examine near surface characteristics of the ice shelf. Data were collected with a Sensors and Software PulseEKKO Pro GPR system with 500 MHz dipole antennas. The antennas were mounted in a plastic sled and towed behind a snowmobile in transects across the Milne Ice Shelf at a speed of ~10 km hr^{-1}. Positioning was provided with a built-in single frequency GPS that recorded the location of each GPR trace to an accuracy of ~5 m. Traces were sampled at a temporal resolution of 0.2 ns over a total time window of 1000 ns, stacked eight times, and recorded every 0.2 s along the transects. The GPR transects were designed to sample the entire Milne Ice Shelf from the northern edge of the Outer Unit to the southern part of the Central Unit, to determine any spatial variability in subsurface layering. The GPR data were processed in EKKO_Project Version 4 using a signal saturation correction ('dewow'), frequency filtering (vertical bandpass) and radar gain adjustments (spreading and exponential calibrated compensation). Duplicate traces, generated when the snowmobile was stationary, were deleted.

To interpret and validate the GPR radargrams, a 7 m ice core was extracted from M1 (Figure 4.1), using a Kovacs Mark II ice coring system in May 2013. Upon extraction, each ice core segment was measured lengthwise, photographed, cut into sections with an ice saw and weighed. A visual examination of stratigraphy was made to assess each core segment for the presence of features characteristic of different facies, such as firn or ice layers. The radio-wave velocity (RWV) was calculated using the mean density of the 7 m core at M1 and four 2 m ice cores at M3, M4, M5 and M8 (described in Richer-McCallum, 2015) nearest the GPR transect using the methods described by Kovacs et al (1995). Measured densities ranged from 896 kg m^3 to 864 kg m^3, equating to a RWV ranging from 0.171 m ns^{-1} (M3; Central Unit) to 0.173 m ns^{-1} (M5; Outer Unit), respectively. This compares closely to a RWV of 0.170 m ns^{-1} determined by Mortimer et al. (2012) from a common midpoint survey on Milne epishelf lake in May 2009.

To examine the spatial distribution of ice facies across the entire ice shelf, and any change in their distribution through time, backscatter properties in synthetic aperture radar (SAR) satellite imagery were analyzed. European Remote-Sensing Satellite-1 (ERS-1), Radarsat-1, and Radarsat-2 images acquired in winter and early spring (to avoid any influence from surface melt) provided data from 1992 to 2018 (Table 4.2). The ERS-1 and Radarsat-1 data were provided by

the Alaska Satellite Facility, and the Radarsat-2 data were acquired through the Canadian Space Agency. To examine the variation in SAR backscatter in the Outer and Central units in relation to the GPR measurements, a Radarsat-2 image from winter 2013 was radiometrically-corrected to a normalized radar cross-section (σ^0) in a linear power scale. A low pass 3 × 3 averaging filter was applied over each raster cell to smooth the image and minimize speckle in ArcGIS Desktop 10.6. The backscatter values were then extracted along a 17 km transect stretching from the northern edge of the Outer Unit to the southern edge of the Central Unit and compared with backscatter values calibrated to sigma nought in SAR scenes from the past 26 years (1992, 1998, 2006, 2013, 2015 and 2018) to determine if their values have changed over time.

4.3.4 Area change

To determine changes in area of the Milne Ice Shelf between 1959 and 2018 we combined the outlines of Mueller et al. (2017b) produced for 12 individual years between 1959 and 2015, with the ice shelf outline derived from a Landsat-8 image from July 23, 2018 in ArcGIS Desktop 10.6. The 2018 Landsat image aligned well with the vector layers and therefore did not require additional georeferencing. For the area measurements between 1959 and 2015, Mueller et al. (2017a) calculated a root mean square error of 0.26%. The error generated in this study is derived from the sum of the error associated with the resolution of the satellite imagery and the operator error (i.e., variation given by repeat digitization). The error related to the image resolution (σ_{area}) was derived using (Ghilani, 2000):

$$\boldsymbol{\sigma_{area} = D\sigma_D\sqrt{2}} \tag{4.2}$$

where D is the equivalent-area square (square root of the ice shelf outline), and σ_D is the uncertainty in the image (half the spatial resolution). The operator error was quantified by digitizing the Milne Ice Shelf with the same imagery on five occasions. The standard deviation between the five digitization attempts was 0.14%, which when combined with σ_{area} gives a total error of 0.21%.

4.4 RESULTS

4.4.1 Surface mass balance

For the 10-year period from 2008 to 2017, the mean annual surface mass balance of the Milne Ice Shelf was -0.30 ±0.02 m water equivalent (w. eq.). Over this period winter snow accumulation remained relatively low (Table 4.1; Figure 4.3); for sites visited in spring 2008, 2009, 2011 and 2013, mean winter accumulation ranged from 0.09 m w. eq. in 2013 to 0.26 m w. eq. in 2009/10. For sites visited in summer (late-June/July), remaining snow from the winter ranged from 0.01 ±0.004 m w. eq. in 2016 to 0.12 ±0.06 m w. eq. in 2014. In contrast, summer ablation has been more variable between years and has been the dominant control on net annual surface mass balance. The mean summer balance has remained predominantly negative, ranging from -1.07 m w. eq. in 2012 to -0.14 m w. eq. in 2014 (Table 4.1; Figure 4.3). The only positive summer balance on record was 2013, with a mean of 0.06 m w. eq.

Surface mass balance changes were not uniform across the ice shelf. As a function of distance from the epishelf lake (at the rear; Figure 4.1), the summer balance at each ablation stake became progressively less negative with proximity to the northern coastline (Figure 4.4). Winter balances did not show such a strong relationship, although increases in accumulation with distance towards the coastline were evident in most years (Figure 4.5). Separated by region, the Outer Unit of the ice shelf had a total cumulative balance of -1.47 ±0.16 m w. eq. for the 10-year period, whereas the Central Unit had a total cumulative balance of -4.92 ±0.02 m w. eq. over this time (Figure 4.3bc).

4.4.2 Microclimatology of the Milne Ice Shelf

A comparison of weather data recorded at the AWS at M1, M3 and M5 show marked gradients across the ice shelf. From July 2012 to April 2013, when all 3 stations were operational (Figure 4.2), mean summer (June-July-August) air temperatures increased with distance from the ocean, with values of 1°C and 0.8°C at M1 and M3 , respectively, compared to 0.2°C at M5 (Figure 4.6a). In winter (December-January-February), this pattern was reversed, when a mean air temperature of -36.4°C was found for M1 and M3, while M5 had a mean winter temperature of -35.1°C. The remainder of the mean monthly temperature data with overlapping time series (May 2013 to October 2015) at M1 and M3 showed a similar relationship to each other (Figure 4.6a).

Mean daily relative humidity values were greatest near the coast over the 10-month record when all three AWS were operating (July 2012 to April 2013), with a mean value of 88.7% at M5, 86.7% at M3 and 85.8% at M1 (Figure 4.6b). The remaining data from M1 and M3 between May 2013 and October 2015 were similar, with M3 an average of 0.58% higher relative humidly compared to M1.

Incoming solar radiation measurements were only ever available from two stations at once, but mean values were consistently lower towards the ocean. At the start of the measurement period, from July 2012 to April 2013, the mean incoming radiation at M5 was 48.0 W m^{-2}, compared to 62.7 W m^{-2} at M3 (Figure 4.6c). From May 2013 to July 2016, M3 consistently recorded higher incoming solar radiation during all months with daylight compared to M1. On average, the mean monthly solar radiation recorded at M3 was 14.66 W m^2 higher than at M1.

Wind speed and direction were recorded at M3-AWS from July 2014 to August 2018. Winds from the west were most frequent and comprised >21% of all recorded wind events (Figure 4.7). Winds from the south-east and south-south-east (>7.95% and >9% of all wind events, respectively) may be attributed to katabatic winds flowing down the Milne Glacier and being channeled along the fiord (Figure 4.1c). Winds from the north were less frequent, occurring <6% of the time. The highest wind speeds (>10 m s^{-1}) recorded at M3-AWS were encountered during storms with south-westerly winds, but were infrequent, occurring 0.13% of the time (Figure 4.7). Winds speeds between 6 and 8 m s^{-1}, however, make up ~2% of all wind events and tended to come from the south-west as well. These strong gusty winds are likely a result of the surrounding mountainous topography, where winds blow off the ice caps and glaciers flowing down the west side of Milne Fiord.

4.4.3 Long-term air temperature

The AWS installed in Purple Valley (Figure 4.1) provides meteorological observations over almost the entire mass balance observation period. Based on air temperature observations with complete years (January 1, 2010 to December 31, 2017), the mean annual air temperature was -18.58°C. From June 1, 2008 to August 31, 2017, the mean summer (June-August) surface air temperature was 1.71°C. The warmest summer on record was in 2012, when mean air temperatures reached 3.41°C (Figure 4.8a). The coolest summer occurred in 2013, with a mean

air temperature of -1.11°C, with August 2013 the coolest summer month on record, with a mean temperature of -3.57°C.

From this dataset the positive degree days (PDDs; cumulative annual total of daily above-freezing mean temperatures) were a mean of 227 yr^{-1}, with large inter-annual variability (Figure 4.8b). The years with highest PDDs were in 2011, 2012 and 2016, with PDDs >315 yr^{-1} and a maximum of 325 yr^{-1} in 2012. The lowest PDDs were recorded in 2013 at 105 yr^{-1}, followed by 119 yr^{-1} in 2014.

4.4.4 SAR and GPR analysis

The GPR profiles collected in May 2013 show layering from ~2 to ~20 m below the surface in the Outer Unit of the Milne Ice Shelf (Figure 4.9). Reflections in the glacier sub-surface can be caused by changes in water content, chemical impurities, crystal orientation, and ice density (Plewes and Hubbard, 2001). However the spatially extensive layering seen along the outer unit is most consistent with firn-ice transition (previous summer's glacier surface) that rises upwards to the surface towards the central unit (Figure 4.9b), a characteristic pattern observed between the boundary of firn zones on Arctic glaciers (e.g., Devon Ice Cap, Sylvestre et al., 2013; Austfonna, Dunse et al., 2009). Conversely, the GPR profiles recorded low backscatter across the Central Unit near the rear of the ice shelf (with the exception of a few point returns assumed to be from small crevasses), with only one strong near-surface layer at the snow ice interface from the last summer surface (Figure 4.9d). The lack of internal scatter below the surface indicates that no strong dielectric contrast was present in this part of the ice shelf, and therefore that there is little variability in the internal properties there. The 7 m long core extracted from the M1 site in May 2013 was composed of clear ice throughout, with no internal layering and densities of ~900 kg m^2.

The areas of subsurface layering detected in the 2013 GPR results correspond closely with the location of high SAR backscatter across the Outer unit of the Milne Ice Shelf in SAR satellite imagery (Figure 4.9a Inset). Based on the Radarsat-2 image of the ice shelf from March 2013, a 13 km transect from the northern edge of the Outer Unit to the southern edge of the Central Unit shows backscatter values ranging from –19.36 to –5.51 dB, with a mean of -8.09 dB (Figure 4.9a). The first 6 km of the transect (from the coast) had the highest backscatter values with an average of -6.17 dB. The remainder of the transect had relatively low backscatter values with an

average of -11.06 dB across the Central Unit. Additional SAR scenes from 1992, 1998, 2006, 2015 and 2018 show that the transition between high and low backscatter has remained in essentially the same position over the past 26 years (~17 km from the back of the ice shelf; Figure 4.10).

4.5 DISCUSSION

4.5.1 Mass balance of the Milne Ice Shelf

The mass balance of the Milne Ice Shelf exhibits a horizontal gradient with distance from the ocean, with net annual ablation generally corresponding with the location of the Central Unit and net annual accumulation corresponding with the location of the Outer Unit. The GPR transects, SAR backscatter analysis and ice core record are consistent with this pattern, with the Outer Unit primarily composed of meteoric ice with internal layering representative of net annual accumulation in the past, while the Central Unit is composed of solid ice with no internal layering, reflective of a region with net annual ablation. The internal layering present in the outer unit rises towards the surface with distance along the GPR transect towards the Central Unit (Figure 4.9ab), indicative of the long-term decrease in accumulation with distance from the ocean. This mass balance gradient is reflected in the thickness of the ice shelf, and how the thickness is changing over time. Based on GPR transects across the ice shelf in 2008/09, Mortimer et al. (2012) reported that the average ice thickness of the Outer Unit was 70-80 m, and ~50 m for the Central Unit. In terms of changes between 1983 and 2008/09, Mortimer et al. (2012; their Figure 4c) showed that the majority of the Outer Unit changed between -7.5 and +7.5 m, while the majority of the Central Unit changed by -15 to -30 m.

The marked difference in mass balance, physical characteristics and thickness suggests that, similar to a traditional glacier, the ice shelf can be divided into an accumulation zone (Outer Unit) and ablation zone (Central Unit), divided by a transition area or equilibrium line (EL; Mueller and Vincent, 2006). This is despite the fact that the ice shelf is almost completely flat and reaches a height of no more than ~10 m above sea level. These distinctions are particularly apparent in 2009, 2013 and 2014, when the Central Unit ablated while the Outer Unit accumulated (Figure 4.11). In these years the EL was positioned at approximately ~14 km from the rear of the ice shelf in 2009, ~9 km from the rear of the ice shelf in 2013 and ~14 km from the rear of the ice shelf in 2014 (Figure 4.11). This compares well with the GPR and SAR data

that show sub-surface layers tapering off and a distinct drop in the 1991-2018 mean backscatter values ~12-13 km away from the rear of the ice shelf, respectively (Figures 4.9 and 4.10f).

The reason for marked difference in mass balance between the Outer and Central units can be primarily attributed to the climatological gradient across the ice shelf, including changes in air temperature and solar radiation (Figure 4.6). Climatological observations at the Outer Unit show lower summer temperature and solar radiation compared to the Central Unit. The average rate of surface lowering, as recorded by the snow depth sounders between June 28, 2012 and August 9, 2012, was -3.52 cm day^{-1} at M3 (Central Unit) compared to -1.73 cm day^{-1} at M5 (Outer Unit; Figure 4.6d), with total cumulative losses of 147.68 cm and 72.83 cm, respectively. The mean gradient in summer mass balance across the ice shelf, derived from the average slope of the best fit lines for each mass balance year (Figure 4.4), is 3.2 cm w. eq. of additional melt per km, equivalent to ~64 cm w eq. more melt at the rear of the ice shelf compared to the front, on average. In contrast, the mean gradient in winter balance derived from the average slope of the best fit lines for each mass balance year (Figure 4.5), is only 0.5 cm w. eq. km^{-1}, equivalent to ~10 cm w. eq. more accumulation at the front of the ice shelf than the rear over its ~20 km length. Based on these differences, the summer balance gradient dominates over the winter balance gradient, which highlights the importance of summer melt on the spatial variability in surface mass balance.

The lower ablation rate across the Outer Unit is characteristic of the 'Arctic Ocean Effect', whereby the ocean acts as a local moisture source that leads to increased precipitation along a narrow zone along the coastline (Koerner, 1979; Braun, 2017). This moisture source also results in more frequent fog and low stratus clouds along the coastline, as often observed during fieldwork, which explains the consistently lower solar radiation inputs at the Outer Unit than the Central Unit. The biggest absolute difference in solar radiation input occurred in April, when mean solar radiation values were 55.4 W m^2 (30.8%) lower at M5 compared to M3. This is also the month when the largest difference in relative humidity occurred between these stations, with frequent near-coastal fog observed during fieldwork at this time of year.

The high incidence of coastal fog and low cloud has also been observed elsewhere near Sverdrup Glacier (north-west Devon Ice Cap), Ward Hunt Island and Meighen Ice Cap, where it has been suggested to be a factor in reducing ablation rates (Sagar, 1962; Paterson, 1969; Hattersley-

Smith and Serson, 1970; Koerner, 2005; Mueller and Vincent 2006). Koerner (2005) found that the mass balance gradient (from 1961-2003) was disrupted by limited ablation below 350 m at Sverdrup Glacier, and could possibly be linked to fog being generated from increasing open water (in summer) in Jones Sound. According to the spatial distribution of surface mass balance at Ward Hunt Ice Shelf, ablation stakes installed in marine ice sites that surround Ward Hunt Island had a significantly higher ablation (mean: 0.75 ±0.17 m w. eq.) compared to the stake clusters installed on meteoric ice sites nearer the ocean (0.29 ±0.05 m w. eq.). Mueller and Vincent (2006) suggested that the spatial variability in ablation could be linked to the distribution of fog. Walker Hill (450 m above sea level) on Ward Hunt Island acts as a topographic barrier that prevents fog from reaching the lee of the island, which allows increased solar radiation to reach the ice surface and increase ablation on the marine ice sites (Mueller and Vincent, 2006). According to Alt (1979), Meighen Ice Cap, lying at 268 m above sea level, owes its existence and positive mass balance years to synoptic conditions that produce fog.

Although our record is short, PDDs show large interannual variability, and the month of July accounts for the majority of summer warmth. There is a strong and significant relationship between PDDs and mean annual summer balance (R^2=0.64, p=0.017; Figure 4.8c). The one positive summer balance year in 2013 was associated with PDDs of 105 yr^{-1}, while the summer balance years that lost >-0.3 m w. eq. (2009/10, 2011, 2012, 2015, and 2016) had PDD totals >200 yr^{-1}. The lowest summer balance (-1.07 m w. eq.) in 2012 and was accompanied by PDDs of 325 yr^{-1}.

The relationship between PDDs and corresponding mass balance is similar to that observed on the St Patrick Bay Ice Caps, north-east Ellesmere Island, where positive mass balance years were associated with summer PDDs <190 yr^{-1} (Bradley and Serreze, 1987). In examining the connection between PDDs and ice shelf calving along the coastline of northern Ellesmere Island, Copland et al. (2007) found that periods of frequent ice shelf calving occurred between 1948 and 1963 when PDDs were typically >200 yr^{-1}, followed by a period of little calving when PDDs rarely exceeded 200 yr^{-1}. The period of increased ice shelf break up between the mid-1990s and mid-2000s occurred after PDDs returned to >200 yr^{-1}, with the complete loss of the Ayles Ice Shelf in 2005 when PDDs exceeded 300 yr^{-1} (Copland et al., 2007).

4.5.2 Historical changes

The consistency between areas of high and low backscatter in the GPR data and SAR imagery is in agreement with the study by Mueller et al. (2006), who used SAR imagery to map out glacier facies across the ice shelf. Similar to studies on Arctic glaciers (Engeset et al., 2002; Casey and Kelly, 2010), high backscatter in SAR imagery is indicative of the presence of firn in the accumulation area, whereas low backscatter indicates the presence of glacier ice in the ablation area. With the availability of SAR data from the past 26 years, this enables a determination of whether the location of the accumulation and ablation zones, and EL, have changed over time (Figures 4.10 and 4.11). This analysis indicates that the EL, defined as the boundary between the Outer and Central units, has remained in broadly the same position since at least 1992 (Figure 4.10). However, the area of the Central Unit has shrunk as a result of fracture development and propagation, and calving from the rear of the ice shelf (Figure 4.12).

Mortimer et al. (2012) measured area changes across the Milne Ice Shelf from 1950-2009, and revealed that the majority of losses occurred at the rear of the ice shelf, where the previous Inner Unit and part of the Central Unit deteriorated and were replaced by the epishelf lake, over an area totaling 59 km^2. Since 2009, the deterioration at the rear of the ice shelf has continued; between 2009 and 2018 the extent of the Central Unit has reduced by 9.8 km^2 (Figure 4.12), similar to the long-term loss rate of ~1 km^2 yr^{-1}. Area loss has also continued due to the expansion of marginal ice-dammed lakes both in the Central Unit and at the boundary of the Central and Outer Unit. The development and expansion of fractures that penetrate the Central Unit account for an additional ~2 km^2 of area loss. Unlike the rear of the ice shelf, the front of the ice shelf has remained quasi-stable since 1974 (Jeffries 1986b; Mortimer et al., 2012), although in 2012/13 a 3 km^2 portion of the ice shelf did calve away near Cape Evans (Mueller et al., 2017a). Similar recent observations of accelerated deterioration at the rear of an ice shelf have also been made at the nearby Petersen Ice Shelf, ~15 km south-west of the Milne, as thin meltwater-filled troughs fractured into individual ridges and became drifting ice islands (White et al., 2015; Mueller et al., 2017a). The Ward Hunt Ice Shelf, ~80 km to the east of the Milne, developed extensive fractures at its rear, between Disraeli Fiord and Ward Hunt Island (centrally located within the Ward Hunt Ice Shelf; Mueller and Vincent, 2003). By July-August 2008 the Ward Hunt Ice Shelf lost 25% of its adjacent lake ice cover, which was followed by ice shelf

break up along the northern edge and southern edge into Disraeli Fiord (Mueller and Vincent, 2003; Vincent et al., 2009).

4.5.3 Importance of surface vs. basal mass balance

Surface losses vary by region of the ice shelf, with cumulative losses amounting to 4.92 ±0.02 m w. eq. in the Central Unit and 1.47 ±0.16 m w. eq. in the Outer Unit over the period 2008-2017, compared to a mean cumulative loss for the ice shelf as a whole of 2.69 ±0.11 m w. eq. (Figure 4.3). However, these changes do not account for gains or losses from the basal surface. An estimate of these can be provided by making comparisons with the findings of Mortimer et al. (2012), who showed that the Milne Ice Shelf thinned by an average of 0.26 ±0.09 m w. eq. yr^{-1} between 1981 and 2008/2009. If the rate of mean annual surface mass balance (-0.30 ±0.02 m w. eq.) for the Milne Ice Shelf from 2008 to 2017 is compared to this rate, then the basal surface would be gaining mass at 0.04 ±0.11 m w. eq. yr^{-1}. However, the mean thickness changes calculated by Mortimer et al. (2012) were not uniform across the ice shelf, with the Central Unit reducing in thickness by ~0.37 m w. eq. yr^{-1}, whereas the Outer Unit thinned by ~0.10 m w. eq. yr^{-1}. Based on a mean annual surface mass balance of -0.16 ±0.03 m w. eq. yr^{-1} (2008-2017) for the Outer Unit and -0.55 ±0.006 m w. eq. yr^{-1} for the Central Unit, this suggests that recent mass balance changes on the ice shelf can be explained entirely by surface processes. Of course, differences in measurement periods and methods between the studies makes direct comparisons difficult, but this simple calculation indicates that basal melt may not be as important to overall thinning as previously thought, at least over the past 10 years (c.f., Mortimer et al., 2012; Braun, 2017).

4.6 CONCLUSIONS

Our findings indicate that the mass balance of the Milne Ice Shelf is predominantly controlled by the microclimatology that exists as result of the ice shelf position within Milne Fiord. The persistence and relative stability of the Outer Unit is linked to cooler temperatures, lower solar radiation and higher snowfall, which have suppressed ablation. In contrast, the Central Unit is subject to warmer temperatures, higher solar radiation and lower snowfall. Past studies have shown that input from tributary glaciers contributed to portions of the Central Unit (Jeffries 1986b; Mortimer et al., 2012; Richer-McCallum, 2015), but since 2011 all but one of these tributary glaciers have become disconnected and are no longer a significant source of

replenishment (Mortimer et al., 2012; Figure 4.12). The lack of glacier inflow, in combination with relatively warmer temperatures and higher solar radiation input, have led to higher rates of ablation compared to the Outer Unit.

The Milne Ice Shelf is a remnant of what was once the continuous Ellesmere Ice Shelf that fringed the northern coast of Ellesmere Island at the start of the 20th century and developed under colder conditions of the past (Vincent et al., 2001). Although the Milne Ice Shelf has undergone changes over the past century, it is more stable than any of the other ice shelves on northern Ellesmere Island. The physiography of Milne Fiord likely assists with this, by providing points of stability along its margins where the ice shelf connects with the walls of the fiord (Jeffries 1986a; Veillette et al 2008). This relative stability is changing, however, as marginal lakes expand and the rear of the ice shelf starts to disintegrate. If the current rate of ice loss (0.16 ±0.03 m w. eq. yr^{-1}.) is assumed to remain constant, the ~63 m thick Outer Unit (Mortimer et al., 2012) would take >350 years to disappear from surface ablation alone. In contrast, the Central Unit would disappear in only ~74 years from surface ablation alone with a mean thickness of ~45 m (Mortimer et al., 2012) and mean surface mass balance rate of -0.55 ±0.006 m w. eq. yr^{-1}. However, the Milne Ice Shelf, which is already heavily fractured (Figure 4.1), is likely to break up well before these dates when the occurrence of calving events observed over the past ~40 years is included, particularly from the inland portion of the Central Unit (Mortimer et al., 2012; Mueller et al., 2017a). The break-up from the back of the Central Unit also demonstrates that the ice shelf becomes increasingly unstable and easier to fragment as it continues to thin. Therefore, as the climate continues to warm, it seems likely that the Central Unit of the Milne Ice Shelf is likely to disappear by the middle part of this century, and the Outer Unit by the end of it, if not before.

Table 4.1: Mean winter, summer and net balances for each year or period.

Balance year or period	Number of Stakes		Number of snow pits[b]	Winter accumulation (m w. eq.)[c]	Summer ablation (m w. eq.)	Net balance (m w. eq.)
	Outer unit	Central unit				
2008	3	1	4	0.25	-0.38	-0.13
2009/10[a]	4	1	5	0.26	-0.34	-0.09
2011	4	4	8	0.18	-0.62	-0.44
2012	3	1	**4**	0.05 ±0.020	-1.07	-1.01 ±0.020
2013	3	2	5	0.09	0.06	0.15
2014	4	2	**6**	0.12 ±0.060	-0.17	-0.04 ±0.060
2015	4	2	**6**	0.03 ±0.010	-0.66	-0.63 ±0.010
2016	2	2	**4**	0.01 ±0.004	-0.36	-0.35 ±0.004
2017	2	2	**4**	0.03 ±0.020	-0.18	-0.15 ±0.020

[a]The field site was not visited in 2010, therefore the summer and winter balance were calculated from the two-year average.
[b]Values in bold represent sites visited in summer when only snow depths were recorded.
[c]Error range represents the range of densities (i.e., 300-700 kg m^3) for sites that were visited in summer when only snow depth was recorded.

Table 4.2: Satellite imagery used in this study.

Sensor	Date, time (UTC) (YYYY-MM-DD, HH:MM:SS)	Resolution (m)
SAR		
ERS-1 Standard (VV)	1992-01-29, 00:11:05	12.5
Radarsat-1 Standard (HH)	1998-04-16, 22:15:02	12.5
Radarsat-1 Standard (HH)	2006-01-14, 19:50:16	12.5
Radarsat-2 ScanSAR wide (HH)	2013-03-26, 21:33:19	50.04
Radarsat-2 ScanSAR wide (HH)	2015-03-22, 20:17:20	50.05
Radarsat-2 Fine wide (HH)	2018-11-27, 14:19:02	6.87
Optical		
ASTER L1T	2009-07-10, 21:18:07	15.02
ASTER L1T	2012-07-15, 22:25:09	15.01
Landsat-8 (OLI)	2018-07-23, 19:45:39 to 19:46:11	15 (Pansharpened)
MODIS	2015-07-09, 01:40:00	256

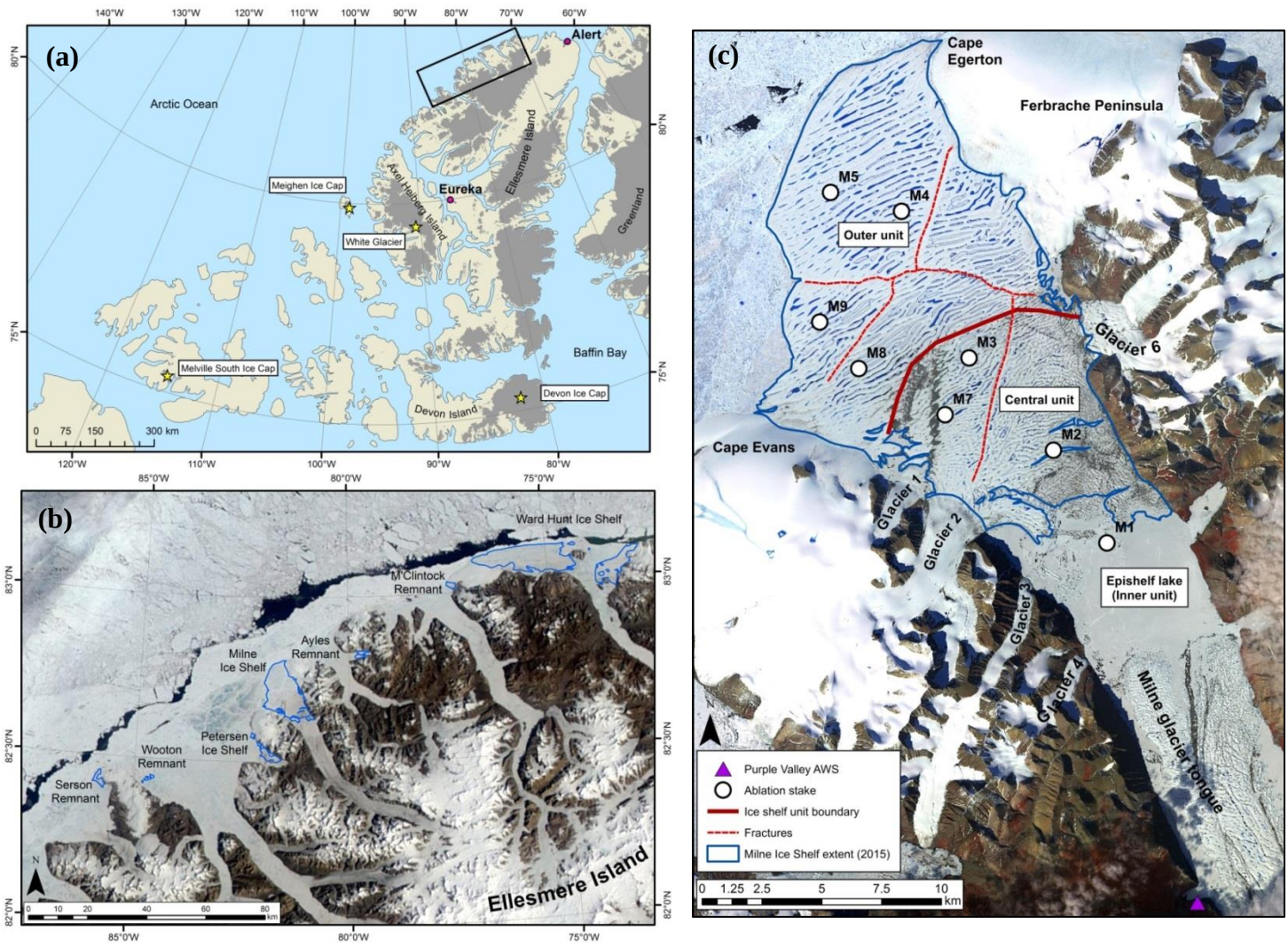

Figure 4.1: (a) Location of study area (in black box) in the Queen Elizabeth Islands. (b) Ellesmere Island ice shelves and ice shelf remnants as of 2015 (Mueller et al, 2017b) Base image: MODIS, July 9, 2015. (c) The Milne Ice Shelf showing its 2015 extent (Mueller et al, 2017b), the location of each mass balance site and the unit boundaries (i.e. outer, central and inner units) first described by Jeffries (1986b). Base image: Landsat-8, July 31, 2018. Note: the M1 site and automatic weather station are located on an ice island that drifted to the south of the main ice shelf in summer 2012.

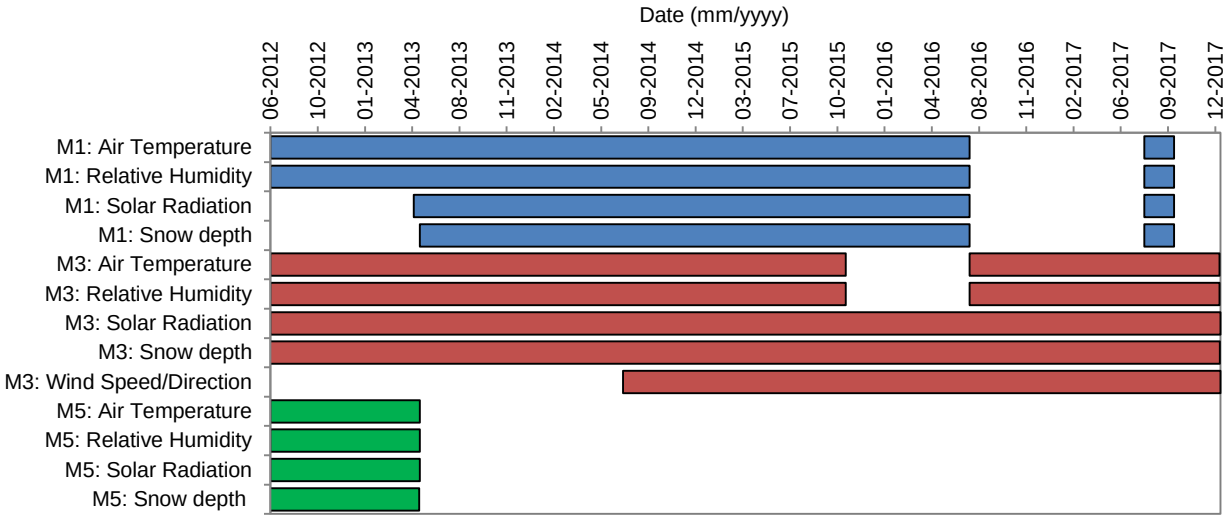

Figure 4.2: Measurement periods at AWS-M1, AWS-M3 and AWS-M5.

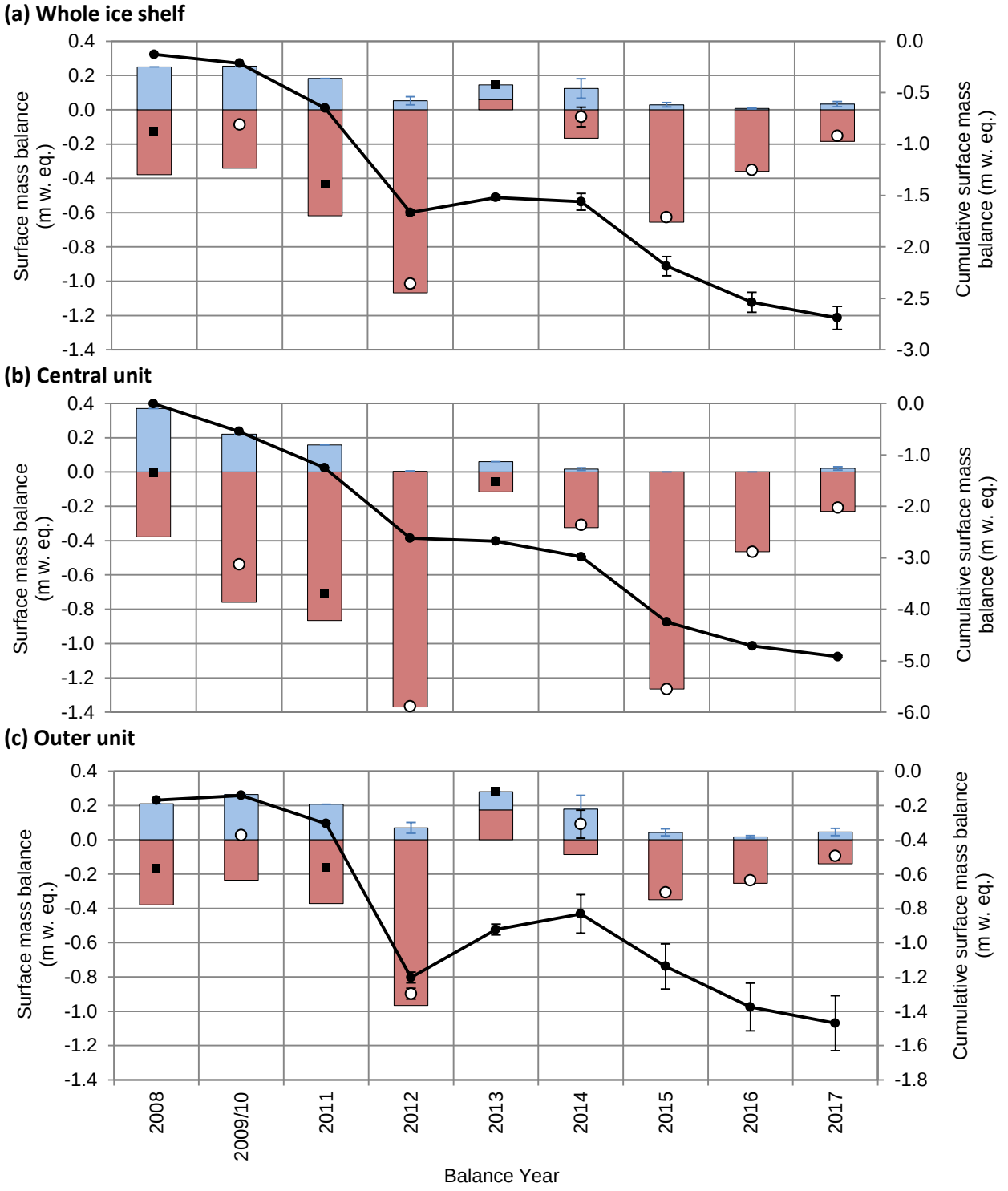

Figure 4.3: The 2008-2017 mean annual and cumulative surface mass balance of (a) the entire Milne Ice Shelf, (b) Central Unit of the ice shelf, (c) Outer Unit of the ice shelf: winter (blue bar), summer (red bar), annual mass balance (black square), estimated annual mass balance (where winter balances are a range; white circle) and cumulative mass balance (black line). The summer balance for 2009/10 is the average of the 2-year period.

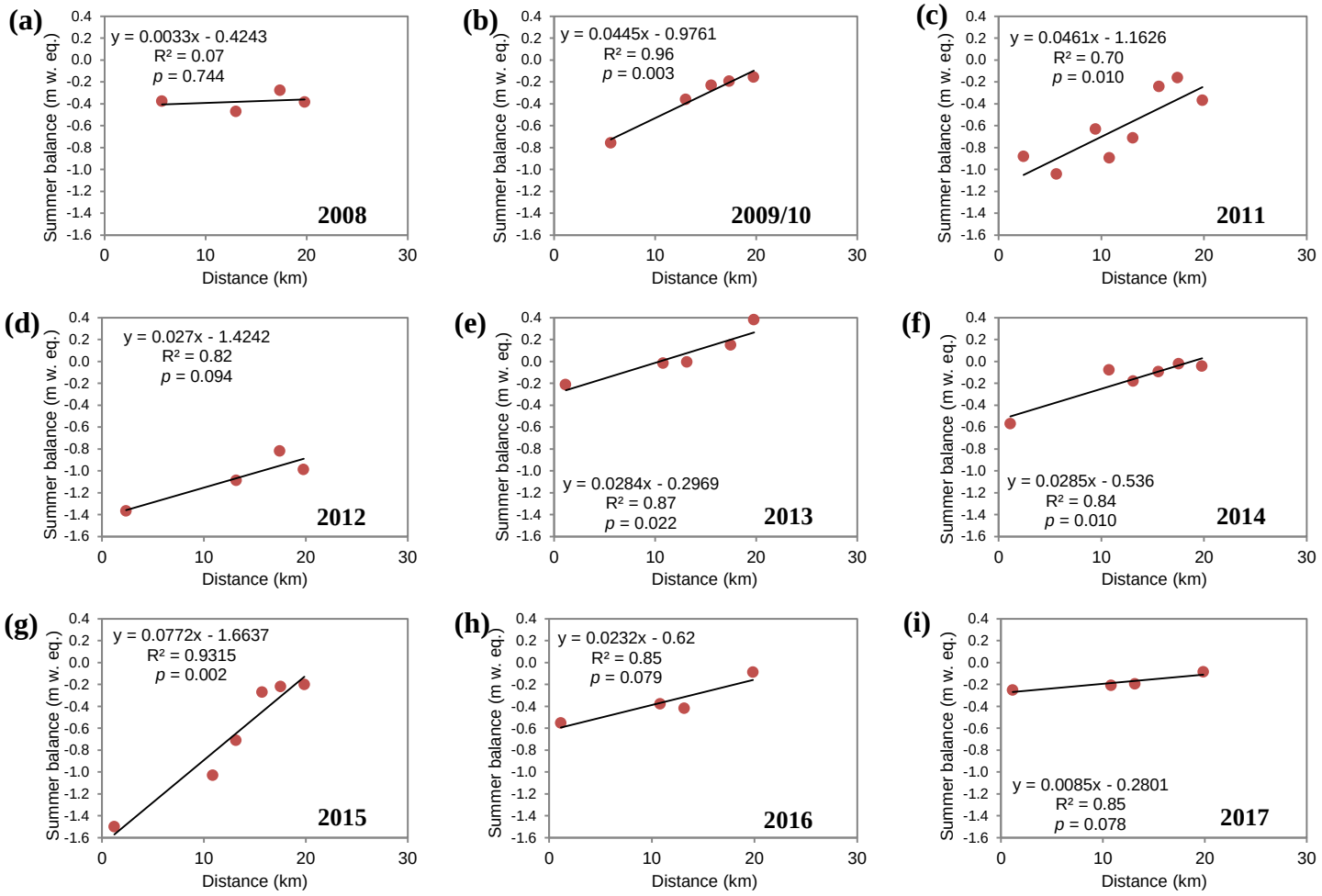

Figure 4.4: Summer balance measured at each ablation stake across the Milne Ice Shelf, plotted as a function of distance from the rear of the ice shelf, for balance year: (a) 2008; (b) 2009/10; (c) 2011; (d) 2012; (e) 2013; (f) 2014; (g) 2015; (h) 2016; and (i) 2017. The average slope of the best fit line for 2008-2017 is 0.0319x.

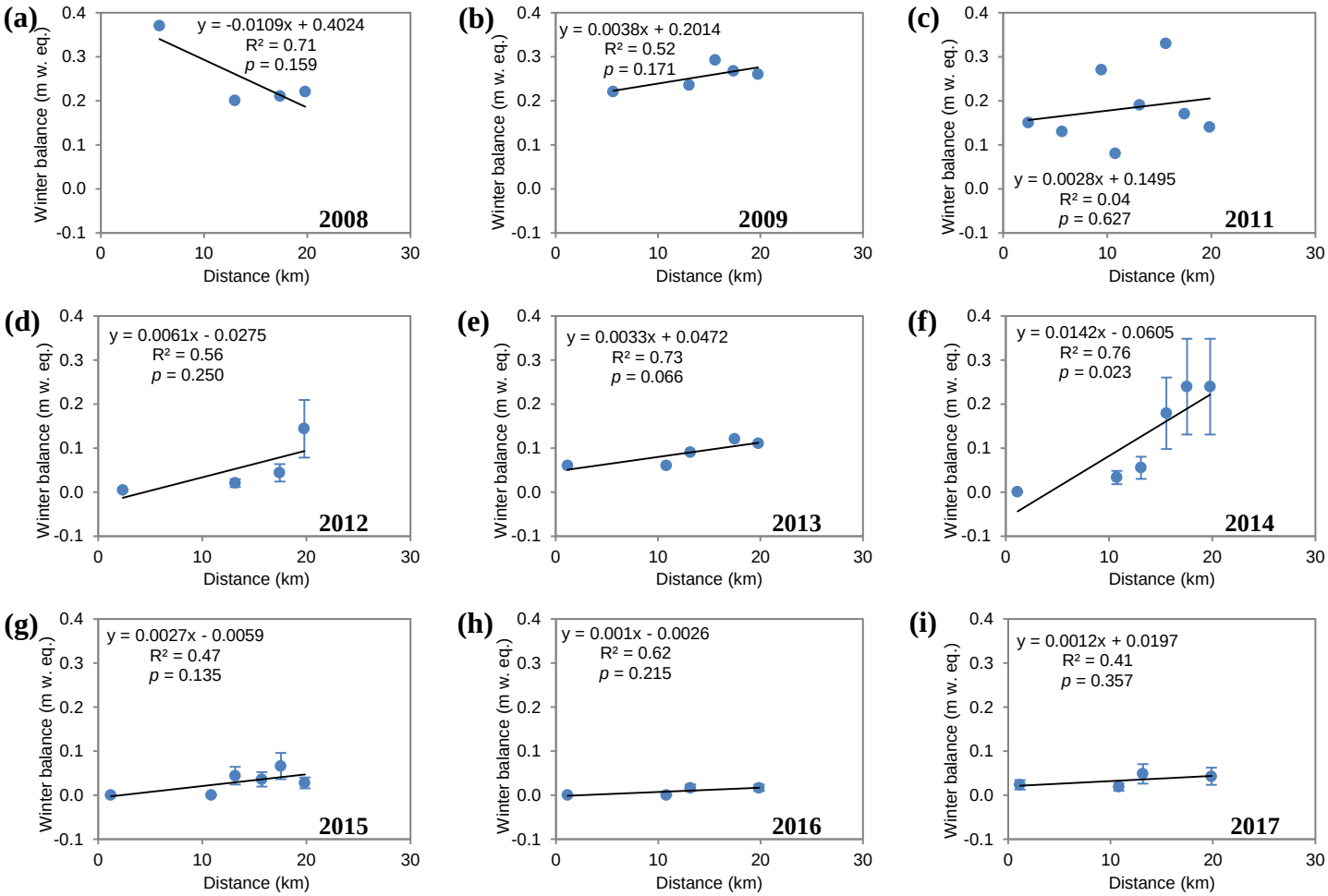

Figure 4.5: Winter balance measured at each ablation stake across the Milne Ice Shelf, plotted as a function of distance from the rear of the ice shelf, for balance year: (a) 2008; (b) 2009/2010; (c) 2011; (d) 2012; (e) 2013; (f) 2014; (g) 2015; (h) 2016; and (i) 2017. The error bars represent the range of snow densities applied to snow depth measurements in years when density was not measured in the field. Winter balance measurements were not made in 2010. The average slope of the best fit line for 2008-2017 is 0.0051x

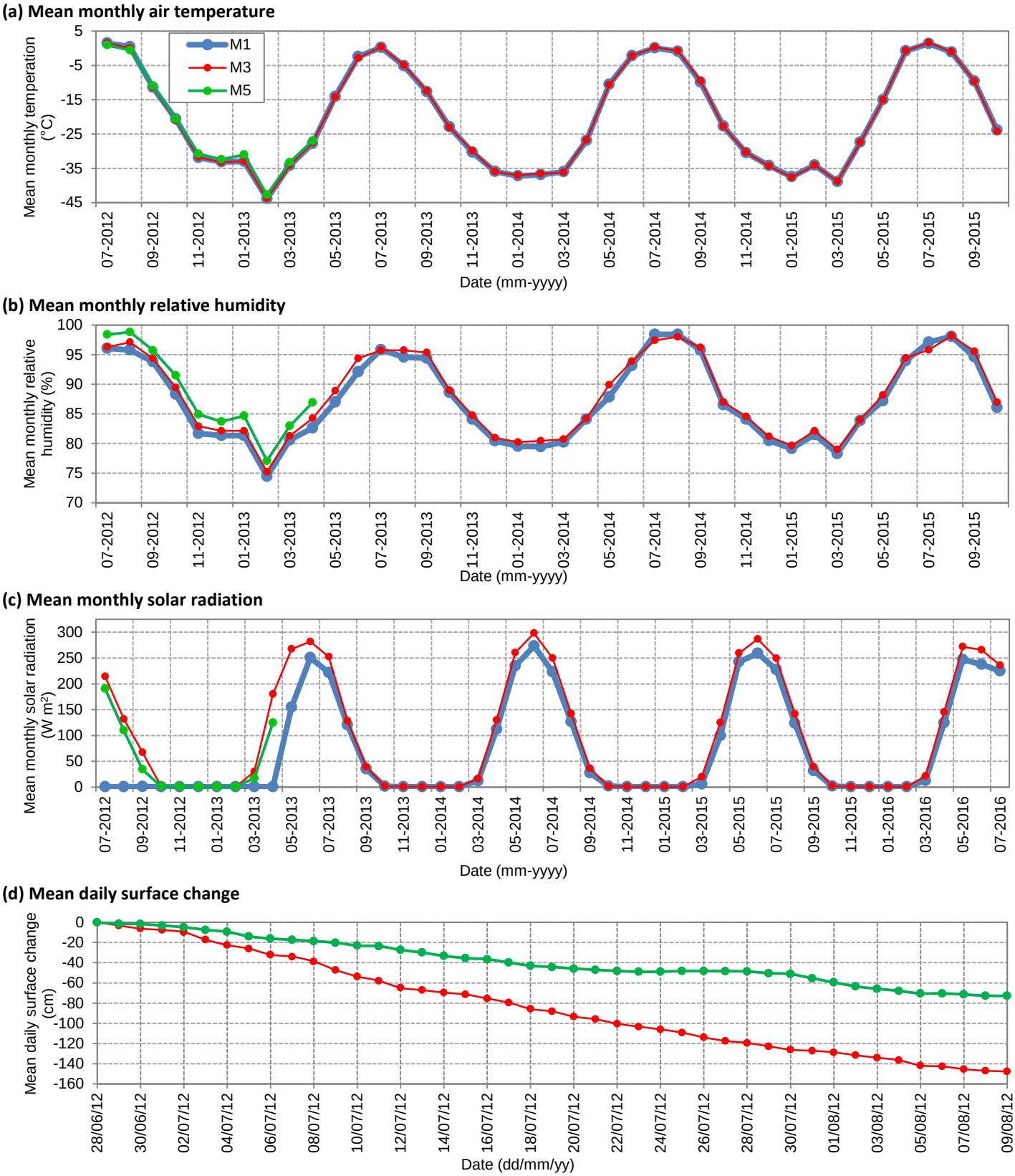

Figure 4.6: Mean monthly observations from M1-AWS, M3-AWS and M5-AWS of: (a) air temperature, (b) relative humidity, (c) incoming solar radiation, and (d) mean daily surface change recorded from the snow depth sounders at M3-AWS and M5-AWS.

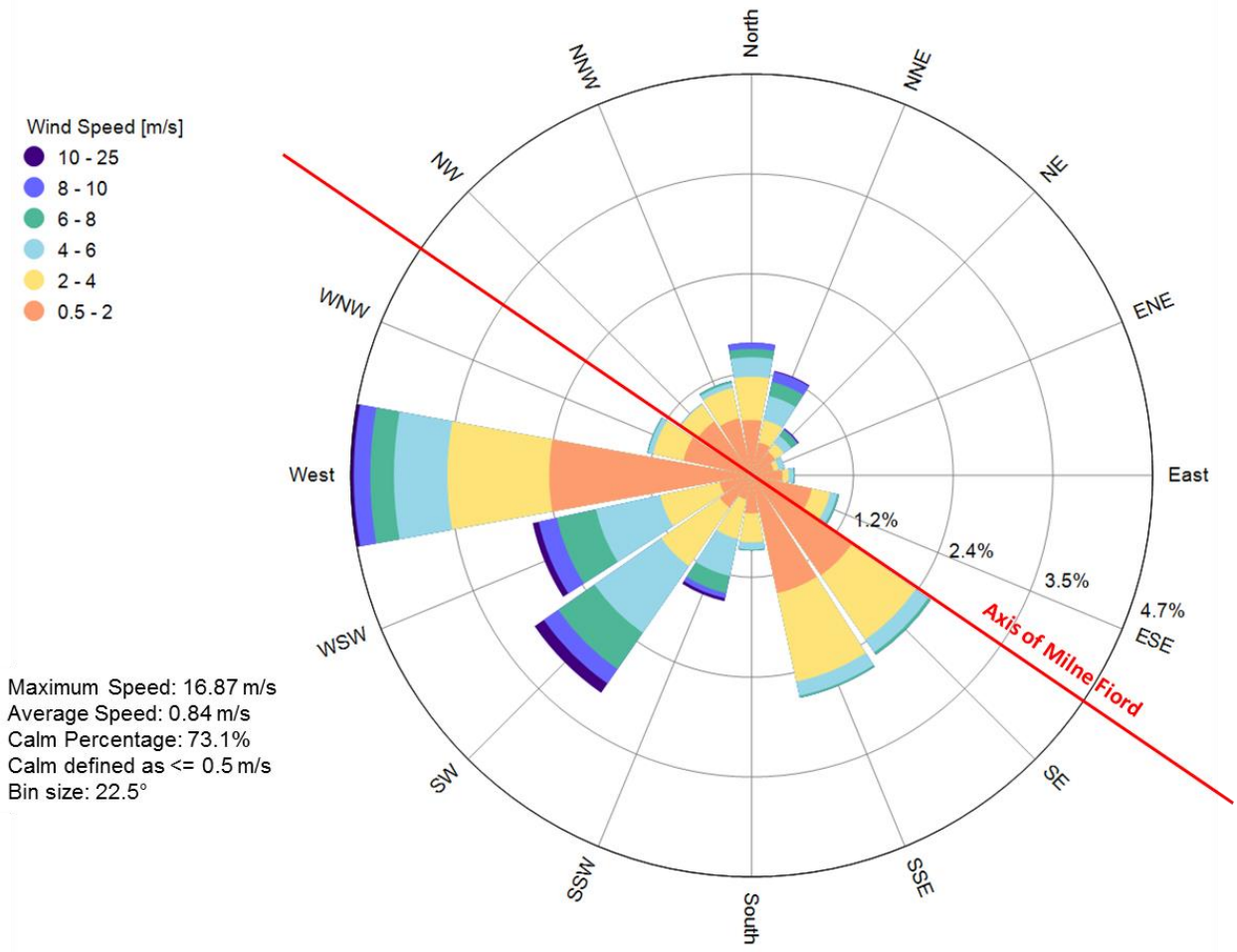

Figure 4.7: Frequency (%) of wind speed from each direction at AWS-M3 from July 15, 2014 to July 8, 2018, based on hourly measurements.

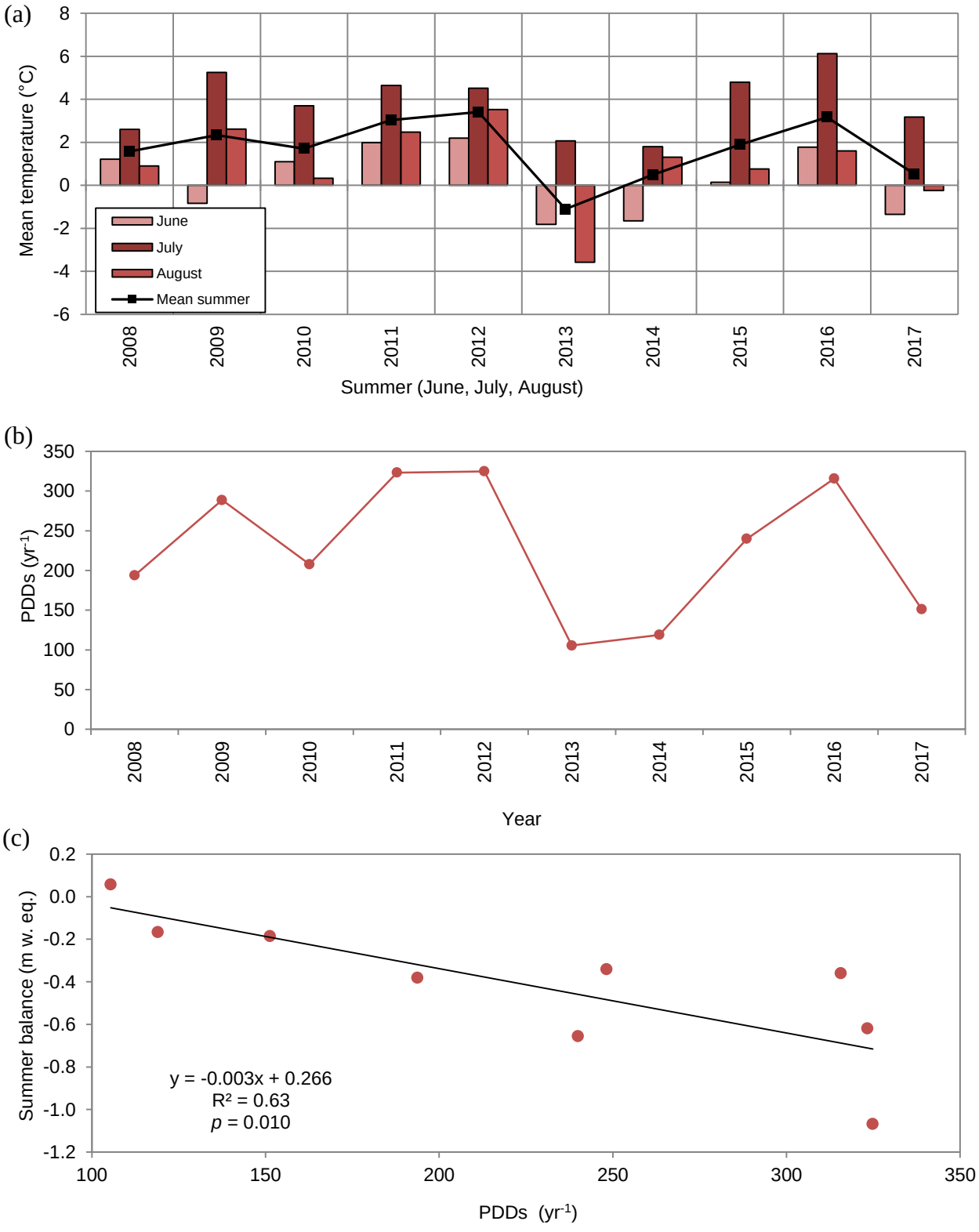

Figure 4.8: Surface air temperatures for the Milne Ice Shelf derived from AWS-PV (2008-2017): (a) mean summer surface air temperatures; (b) annual PDDs and (c) relationship between PDDs and mean annual summer balance.

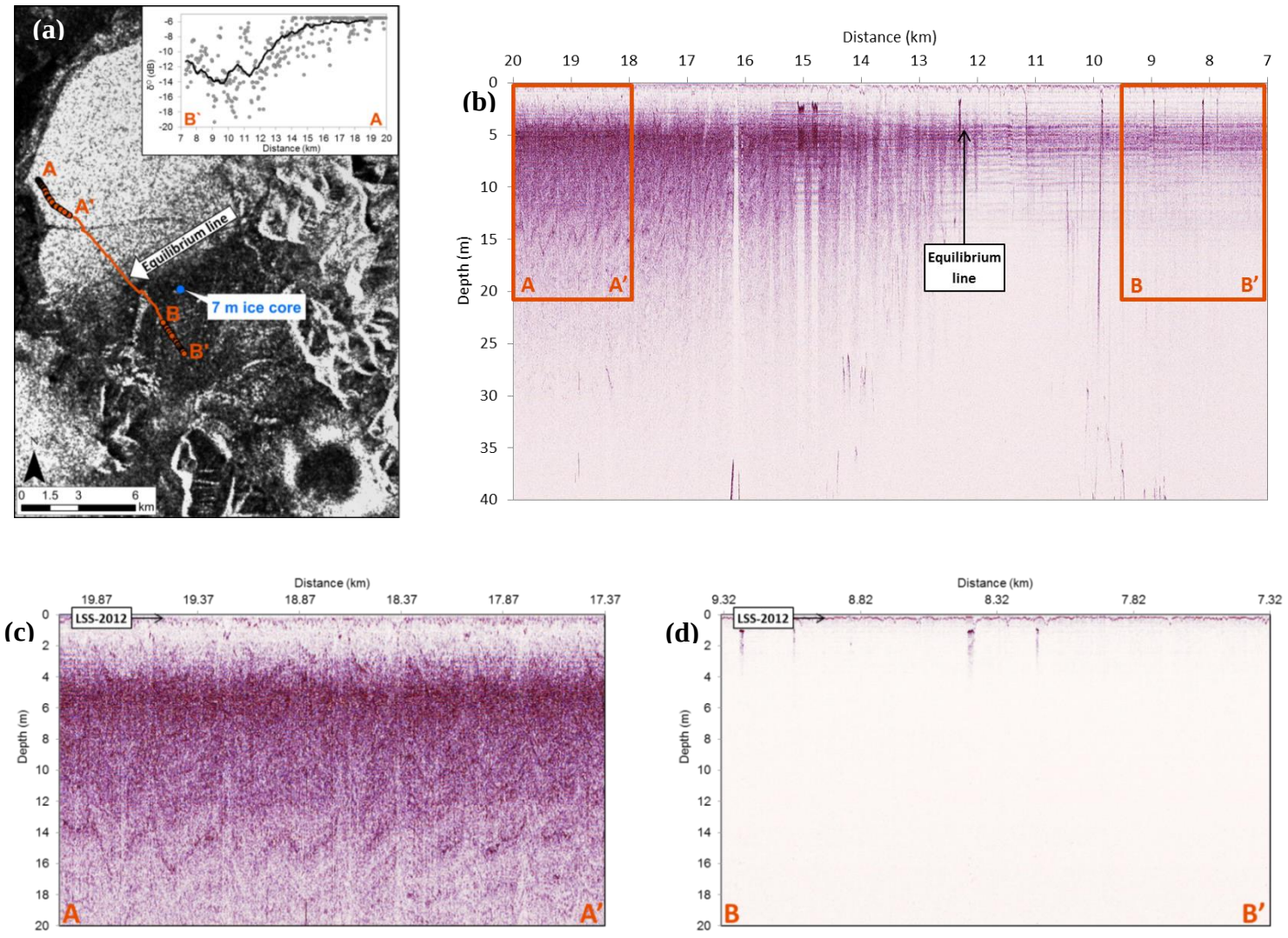

Figure 4.9: (a) Location of the 500 MHz GPR transect collected in May 2013 across the Milne Ice Shelf (base image: Radarsat-2 ScanSAR wide, HH, March 26, 2013, 21:31:19); (b) ~13 km long transect (A to B') spanning from the Outer Unit to the Central Unit; (c) 2.68 km long transect (A to A') along the Outer Unit that shows strong sub-surface layering, including the last summer surface from 2012 (LSS-2012); (d) 2.01 km long transect (B to B') along the Central Unit of the Milne Ice Shelf. Approximate position of the EL (a, b) is indicated where sub-surface layering reaches the surface. Inset graph (a): backscatter values (σ^0) with a 35 m running average, extracted from the SAR image along the GPR transect. Horizontal axis represents distance away from the rear of the ice shelf.

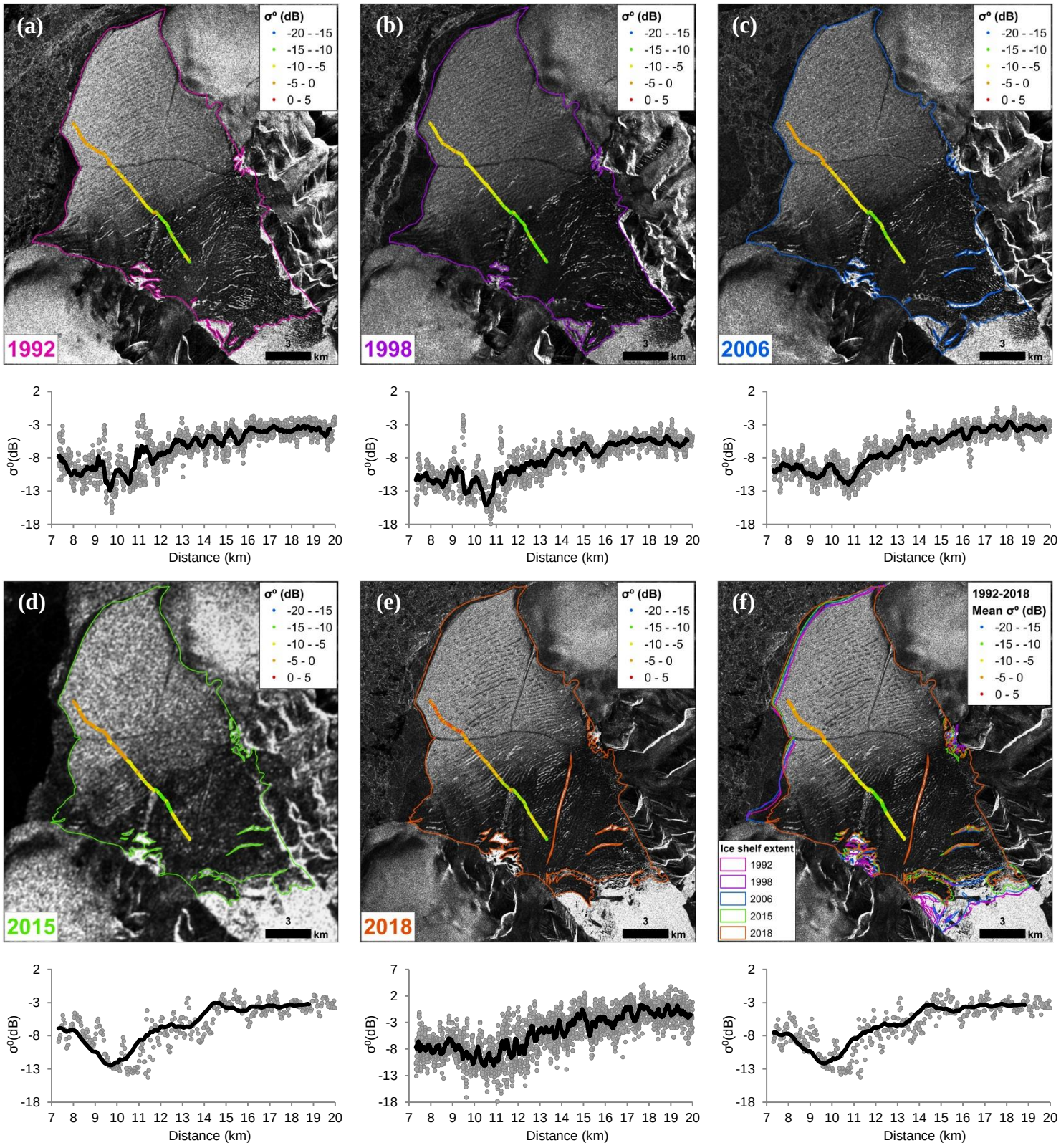

Figure 4.10: Backscatter values extracted from a 13 km long transect extending from the Outer Unit to the Central Unit: (a) ERS-1: January 29, 1992; (b) Radarsat-1: April 16, 1998; (c) Radarsat-1: January 14, 2006; (d) Radarsat-2: March 22, 2015; (e-f) Radarsat-2: November 27, 2018. Ice shelf outlines from 1992-2015 from Mueller et al. (2017b). Each graph shows the backscatter values (σ^0) with a 35 m running average, extracted from each transect for each year (a-e) and the average of these values from 1992-2018 (f). The distance on the horizontal axis represents the distance from the rear of the ice shelf.

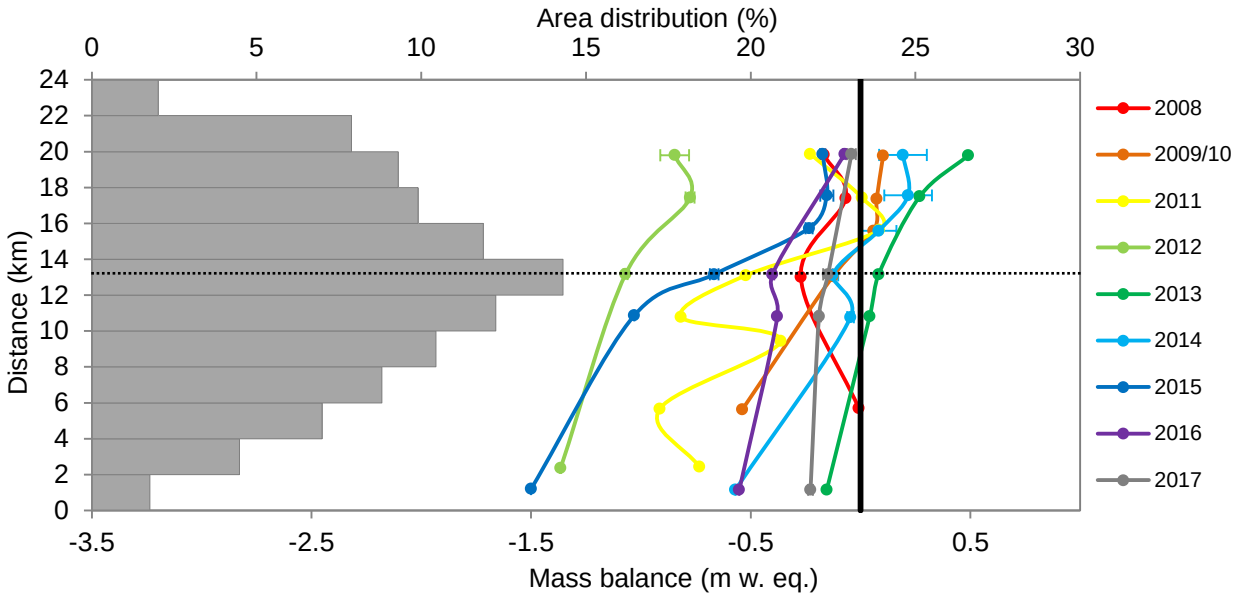

Figure 4.11: Horizontal gradients in net annual mass balance for the Milne Ice Shelf derived from point balance observations for balance years 2008 to 2017. Gray horizontal bars represent the area-distance distribution of Milne Ice Shelf in winter 2015 (Mueller et al., 2017b). The black dotted line shows the approximate position of the long-term EL based on the backscatter brightness in 2013 (Fig. 4.9a). Distance is from rear of the ice shelf; 24 km is the seaward edge.

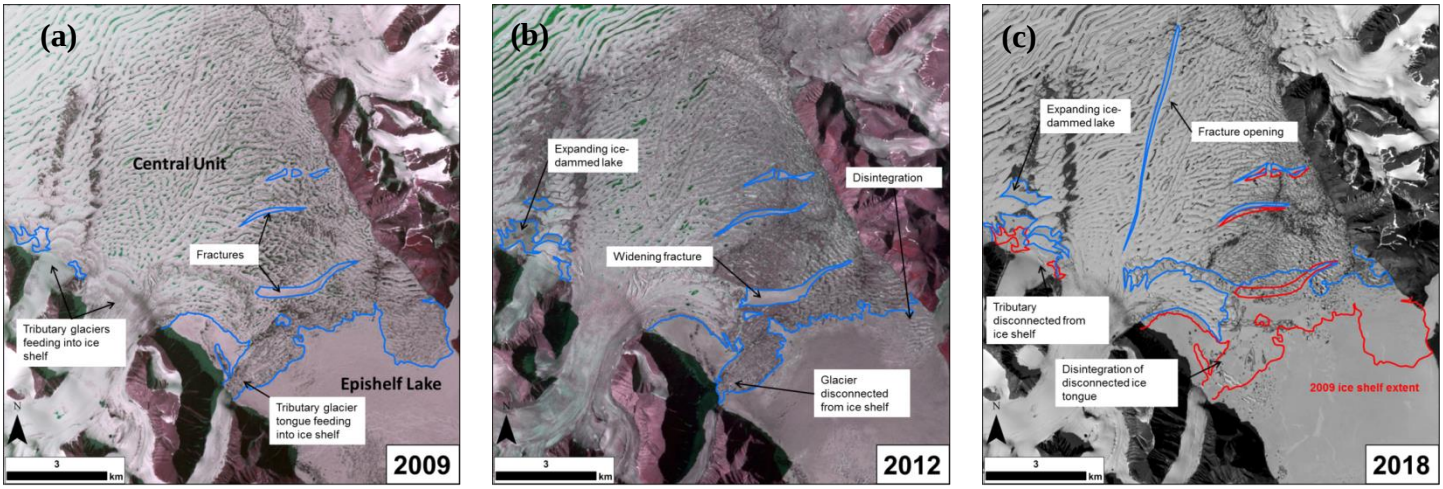

Figure 4.12: Temporal changes in the Central Unit of the Milne Ice Shelf, highlighting the development and widening of fractures, and the decrease in the extent of the ice shelf: (a) ASTER L1T, 2009-07-10; (b) ASTER L1T, 2012-07-15; and (c) Landsat-8, 2018-07-31 (panchromatic band).

CHAPTER 5: CONCLUSIONS

5.1 SYNTHESIS

This study has demonstrated the impact that climate change is having on the glaciers across Northern Ellesmere Island. Remote sensing measurements were used to describe the spatial and temporal variations in glacier area change across this region, with a particular focus on the marine-terminating glaciers in Yelverton Bay. Field measurements were used to examine the processes controlling the mass balance across one of the few remaining ice shelves on the northern coast of Ellesmere Island. The thesis began by setting the glaciological context for recent area changes by describing different glacier responses to climate warming. Next, the factors influencing the recent loss of glacier ice tongues in the Yelverton Bay region were investigated in relation to climatological and oceanographic forcings. Finally, the mass balance of the most stable remaining ice shelf was calculated and compared with local climatology to examine the current stability and implications for future change.

The first goal of this study was to create a comprehensive inventory for all glaciers and ice shelves on Northern Ellesmere Island, which includes area measurements derived from optical satellite imagery in ~1999 and ~2015. This inventory also includes updated basin delineations that were automatically generated using the high-resolution ArcticDEM and manually refined using optical satellite imagery. In addition, the ArcticDEM was used to create terrain parameters for each glacier basin (i.e., elevation, slope, aspect). The new inventory enabled the calculation of glacier area changes in relation to the unique characteristics of all 1773 glaciers. Regional ice coverage decreased by ~5.9% over the 16 years, and ice shelves had the highest losses relative to their size (~42.4% decrease). Statistical analysis revealed that the highest shrinkage rates occurred on small glaciers with lower mean elevations and shorter flow lengths (i.e., small ice caps), a trend that is consistent with area change measurements for Northern Ellesmere Island between ~1960 and ~2000 (Sharp et al., 2014). The loss of small ice caps has also been identified from area measurements on nearby Axel Heiberg Island, where 90% of ice masses <0.2 km^2 disappeared between 1958 and 2000 (Thomson et al., 2011). Changes in marine-terminating glaciers and ice shelves highlighted the marked loss of 19 ice tongues and the

complete loss, or substantial loss, from most ice shelves. Several ice tongues were lost from the Yelverton Bay region, although the nearby Milne Ice Shelf remained relatively stable. These observations motivated the studies in Chapters 3 and 4.

To better understand the patterns and causes of ice tongue changes, aerial photography and optical satellite imagery were used to document their changes in the Yelverton Bay region since 1959, including an assessment of changes in the surrounding marine ice (i.e., sea ice, sikussak, and mélange). From 1959-2017, the total ice tongue area decreased by ~89% (49.07 km^2), with >60% of losses occurring from 2005-2009. Ice tongue losses since 2005 were initiated when the multi-year landfast sea ice (MLSI) abutting their termini was replaced by open water and first-year ice, and mean mid-depth (i.e., 100 and 200 m; 2006-2012) ocean temperatures were nearly 1°C warmer than between 1999-2005. The loss of MLSI from within the study region began a cascade of changes that led to the break-up of the sikussak and ice tongues. Despite the recent decrease to pre-2006 ocean temperatures, open water continues to occur in the summer in the Yelverton Bay region, which prevents the regrowth of MLSI and therefore ice tongues, meaning that their losses are likely to continue in the future.

The ice shelf measurements captured in the first part of this study showed that the Milne Ice Shelf had undergone relatively little change in its area compared to its counterparts, and that the changes have been concentrated at its landward (southern) edge. A 10-year record of ablation stake and snow measurements reveals a marked surface mass balance gradient across the ice shelf, whereby ablation decreases with proximity to the seaward margin. The ablation gradient is reflected in the microclimatology recorded at three automated weather stations sites installed across the ice shelf, with air temperature and solar radiation decreasing towards the coastline, while snow accumulation and humidity increases. The lower solar radiation inputs and increased humidity are consistent with near-coastal fog, which has been observed during field work in spring and summer. The presence of a long-term mass balance gradient is apparent from ground-penetrating radar (GPR) measurements that show sub-surface layering limited to the outer unit of the ice shelf, indicative of a region of long-term net accumulation. As a result of this mass balance gradient, the ice shelf has demonstrated relative stability and greater thicknesses across its seaward half, with some positive annual mass balance years over the past decade. The

landward side of the ice shelf, however, is thinnest and weakest, with strongly negative mass balance over the past decade, which has resulted in area losses that are likely to continue.

The combined results provide some insight into the response of land-terminating glaciers, marine-terminating glaciers and ice shelves on Northern Ellesmere Island to a changing climate. Overall, the ice coverage over Northern Ellesmere Island has decreased by ~5.9% since 1999, and this change is linked to long-term (1948-2016) increases in temperature, particularly in fall and winter (0.74 and 0.65°C decade^{-1}, respectively), but also in summer where mean temperatures have become positive since 2007. Based on the ELA trend surface modeled by Miller et al. (1975) for 1960, 35.2% of the ice-covered areas in 1999 were in the ablation area. Long-term mass balance measurements from White Glacier, on Axel Heiberg Island, have shown a ~200 m rise in the ELA since 1999 (Thomson et al., 2017). If this is taken as an indication to how ELA heights have changed on Northern Ellesmere Island, then 60.2% of the ice cover is now in the ablation zone. This helps to explain the cause of the rapid loss of small ice caps at lower elevations, including the complete loss of three ice caps observed in this study. Miller et al. (1975) and Wolken et al. (2008) also described the northern coastline of Ellesmere Island as having some of the lowest ELA levels (<200 m) in the Canadian Arctic in 1960, an attribute that has facilitated the persistence of ice shelves and floating termini (Braun et al., 2004). However, the northern coast of Ellesmere Island has undergone substantial changes to its marine environment in recent decades (e.g., loss of MLSI and increased open water), and recent changes in the ice shelves and ice tongues highlighted here show that this region is unlikely to be able to sustain a permanent floating ice cover into the future.

5.2 KEY CONTRIBUTIONS

This thesis has provided several key contributions to Canadian Arctic glaciology. First, the glacier area database offers a comprehensive record of ice area and ice area change (in ~1999 and ~2015) for all glaciers and ice shelves across northern Ellesmere Island. This study builds upon the Global Land Ice Measurements from Space database by manually correcting individual basin divides and extents in ~1999 and extending this database to ~2015. Furthermore, for the first time, this study provides a temporal and spatial analysis of how glacier area is changing based on ice type (i.e., land-terminating, marine-terminating, marine-terminating ice tongue, and ice shelf), physiography and location.

Second, this thesis, for the first time, quantifies and analyses the loss of glacier ice tongues in the Yelverton Bay region. The results of this study highlight the importance of changing marine ice conditions on the stability of floating glacier tongues. These findings contribute to a growing body of literature documenting the role of sea ice and ice mélange or sikussak on glacier tongue stability, that up until now has been primarily focused on Greenland and Antarctica (e.g., Amundson et al., 2010; Cassotto et al., 2015; Moon et al., 2015; Miles et al., 2017).

Third, the 10-year record of mass balance and climate measurements across the Milne Ice Shelf conducted in this study provides new insight into mass balance processes across an Arctic ice shelf. Previous mass balance studies for the Ellesmere ice shelves had been limited to intermittent records between 1951 and 2000 on the Ward Hunt Ice Shelf, and a single year of surface mass balance measurements across the Petersen Ice Shelf (Braun et al., 2004; White et al., 2015). Furthermore, the surface mass balance records from Ward Hunt were mostly derived from stake-farms that did not properly capture the spatial variability in surface mass balance. For the first time, Chapter 4 suggests that much like a traditional mountain glacier, the Milne Ice Shelf has a surface mass balance gradient, except that rather than varying with elevation, the surface mass balance varies with distance from the ocean front. This study proposes that fog may be an important mechanism for preserving winter accumulation and suppressing summer ablation from the seaward margin of the Milne Ice Shelf, while the landward margin is exposed to higher air temperatures and high inputs of solar radiation, resulting in increased thinning and calving. Based on the surface ablation patterns shown for the Milne Ice Shelf and described in previous studies (i.e., Mueller and Vincent, 2006; Mortimer et al., 2012; White et al., 2015; Mueller et al., 2017a), Ellesmere Ice Shelves appear to be particularly prone to break-up from their landward margins. This pattern seems to be unique to this part of the world, as all other ice shelves in Antarctica break up from their seaward margin.

5.3 FUTURE RESEARCH DIRECTIONS

This thesis shows the importance of long-term glacier monitoring programs to understand how glaciers are changing. Long-term area change and annual mass balance measurements help quantify glacier losses and the pace of these losses. The Northern Ellesmere glacier inventory for ~1999 and ~2015, and the 10-year surface mass balance record for the Milne Ice Shelf collected for this thesis, provide baselines from which future measurements can be made. Currently, there

are no mass balance reference glaciers for Northern Ellesmere Island, which limits the ability to incorporate their variations into regional mass balance estimates, so the mass balance monitoring of the Milne Ice Shelf should be continued and data contributed to the World Glacier Monitoring Service. It is essential that long-term records such as these continue to be built upon to monitor changing glacial landscapes in a warming climate.

In Chapter 3, the TOPAZ4 Arctic Ocean Reanalysis dataset, supplied by Copernicus Marine Environment Monitoring Service, was used to generate ocean temperatures in the Yelverton Bay region. However, this ocean database contains no direct measurements for model validation from the northern coast of Ellesmere Island, which highlights the need to collect oceanographic data in this region to create improved models and capture ocean changes through time. Ocean temperature data also needs to be collected data from within glacial fiords, to assess the extent to which any offshore oceanic changes may be transmitted to the glacier front. The role of changing ocean temperatures is particularly important in areas such as the northern coast of Ellesmere Island, where floating glacier and sea ice cover have recently changed, after years of permanence and semi-permanence.

The relationship between surface mass balance and climate for the Milne Ice Shelf suggests that decreasing solar radiation and air temperature with proximity to the seaward edge influence the surface ablation gradient. These observations, however, were based on limited climatological data (June 2012 to April 2013) due to instrument failure from the northernmost station. Further study could use satellite imagery and time-lapse photography to investigate the detailed role of fog in these processes, and investigate whether the frequency of fog is changing over time in response to the increased frequency of open water along the northern coastline.

Surface mass balance across the Milne Ice Shelf has provided reliable estimates of surface lowering, although basal measurements are necessary to quantify the full controls on ice shelf mass balance. In Chapter 4, a comparison of recent mass balance measurements and those of Mortimer et al. (2012) suggests that basal melt may not be as significant as previously thought. However, direct measurements are needed to further investigate this, which could be undertaken from point GPR measurements at each ablation stake across the ice shelf, to quantify the gains or losses at the basal interface. The deployment of remotely operated underwater vehicles may also serve to make observations of basal processes beneath the ice shelf.

5.4 SUMMARY

Northern Ellesmere Island is a unique and important region of the Queen Elizabeth Islands because it contains the largest single icefield, and the only ice shelves and marine-terminating glaciers with ice tongues in the Canadian Arctic. This thesis presented a comprehensive assessment of area changes for all glaciers on Northern Ellesmere Island, and investigated the potential links to changes in atmospheric and oceanographic temperatures. A clear conclusion from this analysis is that between ~1999 and ~2015 the ice-cover has rapidly decreased (by an average of ~5.9%), and that no individual glacier has advanced. Two main trends from these area changes include the rapid loss of small, low elevation, land-terminating glaciers and the loss of floating glacier termini and ice shelves. Along with increasing air temperatures, the loss of ice tongues in the Yelverton Bay region was initiated by increasing ocean temperatures, the loss of MLSI and the subsequent destabilization and loss of sikussak around the majority of ice tongues. Continued open water has prevented the reestablishment of MLSI and thus prevents the ice tongues from reforming. The same factors have led to the break up and loss of ice shelves such as the Ayles and Markham ice shelves. Although the Milne Ice Shelf has been subject to the same conditions, it has remained relatively stable, although recently increased thinning has led to break-up and calving along its landward margin.

Given the above, and projections for increasing air temperatures in the future, the ice-covered of Northern Ellesmere Island environment will continue to shrink. On land, small ice caps will be the first to vanish and the remaining ice-covered areas will likely to be limited to larger ice caps and icefields at higher elevations. Recent changes to floating glacier termini and ice shelves, along with MLSI, suggest that the northern coastline is approaching a future free of floating ice. This is why further research is necessary to investigate current knowledge gaps such as ocean temperature changes, and to continue monitoring glacier changes as they happen in the future.

CHAPTER 6: REFERENCES

Abdalati W, Krabill W, Frederick E, Manizade S, Martin C, Sonntag J, Swift R, Thomas R and Koerner R (2004) Elevation changes of ice caps in the Canadian Arctic Archipelago. *Journal of Geophysical Research*, **109**(F04007), doi: 10.1029/2003JF000045

Alt BT (1979) Investigation of summer synoptic climate controls on the mass balance of Meighen Ice Cap. *Atmosphere-Ocean*, **17**(3), doi: 10.1080/07055900.1979.9649060

Alt BT (1987) Developing synoptic analogs for extreme mass balance conditions on Queen Elizabeth Island ice caps. *Journal of Applied Meteorology*, **26**, 1605-1623, doi: 10.1175/1520-0450

Amundsen JM, Fahnestock M, Truffer M, Brown J, Lüthi MP and Motyka RJ (2010) Ice mélange dynamics and implications for terminus stability, Jakobshavn Isbrae, Greenland. *Journal of Geophysical Research*, **115**(F1), doi: 10.1029/2009JF001405

Andrews JT (2002) Glaciers of Baffin Island. In Williams Jr RS and Ferrigno JG eds. *Satellite Image Atlas of the World*, U.S. Geological Survey Professional Paper, 1386-J-1, J165-J195

Antoniades D, Francus P, Pienitz R, St-Onge G and Vincent W (2011) Holocene dynamics of the Arctic's largest ice shelf. *Proceedings of the National Academy of Sciences of the United States of America*, **108**(47), 18899-18904, doi: 10.1073/pnas.1106378108

Belkin IM and Kessel SA (2017) Russian drifting stations on Arctic ice islands. In Copland L and Mueller DR, eds. Arctic Ice Shelves and Ice Islands, Springer, Dordrecht, 367–393

Bezeau P, Sharp M and Gascon G (2015) Variability in summer anticyclonic circulation over the Canadian Arctic Archipelago and west Greenland in the late 20th/early 21st centuries and its effect on glacier mass balance. *International Journal of Climatology*, **35**, 540-557, doi: 10.1002/joc.4000

Box JE, Colgan WT, Wouters B, Burgess DO, O'Neel S, Thomson LI and Mernild SH (2018) Global sea-level contribution from Arctic land ice: 1971-2017. *Environmental Research Letters*, **13**, doi: 10.1088/1748-9326/aaf2ed

Bradley RS and Serreze MC (1987) Mass balance of two High Arctic plateau ice caps. *Journal of Glaciology*, **33**(113), 123-128

Braun C (2017) The surface mass balance of the Ward Hunt Ice Shelf and Ward Hunt Ice Rise. In Copland L and Mueller DR, eds. *Arctic Ice Shelves and Ice Islands*, Springer, Dordrecht, 149–183

Braun C, Hardy DR and Bradley RS (2004) Mass balance and area changes of four high arctic plateau ice caps, 1959-2002. *Geografiska Annaler*, **86A**, 43-52

Burgess DO (2017) *Mass balance of ice caps in the Queen Elizabeth Islands, Arctic Canada: 2014-2015*. Geological Survey of Canada, Open File 8223, 38 p., doi: 10.4095/300231

Canadian Ice Service (CIS) (2005) *Manual of Standard Procedures for Observing and Reporting Ice Conditions (MANICE)*, revised 9th edn. Meteorological Service of Canada, Environment Canada, Ottawa, ON.

Carr JR, Stokes CR and Vieli A (2013) Recent progress in understanding marine-terminating Arctic outlet glacier response to climatic and oceanic forcing: twenty years of rapid change. *Progress in Physical Geography*, **37**(4), 435-466, doi: 10.1177/0309133313483163

Carr JR, Stokes C and Vieli A (2014) Recent retreat of major outlet glaciers on Novaya Zemlya, Russian Arctic, influenced by fjord geometry and sea-ice conditions. *Journal of Glaciology*, **60**(219), 155-170, doi: 10.3189/2014JoG13J122

Carr JR, Stokes CR and Vieli A (2017) Threefold increase in marine-terminating outlet glacier retreat rates across the Atlantic Arctic: 1992-2010. *Annals of Glaciology*, **58**(74), 72-91, doi: 10.1017/aog.2017.3

Casey JA and Kelly R (2010) Estimating the equilibrium line of Devon Ice Cap, Nunavut, from RADARSAT-1 ScanSAR wide imagery. *Canadian Journal of Remote Sensing*, **36**(1), S41-S55

Cassotto R, Fahnestock M, Amundson JM, Truffer M and Joughin I (2015) Seasonal and interannual variations in ice melange and its impact on terminus stability, Jakobshavn Isbrae, Greenland. *Journal of Glaciology*, **61**(225), doi: 10.3189/2015JoG13J235

Copland L (1998) The use of terrain analysis in the evaluation of snow cover over an alpine glacier, In Lane SN, Richards KS and Chandler JH eds., *Landform Monitoring, Modelling and Analysis*. John Wiley & Sons, Chichester

Copland L, Sharp MJ and Dowdeswell JA (2003) The distribution and flow characteristics of surge-type glaciers in the Canadian High Arctic. *Annals of Glaciology*, **36**, 73-81

Copland L, Mueller DR and Weir L (2007) Rapid loss of the Ayles Ice Shelf, Ellesmere Island, Canada. *Geophysical Research Letters*, **34**(21), doi: 10.1029/2007GL031809

Copland L, Mortimer C, White A, Richer McCallum M and Mueller D (2017) Factors contributing to recent Arctic Ice Shelf losses. In Copland L and Mueller DR, eds., *Arctic Ice Shelves and Ice Islands*, Springer, Dordrecht, 263-285

Dowdeswell JA and Jeffries MO (2017) Arctic Ice Shelves: an introduction. In Copland L and Mueller DR, eds., *Arctic Ice Shelves and Ice Islands*, Springer, Dordrecht, 3-21

Dunse T, Schuler TV, Hagen JO, Eiken T, Brandt O and Høgda KA (2009) Recent fluctuations in the extent of the firn area of Austfonna, Svalbard, inferred from GPR. *Annals of Glaciology*, **50**(50), 155-162, doi: 10.3189/172756409787769780

Dyurgerov M, Meier MF and Bahr DB (2009) A new index of glacier area change: a tool for glacier monitoring. *Journal of Glaciology*, **55**(192), 710-716

Engeset R, Kohler J, Melvold K and Lunden B (2002) Change detection and monitoring of glacier mass balance and facies using ERS SAR winter images over Svalbard. *International Journal of Remote Sensing*, **23**(10), 2023-2050

England JH, Evans DA and Lakeman TR (2017) Holocene history of Arctic ice shelves. In Copland L and Mueller D, eds., *Arctic Ice Shelves and Ice Islands*, Springer, Dordrecht, 185-205

Ghilani CD (2000) Demystifying area uncertainty: more or less. *Surveying and Land Information Systems*, **60**(3), 177-182

GLIMS and NSIDC (2005, updated 2018): Global Land Ice Measurements from Space glacier database. Compiled and made available by the international GLIMS community and the National Snow and Ice Data Center

Hamilton AK, Laval BE, Mueller DR, Vincent WF and Copland L (2017) Dynamic response of an Arctic epishelf lake to seasonal and long-term forcing: implications for ice shelf thickness. *The Cryosphere*, **11**, 2189-2211

Harig C and Simons FJ (2016) Ice mass loss in Greenland, the Gulf of Alaska, and the Canadian Archipelago: Seasonal cycles and decadal trends. *Geophysical Research Letters*, **43**(7), 3150-3159, doi: 10.1002/2016GL067759

Hattersley-Smith G (1957) The rolls on the Ellesmere ice shelf. *Arctic*, **10**, 32-44

Hattersley-Smith G (1963) The Ward Hunt Ice Shelf: recent changes of the ice front. *Journal of Glaciology*, **4**(34), 415-424, doi: 10.3189/S0022143000027830

Hattersley-Smith G. (1969) Recent observations on the surging Otto Glacier, Ellesmere Island. *Canadian Journal of Earth Sciences*, **6**, 883-888

Hattersley-Smith G and Serson H (1970), Mass balance of the Ward Hunt Ice Rise and Ice Shelf: A 10 year record. *Journal of Glacio*logy, **9**(56), 247-252

Hattersley-Smith G and Serson H (1973) Reconnaissance of a small ice cap near St. Patrick Bay, Robeson Channel, Northern Ellesmere Island, Canada. *Journal of Glaciology*, **12**(66), 417-421

Holland DM, Thomas RH, De Young B, Ribergaard MH and Lyberth B (2008) Acceleration of Jakobshavn Isbrae triggered by warm subsurface ocean waters. *Nature Geoscience*, **1**, 1-6, doi: 10.1038/ngeo316

Howell SEL, Duguay CR and Markus T (2009) Sea ice conditions and melt season duration variability within the Canadian Arctic Archipelago: 1979-2008. *Geophysical Research Letters*, **36**(L10502), doi: 10.1029/2009GL037681

Jeffries MO (1984) Milne Glacier, Northern Ellesmere Island, N.W.T., Canada: a surging glacier? *Journal of Glaciology*, **30**(105), 251-253

Jeffries MO (1985) *Physical, chemical and isotopic investigations of Ward Hunt Ice Shelf and Milne Ice Shelf, Ellesmere Island, NWT*. PhD Thesis, University of Calgary, 358 pp

Jeffries MO (1986a) Glaciers and the morphology and structure of Milne Ice Shelf, Ellesmere Island, N.W.T, Canada. *Arctic and Alpine Research*, **18**(4), 397-405

Jeffries MO (1986b) Ice island calvings and ice shelf changes, Milne Ice Shelf and Ayles Ice Shelf, Ellesmere Island, N.W.T. *Arctic*, **39**(1), 15-19

Jeffries MO (1992) Arctic ice shelves and ice islands: origin, growth and disintegration, physical characteristics, structural-stratigraphic variability, and dynamics. *Reviews in Geophysics*, **30**(3), 245–267

Jeffries MO, Reynolds GJ and Miller JM (1992) First Landsat multi-spectral scanner images of the Canadian Arctic north of 80°N. *Polar Record*, **28**(164), doi: 10.1017/S0032247400020192

Jeffries MO (2002) Ellesmere Island Ice Shelves and Ice Islands. In Williams RS and Ferrigno JG, eds., *Satellite Image Atlas of Glaciers of the World: Glaciers of North America*, United States Geological Survey, Washington, D. C, J147-J164

Jeffries MO (2017) The Ellesmere Ice Shelves, Nunavut, Canada. In Copland L and Mueller DR, eds., *Arctic Ice Shelves and Ice Islands*, Springer, Dordrecht, 23-54

Jeffries MO and Serson HV (1986) Survey and mapping of recent ice shelf changes and landfast sea ice growth along the north coast of Ellesmere Island, NWT, Canada. *Annals of Glaciology*, **8**, 96-99, doi: 10.3189/S0260305500001221

Jenkins A (2011) Convection-driven melting near the grounding lines of ice shelves and tidewater glaciers. *Journal of Physical Oceanography*, **41**, 2279-2294, doi: 10.1175/JPO-D-11-03.1

Jenson SK and Domingue JO (1988) Extracting topographic structure from digital elevation data for geographic information analysis. *Photogrammetric Engineering and Remote Sensing*, **54**(11), 1593-1600

Joughin I, Howat IM, Fahnestock M, Smith B, Krabill W, Alley RB, Stern H and Truffer M (2008) Continued evolution of Jakobshavn Isbrae following its rapid speedup. *Journal of Geophysical Research*, **113**(F04006), doi: 10.1029/2008JF001023

Kalnay E and 21 others (1996) The NCEP/NCAR Reanalysis 40-year project. *Bulletin of the American Meteorological Society*, **77**(3), 437-471

Koenig LS, Greenaway KR, Dunbar M and Hattersley-Smith G (1952) Arctic ice islands. *Arctic*, **5**(2), 67-103, doi: 10.14430/arctic3901

Koerner RM (1979) Accumulation, ablation and oxygen isotope variations on the Queen Elizabeth Islands ice caps, Canada. *Journal of Glaciology*, **22**(86), 25-41

Koerner RM (2005) Mass balance of glaciers in the Queen Elizabeth Islands, Nunavut, Canada. *Annals of Glaciology*, **42**, 417-423

Kwok R (2015) Sea ice convergence along the Arctic coasts of Greenland and the Canadian Arctic Archipelago: Variability and extremes (1992-2014). *Geophysical Research Letters*, **42**, 7598-7605, doi: 10.1002/2015GL065462

Kwok R (2018) Arctic sea ice thickness, volume, and multiyear ice coverage: losses and coupled variability (1958-2018). *Environmental Research Letters*, **13**(10), doi: 10.1088/1748-9326/aae3ec

Lemmen DS, Evans DJA and England J (1988) Ice Shelves of northern Ellesmere Island, NWT, Canadian landform examples. *The Canadian Geographer*, **32**, 363-367

Lesins G, Duck TJ and Drummond JR (2010) Climate trends at Eureka in the Canadian high arctic. *Atmosphere-Ocean*, **48**(2), 59-80, doi: 10.3137/AO1103.2010

Leuschen, C., P. Gogineni, F. Rodriguez-Morales, J. Paden, and C. Allen. (2010, updated 2018) IceBridge MCoRDS L2 Ice Thickness, Version 1. [IRMCR2_20140401_03]. Boulder, Colorado USA. NASA National Snow and Ice Data Center Distributed Active Archive Center, doi: 10.5067/GDQ0CUCVTE2Q

Luckman A, Benn DI, Cottier F, Bevan S, Nilsen F and Inall M (2015) Calving rates at tidewater glacier vary strongly with ocean temperature. *Nature Communications*, **6**, doi: 10.1038/ncomms9566

Maslanik J, Stroeve J, Fowler C and Emery W (2011) Distribution and trends in Arctic sea ice age through spring 2011. *Geophysical Research Letters*, **38**(13), doi: 10.1029/2011GL047735

Massom RA (2003) Recent iceberg calving events in the Ninnis Glacier region, East Antarctica. *Antarctic Science*, **15**(2), 303-313, doi: 10.1017/S0954102003001299

Massom RA, Giles AB, Fricker HA, Warner RC, Legrésy B, Hyland G, Young N and Fraser AD (2010) Examining the interaction between multi-year landfast sea ice and the Mertz Glacier Tongue, East Antarctica: Another factor in ice sheet stability? *Journal of Geophysical Research*, **115**(C12027), doi: 10.1029/2009JC006083

Maxwell JB (1981) Climatic regions of the Canadian Arctic islands. *Arctic*, **34**(3), 225-240

Miles BWJ, Stokes CR and Jamieson SSR (2016) Pan-ice-sheet glacier terminus change in East Antarctica reveals sensitivity of Wilkes Land to sea-ice changes. *Science Advances*, **2**(5, e1501350), doi: 10.1126/sciadv.1501350

Miles BWJ, Stokes CR and Jamieson SSR (2017) Simultaneous disintegration of outlet glaciers in Porpoise Bay (Wilkes Land), East Antarctica, driven by sea ice break-up. *The Cryosphere*, **11**, 427-442, doi: 10.5194/tc-11-427-2017

Millan, R, Mouginot J and Rignot E (2017) Mass budget of the glaciers and ice caps of the Queen Elizabeth Island, Canada, from 1991 to 2015. *Environmental Research Letters*, **12**(024016), doi:10.1088/1748-9326/aa5b04

Miller GH, Bradley RS and Andrews JT (1975) The glaciation level and lowest equilibrium line altitude in the high Canadian Arctic: maps and climatic interpretations. *Arctic and Alpine Research*, **7**(2), 155-168, doi: 10.2307/1550318

Moon T, Joughin I and Smith B (2015) Seasonal to multiyear variability of glacier surface velocity, terminus position, and sea ice/ice mélange in northwest Greenland. *Journal of Geophysical Research: Earth Surface*, **120**(5), 818-833, doi: 10.1002/2015JF003494

Mortimer CA, Copland L and Mueller DR (2012) Volume and area changes of the Milne Ice Shelf, Ellesmere Island, Nunavut, Canada, since 1950. *Journal of Geophysical Research*, **117**(F04011), doi: 10.1029/2011JF002074

Mortimer CA, Sharp M and Wouters B (2016) Glacier surface temperatures in the Canadian High Arctic, 2000-15. *Journal of Glaciology*, **62**(235), 963-975, doi: 10.1017/jog.2016.80

Mortimer CA and Sharp M (2018) Spatiotemporal variability of Canadian High Arctic glacier surface albedo from MODIS data, 2001–2016. *The Cryosphere*, **12**, 701–720, doi: 10.5194/tc-12-701-2018

Mortimer CA, Sharp M and Van Wychen W (2018) Influence of recent warming and ice dynamics on glacier surface elevations in the Canadian High Arctic. *Journal of Glaciology*, **64**(245), 450-464, doi: 10.1017/jog.2018.37

Motyka RJ, Truffer M, Fahnestock M, Mortensen J, Rysgaard S and Howat I (2011) Submarine melting of the 1985 Jakobshavn Isbrae floating tongue and the triggering of the current retreat. *Journal of Geophysical Research*, **116**(F01007), doi: 10.1029/2009JF001632

Mueller DR and Vincent WF (2003) Break-up of the largest Arctic ice shelf and associated loss of an epishelf lake. *Geophysical Research Letters*, **30**(20), doi:10.1029/2003GL017931

Mueller DR and Vincent WF (2006) Microbial habitat dynamics and ablation control on the Ward Hunt Ice Shelf. *Hydrological Processes*, **20**, 857-876, doi: 10.1002/hyp.6113

Mueller DR, Vincent WF and Jeffries MO (2006) Environmental gradients, fragmented habitats, and microbiota of a northern ice shelf cryoecosystem, Ellesmere Island, Canada. *Arctic, Antarctic, and Alpine Research*, **38**(4), 593-608

Mueller DR, Copland L, Hamilton A and Stern D (2008) Examining Arctic Ice Shelves prior to the 2008 breakup. *EOS*, **89**(49), 502-503, doi: 10.1029/2008EO490002

Mueller DR, Copland L and Jeffries MO (2017a) Changes in Canadian Arctic ice shelf extent since 1906. In Copland L and Mueller DR, eds., *Arctic Ice Shelves and Ice Islands*, Springer, Dordrecht, 109–148

Mueller DR, Copland L and Jeffries MO (2017b) Northern Ellesmere Island ice shelf and ice tongue extents, v. 1.0 (1906-2015). Nordicana D28, doi: 10.5885/45455XD-24C73A8A736446CC

Nick FM, Luckman A, Vieli A, Van der Veen CJ, Van As D, Van De Wal RSW, Pattyn F, Hubbard AL and Floricioiu D (2012) The response of Petermann Glacier, Greenland, to large calving events, and its future stability in the context of atmospheric and oceanic warming. *Journal of Glaciology*, **58**(208), 229-239, doi: 10.3189/2012JoG11J242

Noël B, van de Berg WJ, Lhermitte S, Wouters B, Schaffer N and van den Broeke MR (2017) Six decades of glacial mass loss in the Canadian Arctic Archipelago. *Journal of Geophysical Research: Earth Surface*, **123**, 1430-1449, doi: 10.1029/2017JF004304

Østrem G and Brugman M (1991) *Mass Balance Measurements: A Manual for Field and Office Work*. National Hydrology Research Institute, Scientific Report 4, Environment Canada, Saskatoon and Norges Vassdrags og Elektrisitetsveseb, Oslo, 224 pp

Parliamentary Paper v LVI. (1877) *Journals and proceedings of the Arctic expedition of 1875-76 under the command of captain Sir George Nares, R.N.*, K.C.B. London

Paterson WSB (1969) The Meighen Ice Cap, Arctic Canada: Accumulation, ablation and flow. *Journal of Glaciology*, **8**(54), 341- 352

Peary RE (1907) *Nearest the Pole: A narrative of the polar expedition of the Peary Polar Club in the S.S. Roosevelt, 1905-1906*. London, Hutchinson

Pfeffer WT and 19 others (2014) The Randolph Glacier Inventory: a globally complete inventory of glaciers. *Journal of Glaciology*, **60**(221), doi: 10.3189/2014JoG13J176

Pimentel S, Flowers GE, Sharp MJ, Danielson B, Copland L, Van Wychen W, Duncan A and Kavanaugh JL (2017) Modelling intra-annual dynamics of a major marine-terminating Arctic glacier. *Annals of Glaciology,* doi: 10.1017/aog.2017.23

Plewes LA and Hubbard B (2001) A review of the use of radio-echo sounding in glaciology. *Progress in Physical Geography*, **25**(2), 203-236

Pope S, Copland L and Mueller D (2012) Loss of multiyear landfast sea ice from Yelverton Bay, Ellesmere Island, Nunavut, Canada. *Arctic Antarctic and Alpine Research*, **44**(2), 210-221, doi: 10.1657/1938-4246-44.2.210

Pope S, Copland L and Alt B (2017) Recent changes in sea ice plugs along the Northern Canadian Arctic Archipelago. In Copland L and Mueller DR, eds., *Arctic Ice Shelves and Ice Islands*, Springer, Dordrecht, 317-342

Prager BT (1983) *Digital signal processing of UHF radio-echo sounding data from northern Ellesmere Island*. MSc. Thesis, University of British Columbia, 88 pp

Raup B, Kääb A, Kargel JS, Bishop MP, Hamilton G, Lee E, Paul F, Rau F, Soltesz D, Khalsa SJS, Beedle M and Helm C (2007) Remote sensing and GIS technology in the Global Land Ice Measurements from Space (GLIMS) Project. *Computers and Geosciences*, **33**, 104-125

Raup B and Khalsa SJS (2010) *GLIMS analysis tutorial*. National Snow and Ice Data Center, Boulder, CO, https://www.glims.org/MapsAndDocs/assets/GLIMS_Analysis_Tutorial_a4.pdf

Rasmussen K (1921) *Greenland by the polar sea; the story of the Thule Expedition from Melville Bay to Cape Morris Jesup*. Frederick A. Stokes Company, New York, 327 pp

Reeh N, Thomsen HH, Higgins AK and Weidick A (2001) Sea ice and the stability of north and northeast Greenland floating glaciers. *Annals of Glaciology*, **33**(1), 474-480, doi: 10.3189/172756401781818554

Richer-McCallum M (2015) *Analysis of ice types along the northern coast of Ellesmere Island, Nunavut, Canada, and their relationship to synthetic aperture radar (SAR) backscatter*. MSc Thesis, Carleton University, 147 pp

Robel AA (2017) Thinning sea ice weakens buttressing force of iceberg mélange and promotes calving. *Nature Communications*, **8**(14596), doi: 10.1038/ncomms14596

Sackinger WM, Jeffries MO, Li F and Lu M (1991) *Ice Island creation, drift, recurrences, mechanical properties, and Interactions with Arctic offshore oil production structures*. U.S. Department of Energy Final Report DOE/MC/25027-3112, 34 pp

Sagar RB (1962) *Meteorological and glaciological studies: Ice rise station, Ward Hunt Island, May to September 1960*, Res. Pap. 24, 87 pp., Arctic Institute of North America, Calgary, Alberta, Canada.

Serreze MC, Raup B, Braun C, Hardy DR and Bradley RS (2017) Rapid wastage of the Hazen Plateau ice caps, northeastern Ellesmere Island, Nunavut, Canada. *The Cryosphere*, **11**, 169-177, doi: 10.5194/tc-11-169-2017

Sharp M, Burgess DO, Cogley JG, Ecclestone M, Labine C and Wolken GJ (2011) Extreme melt on Canada's Arctic ice caps in the 21st century. *Geophysical Research Letters*, **38**(L11501), doi:10.1029/2011GL047381

Sharp M and 12 others (2014) Remote sensing of recent glacier changes in the Canadian Arctic. In Kargel JS, Bishop MP, Kaab A, Raup BH and Leonard G, eds., *Global Land Ice Measurements from Space: Satellite Multispectral Imaging of Glaciers*. Springer-Praxis. Springer-Verlag, Berlin, Heidelberg, 205–228, doi: 10.1007/978-3-540-79818-7_9

Sohn H, Jezek KC and van der Veen CJ (1998) Jakobshavn Glacier, West Greenland: 30 years of spaceborne observations. *Geophysical Research Letters*, **25**(14), 2699-2702

Sylvestre T, Copland L, Demuth MV and Sharp M (2013) Spatial patterns of snow accumulation across Belcher Glacier, Devon Ice Cap, Nunavut, Canada. *Journal of Glaciology*, **59**(217), 874-882, doi: 10.3189/2013JoG12J227

Thomas RH, Abdalati W, Frederick E and Krabill WB (2003) Investigation of surface melting and dynamic thinning on Jakobshavn Isbrae, Greenland. *Journal of Glaciology*, **49**(165), 231-239, doi: 10.3189/172756503781830764

Thomson LI, Osinski GR and Ommanney SL (2011) Glacier change on Axel Heiberg Island, Nunavut, Canada. *Journal of Glaciology*, **57**(206), 1079-1086, doi: 10.3189/002214311798843287

Thomson LI, Zemp M, Copland L, Cogley JG and Ecclestone MA (2017) Comparison of geodetic and glaciological mass budgets for White Glacier, Axel Heiberg Island, Canada. *Journal of Glaciology*, **63**(237), 55-66, doi: 10.1017/jog.2016.112

Todd J and Christoffersen P (2014) Are seasonal calving dynamics forced by buttressing from ice mélange or undercutting by melting? Outcomes from full-Stokes simulations of Store Glacier, West Greenland. *The Cryosphere*, **8**, 2353-2365

U.S. Geological Survey (2016) Landsat collections. https://landsat.usgs.gov/landsat-collections

van der Veen CJ (1998) Fracture mechanics approach to penetration of surface crevasses on glaciers. *Cold Regions Science and Technology*, **27**, 31-47

Van Wychen W., Davis J, Burgess DO, Copland L, Gray L, Sharp M and Mortimer C (2016) Characterizing interannual variability of glacier dynamics discharge (1999-2015) for the ice masses of Ellesmere and Axel Heiberg Islands, Nunavut, Canada. *Journal of Geophysical Research: Earth Surface*, **121**, 39-63, doi: 10.1002/2015JF003708

Veillette J, Mueller DR, Antoniades D and Vincent WF (2008) Arctic epishelf lakes as sentinel ecosystems: Past, present and future. *Journal of Geophysical Research,* **113**(G04014), doi: 10.1029/2008JG000730

Vieli A and Nick FM (2011) Understanding and modeling rapid dynamic changes of tidewater outlet glaciers: issues and implications. *Surveys in Geophysics,* **32**, 437-458, doi: 10.1007/s10712-011-932-4

Vincent WF, Gibson JAE and Jeffries MO (2001) Ice shelf collapse, climate change and habitat loss in the Canadian High Arctic. *Polar Record*, **37**, 133-142

Vincent WF, Whyte LG, Lovejoy C, Greer CW, Laurion I, Suttle CA, Corbeil J and Mueller DR (2009) Arctic microbial ecosystems and impacts of extreme warming during the International Polar Year. *Polar Science*, **3**, 171-180, doi: 10.1016/j.polar.2009.05.004

Walker PW and Mattox Jr WG (1961) *Glaciological observations in northern Ellesmere Island-1959*, Scientific Report No. 139. Washington, DC: Arctic Institute of Northern America.

Walter JI, Box JE, Tulaczyk S, Brodsky EE, Howat IM, Ahn Y and Brown A (2012) Oceanic mechanical forcing of a marine-terminating Greenland glacier. *Annals of Glaciology*, **53**(60), 181-192, doi: 10.3189/2012AoG60A083

White A, Copland L, Mueller D and Van Wychen W (2015) Assessment of historical changes (1959-2012) and the causes of recent break-ups of the Petersen ice shelf, Nunavut, Canada. *Annals of Glaciology*, **56**(69), 65-76, doi:10.3189/2015AoG69A687

Williamson S, Sharp M, Dowdeswell J and Benham T (2008) Iceberg calving rates from northern Ellesmere Island ice caps, Canadian Arctic, 1999-2003. *Journal of Glaciology*, **54**(186), 391-400

Wolken GJ, England JH and Dyke AS (2008) Changes in late-neoglacial perennial snow/ice extent and equilibrium-line altitudes in the Queen Elizabeth Islands, Arctic Canada. *The Holocene*, **18**(4), 615-627, doi: 10.1177/0959683608089215

Yu Y, Stern H, Fowler C, Fetterer F and Maslanik J (2013) Interannual variability of arctic landfast ice between 1976 and 2007. *Journal of Climate*, **27**(1), 227-243, doi: 10.1175/JCLI-D-13-00178.1

Zhang X, Vincent LA, Hogg, WD and Niitsoo A (2000) Temperature and precipitation trends in Canada during the 20th century. *Atmosphere-Ocean*, **38**(3), 395-429, doi:10.1080/07055900.2000.9649654